

Instruments and Observing Methods  
Report No. 141

WEATHER CLIMATE WATER

# Report on the 3rd WMO International Pyrgeometer Intercomparison (IPgC-III)

(27 September - 15 October 2021, Davos, Switzerland)

J. Gröbner and C. Thomann



WORLD  
METEOROLOGICAL  
ORGANIZATION

This publication is available in pdf format, from the WMO Library website:  
<https://library.wmo.int/>

© **World Meteorological Organization, 2023**

The right of publication in print, electronic and any other form and in any language is reserved by WMO. Short extracts from WMO publications may be reproduced without authorization, provided that the complete source is clearly indicated. Editorial correspondence and requests to publish, reproduce or translate this publication in part or in whole should be addressed to:

Chair, Publications Board  
World Meteorological Organization (WMO)  
7 bis, avenue de la Paix  
P.O. Box 2300  
CH-1211 Geneva 2, Switzerland

Tel: +41 (0) 22 730 8403  
Fax: +41 (0) 22 730 8117  
E-mail: [Publications@wmo.int](mailto:Publications@wmo.int)

NOTE

The designations employed in WMO publications and the presentation of material in this publication do not imply the expression of any opinion whatsoever on the part of WMO concerning the legal status of any country, territory, city or area, or of its authorities, or concerning the delimitation of its frontiers or boundaries.

The mention of specific companies or products does not imply that they are endorsed or recommended by WMO in preference to others of a similar nature which are not mentioned or advertised.

The findings, interpretations and conclusions expressed in WMO publications with named authors are those of the authors alone and do not necessarily reflect those of WMO or its Members.

This publication has been issued without formal editing.

## FOREWORD

The WMO Technical Commission for Observation, Infrastructure and Information Systems (INFCOM), through its Standing Committee on Measurement, Instrumentation and Traceability (SC-MINT), coordinates activities that enable the traceability of measurement to international standards in the context of the WMO Integrated Global Observing System (WIGOS). The intercomparison presented in this report is one of those key activities.

Precise and traceable radiation measurements, including their terrestrial infrared component, are essential for understanding the Earth's energy budget, and for monitoring changes in climate. The World Infrared Standard Group (WISG) was established to serve as an interim reference for the calibration of pyrgeometers to ensure the worldwide comparability of their measurements of terrestrial infrared irradiance.

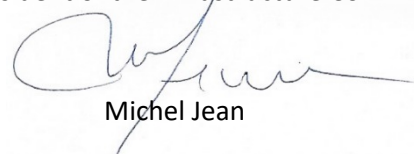
This Third International Pyrgeometer Intercomparison (IPgC-III) was organized by the *Physikalisch-Meteorologisches Observatorium Davos/World Radiation Centre* (PMOD/WRC) in Davos, Switzerland, from 27 September to 15 October 2021. The organization of these intercomparisons every five years has now become a regular practice and follows a clear governance framework agreed by WMO. Exceptionally, IPgC-III had to be postponed by one year, to 2021, because of the COVID-19 pandemic.

IPgC-III demonstrated the stability of the WISG and enabled the calibration of a large number of instruments. It has been shown that there is an apparent offset between the WISG and the International System of Units (SI) and that recent technological developments enable to significantly reduce the uncertainties of potential new reference instruments. IPgC-III was also the occasion for investigating the performance of such modern instruments and how they compare to the WISG. This will be crucial for ensuring the continuity of climate time series in case of reference change.

PMOD/WRC organized this intercomparison again in parallel with two other instrument intercomparisons: the International Pyrheliometer Intercomparison (IPC) and the Filter Radiometer Comparison. PMOD/WRC also organized a Symposium on Radiation Measurement during the same timeframe. This is a very efficient use of resources for those attending, and a unique opportunity for capacity development and sharing of experience among the participants.

I wish to express my sincere gratitude and that of the WMO Infrastructure Commission to the organizers of the IPgC-III, and authors of this report for their valuable work, as well as to all the staff of PMOD for supporting this intercomparison propagating the traceability of terrestrial infrared irradiance measurements to the WMO and broader radiation measurement community.

President of the Infrastructure Commission



Michel Jean

# Report of the Third International Pyrgeometer Comparison from 27 September to 15 October 2021 at PMOD/WRC (IPgC-III)

Julian Gröbner, Christian Thomann

*Physikalisch-Meteorologisches Observatorium Davos, World Radiation Centre*

Infrared Radiometry Section (WRC-IRS)

1	Introduction.....	2
2	Setup and Instrumentation.....	2
3	Laboratory characterisation.....	4
4	Calibration relative to WISG.....	4
4.1	Stability of the WISG .....	6
5	Results .....	6
5.1	Blackbody versus WISG based calibration .....	8
5.2	Solar influence on unshaded pyrgeometers .....	9
6	IRIS, ACP and WISG .....	9
6.1	The Infrared Integrating sphere radiometers (IRIS).....	10
6.2	The Absolute Cavity Pyrgeometers (ACP).....	10
6.3	Results .....	11
7	New WISG coefficients .....	14
8	Conclusion.....	19
9	Annex .....	20

## 1 Introduction

The Third International Pyrgeometer Comparison (IPgC-III) was organised together with the Thirteenth International Pyrheliometer Comparison (IPC-XIII) and the Fifth Filter Radiometer Comparison (FRC-V) from 27 September to 15 October 2021 at the *Physikalisch-Meteorologisches Observatorium Davos*, World Radiation Centre (PMOD/WRC). 28 participants with a total of 40 pyrgeometers participated at this intercomparison. In addition, 4 Infrared Integration Sphere Radiometers (IRIS), 2 from PMOD/WRC, one from BOM, Australia and one from DWD, Germany and 4 Absolute Cavity Pyrgeometers (ACP), 2 from NREL, USA, 1 from DWD, Germany, and 1 from JMA, Japan, were operated during 7 clear-sky nights in view of establishing a new reference for longwave irradiance measurements traceable to SI.



Figure 1. Pictures of the measurement platform of WRC-IRS on top of the PMOD/WRC. Left upper figure: World Infrared Standard Group (WISG), left bottom: the IRIS, right : Pyrgeometers in the foreground, IRIS and ACP in the background.

## 2 Setup and Instrumentation

The intercomparison took place at the PMOD/WRC, Switzerland, from 27 September to 15 October 2021. The outdoor measurement platform is located on the roof of the PMOD/WRC building at 1610 m.a.s.l., 46.813 N, 9.845 E. The measurement site is located in the Swiss Alps and its horizon is limited by mountains. Each pyrgeometer was characterised in the blackbody cavity of PMOD/WRC (Blackbody BB2007) to retrieve the pyrgeometer coefficients according to the standard PMOD formula [1] (see section 3). This procedure lasted for about 10 hours per instrument, so that the duration of the campaign was just sufficient to cycle all instruments.

The pyrgeometers were installed on the measurement platform on shaded and unshaded positions. The specific conditions for each pyrgeometer are described in Table 1. When not otherwise noted, pyrgeometers were placed in PMOD-VHS ventilation and heating units. Most pyrgeometers were connected to the PMOD data acquisition system (DAQ), apart from those denoted otherwise. The measured data were saved as one minute averages.

The calibration of the participating pyrgeometers was performed according to the calibration procedure described in the IOM report No. 120 [1], using the WISG as reference for atmospheric longwave irradiance.

**Table 1. Participant information**

Nb	Pyregeometer	Type	Manufacturer	DAQ	Institution	Remarks
1	PIR 31463F3	PIRmod	Eppley	PMOD	PMOD/WRC	WISG1
2	PIR 31464F3	PIRmod	Eppley	PMOD	PMOD/WRC	WISG2
3	CG4_FT004	CG4	Kipp&Zonen	PMOD	PMOD/WRC	WISG3
4	CG4_010535	CG4	Kipp&Zonen	PMOD	PMOD/WRC	WISG4
5	CG4_FT006	CG4	Kipp&Zonen	PMOD	PMOD/WRC	
6	IR20_105	IR20	Hukseflux	PMOD	PMOD/WRC Hukseflux	No solarblind filter
7	CGR4_110390	CGR4	Kipp&Zonen	PMOD	PMOD/WRC Kipp&Zonen	No solarblind filter
8	CG4_FT005	CG4	Kipp&Zonen	PMOD	PMOD/WRC	Cut-on filter at 6 $\mu$ m
9	CG4_060893	CG4 PT100	Kipp&Zonen	PMOD	AEMET, Spain	
10	CGR4_140081	CGR4 PT100	Kipp&Zonen	PMOD	UNAM, Mexico	
11	CG4_050792	CG4	Kipp&Zonen	PMOD	SMHI, Sweden	
12	CGR4_110348	CGR4 PT100	Kipp&Zonen	PMOD	Meteoswiss, Switzerland	
13	CG4_060881	CG4	Kipp&Zonen	PMOD	NREL, USA	
14	CG4_050783	CG4 PT100	Kipp&Zonen	PMOD	AEMET, Spain	
15	PIR_32227F3	PIR	Eppley	PMOD	Eppley, USA	
16	CGR4_130621	CGR4	Kipp&Zonen	PMOD	KACST, Saudia Arabia	
17	CG4_080066	CG4 PT100	Kipp&Zonen	PMOD	OMSZ, Hungary	
18	MS-21_REF002	MS-21 PT100	EKO	PMOD	EKO Instruments, Japan	EKO ventilation unit
19	CGR4_110378	CGR4 PT100	Kipp&Zonen	PMOD	DWD, Germany	
20	CG4_010567	CG4 PT100	Kipp&Zonen	PMOD	JMA, Japan	
21	MS-20 S19068.06	MS-20 PT100	EKO	PMOD	NIMS, Rep. of Korea	
22	CG4_030665	CG4	Kipp&Zonen	PMOD	CMA, China	
23	IR20-T2_4019	IR-20-T2	Hukseflux	PMOD	Hukseflux, Netherlands	
24	CGR4_160201	CGR4 PT100	Kipp&Zonen	PMOD	SMN, Argentina	
25	CGR4_140016	CGR4 PT100	Kipp&Zonen	PMOD	SHMI, Slovakia	
26	CGR4_130648	CGR4	Kipp&Zonen	PMOD	CHMI, Czech Republic	
27	CGR4_070042	CGR4 PT100	Kipp&Zonen	PMOD	CIEMAT, Spain	Kipp&Zonen CV2 ventilation unit
28	CGR3_110460	CGR3	Kipp&Zonen	PMOD	Udelar, Uruguay	
29	CG4_010536	CG4	Kipp&Zonen	PMOD	OTT Hydromet, Netherlands	
30	EMPIR_01	Prototype	Hukseflux	PMOD	PMOD/WRC, Hukseflux	Diamond dome
31	EMPIR_02	Prototype	Hukseflux	PMOD	PMOD/WRC, Hukseflux	Diamond dome
32	CGR4_100210	CGR4 PT100	Kipp&Zonen	PMOD	Voeikov MGO, Russian Federation	
33	CG4_060869	CG4	Kipp&Zonen	PMOD	CSERS, Libya	
34	CGR4_170224	CGR4 PT100	Kipp&Zonen	PMOD	EMHI, Estonia	
35	CG1_970115	CG1 PT100	Kipp&Zonen	PMOD	TUD, Denmark	
36	PIR_38864F3	PIR	Eppley	PMOD	NOAA, USA	
37	IR20-T2_4041	IR20-T2	Hukseflux	Hukseflux	Hukseflux, Netherlands	Hukseflux VU01 ventilation unit

38	IR30-A1-T2_101	IR30-A1-T2	Hukseflux	Hukseflux	Hukseflux, Netherlands	No ventilation unit
39	IR30-A1-T2_102	IR30-A1-T2	Hukseflux	Hukseflux	Hukseflux, Netherlands	No ventilation unit
40	IR30-A1-T2-WS_100	IR30-A1-T2-WS	Hukseflux	Hukseflux	Hukseflux, Netherlands	No ventilation unit, no solarblind filter
41	IRIS2	IRIS	PMOD/WRC	---	PMOD/WRC	
42	IRIS4	IRIS	PMOD/WRC	---	PMOD/WRC	
43	IRIS3	IRIS	PMOD/WRC	---	BOM, Australia	
44	IRIS5	IRIS	PMOD/WRC	---	DWD, Germany	
45	ACP10	ACP	NREL	NREL	JMA, Japan	
46	ACP57	ACP	NREL	NREL	DWD, Germany	
47	ACP95	ACP	NREL	NREL	NREL, USAA	
48	ACP96	ACP	NREL	NREL	NREL, USA	On Loan to PMOD/WRC

### 3 Laboratory characterisation

Each pyrgeometer was characterised in the blackbody cavity BB2007 of PMOD/WRC [2]. The characterisation procedure consisted in varying the blackbody temperature between +15 °C and -20 °C and the pyrgeometer body temperature between +20 °C and -10 °C to obtain 7 constant temperature levels at which the pyrgeometer coefficients  $C_{BB}$ ,  $k_1$ ,  $k_2$ , and  $k_3$ , were retrieved using the following equation:

$$E = \frac{U}{C_{BB}} (1 + k_1 \sigma T_B^3) + k_2 \sigma T_B^4 - k_3 \sigma (T_D^4 - T_B^4) \quad (1)$$

where  $E$  is the irradiance in  $W m^{-2}$ ,  $U$  the pyrgeometer voltage in volt, and  $T_B$  and  $T_D$  the body and dome temperatures respectively (called PMOD equation from now on).  $k_1$ ,  $k_2$ , and  $k_3$  are pyrgeometer specific coefficients which are retrieved for each pyrgeometer separately and used for the outdoor calibration. The last term in equation 1 is set to zero for pyrgeometers without dome thermistor. For PIR pyrgeometers, the retrieval sensitivity of  $k_3$  is significantly improved by differentially heating the dome of the pyrgeometer by a copper heating ring. This allows heating the dome by about +1 K relative to the body temperature.

The same measurements were used to retrieve the responsivity  $C_{BB}$  and in case of Eppley PIR the dome coefficient  $K$  using the simplified version of equation 1 (often denoted Albrecht equation),

$$E = \frac{U}{C_{BB}} + \sigma T_B^4 - k_3 \sigma (T_D^4 - T_B^4) \quad (2)$$

### 4 Calibration relative to WISG

The calibration of the participating pyrgeometers was performed according to the calibration procedure described in [1], against the WISG which served as reference for atmospheric longwave irradiance. Figure 2 shows the atmospheric downwelling longwave irradiance during the campaign. The data selection used to retrieve the responsivity of the pyrgeometers used the following criteria, as described in [1]:

1. Outliers are removed ( $U > 0.001$  V,  $U < -20$  mV,  $|T_D| > 40$  °C,  $|T_B| > 40$  °C).
2. Any night containing rain is excluded (limit of 0.2 mm/10 min).
3. Stable atmospheric conditions, defined by the standard deviation of the WISG  $< 2$   $W m^{-2}$ .
4. Net radiation measured by the WISG  $< -70$   $W m^{-2}$ .
5. Measurements from one night are used if there are at least 80% valid measurement points.
6. Night is defined when the solar zenith angle is larger than 95°.
7. Relative standard deviation of the 1 min average test pyrgeometer signal  $< 3\%$ .

Furthermore, data is excluded from the calibration if the integrated water vapour (I WV), determined from the time delay of GPS receivers, is below 10 mm. The 95% coverage of the I WV varied between

4.2 mm and 19.1 mm during the campaign (see Figure 3), while the minimum IWV was 2.9 mm on 15 October at 5:00 UTC and the maximum IWV was 21.5 mm on 26 September at 16:00 UTC.

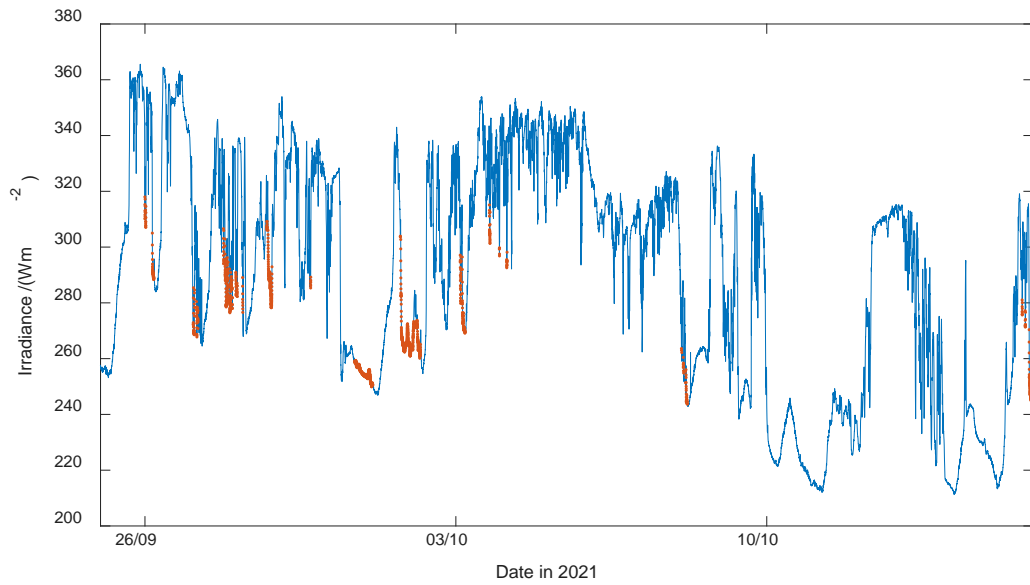


**Figure 2. Downwelling longwave irradiance during the campaign. The red dots represent the data points which satisfy the calibration criteria.**

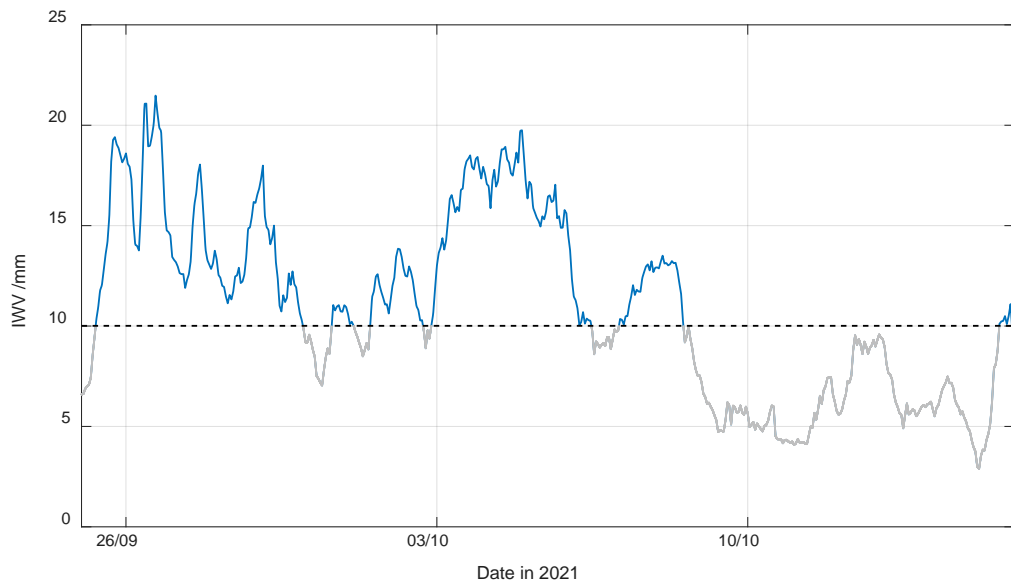


**Figure 3. Integrated water vapour (IWV) from GPS measurements during the IPgC campaign. The threshold for using measurement data points for retrieving the pyrometer responsivity is for IWV larger than 10 mm.**



## 4.1 Stability of the WISG

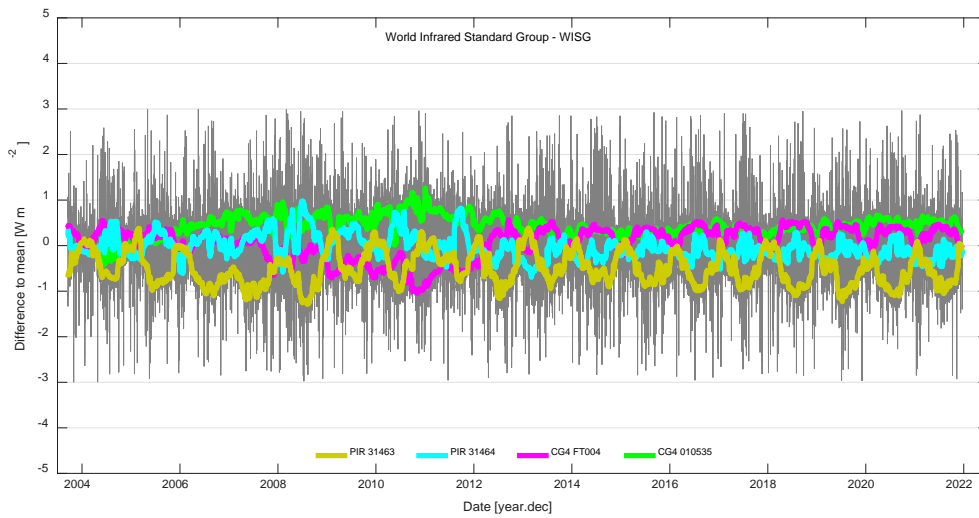


**Figure 4. Night average differences of longwave irradiance measurements between the WISG pyrgeometers relative to their average. The thick lines represent a monthly running average.**

The WISG is operated continuously on the measurement platform of PMOD/WRC. Its stability is monitored by internal consistency checks of the four pyrgeometers comprising the WISG. As can be seen in Figure 4, the pyrgeometers of the WISG typically agree to within  $\pm 1 \text{ W m}^{-2}$ , with minor seasonal variations between individual members of the WISG.

## 5 Results

The results of the blackbody characterisation and the outdoor calibration relative to the WISG are summarised in Table 2. The coefficients  $k_1$ ,  $k_2$ ,  $k_3$  and  $C_{\text{BB}}$  were retrieved with the blackbody as radiation source, while  $C_{\text{WISG}}$  was retrieved using  $k_1$ ,  $k_2$ ,  $k_3$  and the atmospheric downwelling irradiance as source, as measured by the WISG using the original coefficients (see section 7). The responsivities  $C_{\text{WISG}}$  were retrieved using the PMOD ( $C$ ,  $k_1$ ,  $k_2$ ,  $k_3$ ) and Albrecht ( $C$ ,  $k_3$ ) equations, respectively. The figures showing the individual performance of each pyrgeometer are shown in the Annex at the end of this report.

**Table 2. Results from the blackbody characterisation and the calibration relative to the WISG using the original WISG coefficients. The responsivities  $C_{\text{Blackbody}}$  and  $C_{\text{WISG}}$  are given in  $\mu\text{V}/(\text{W m}^{-2})$ . The residuals in  $\text{W m}^{-2}$  in the corresponding column are given for a coverage interval of 95% using the PMOD equation.**

Nb	Pyrgeometer	$k_1$	$k_2$	$k_3$	$C_{\text{Blackbody}} (C_{\text{BB}})$		$C_{\text{WISG}} (C_{\text{WISG}})$		Residuals in $\text{W m}^{-2}$ rel. to WISG (95%)	shaded/ unshaded
					$k_1, k_2, k_3$	Albrecht	$k_1, k_2, k_3$	Albrecht		
1	PIR_31463F3	0.069	0.9957	3.2	3.700	3.315	3.885	3.504	0.64	S
2	PIR_31464F3	0.046	0.9957	2.8	3.942	3.629	4.026	3.733	0.58	S
3	CG4_FT004	-0.042	0.9977	0	11.71	12.47	12.23	12.80	0.31	S
4	CG4_010535	-0.029	0.9981	0	8.808	8.730	9.460	9.742	0.24	S
5	CG4_FT006	0.072	1.0003	0	11.99	11.03	11.62	10.66	0.53	S
6	IR20_105	-0.029	1.0009	0	15.50	16.18	15.08	15.72	0.62	U
7	CGR4_110390	0.000	0.9993	0	8.910	9.020	8.398	8.368	0.58	U
8	CG4_FT005	0.049	0.9983	0	9.055	9.442	9.673	9.036	0.31	S
9	CG4_060893	-0.010	0.9979	0	7.903	7.850	7.435	7.459	0.57	U
10	CGR4_140081	-0.010	0.9980	0	9.537	9.513	9.405	9.441	0.29	S
11	CG4_050792	0.053	0.9991	0	8.964	8.365	8.783	8.208	0.42	U
12	CGR4_110348	0.040	0.9978	0	11.69	11.01	11.55	10.90	0.35	S
13	CG4_060881	0.016	0.9979	0	8.541	8.266	8.215	7.976	0.57	S
14	CG4_050783	0.020	0.9974	0	9.830	9.411	9.619	9.280	0.37	U
15	PIR_32227F3	-0.046	0.9956	2.5	3.745	3.867	3.833	3.999	0.31	S
16	CGR4_130621	-0.0231	0.9986	0	11.75	11.99	11.39	11.68	0.45	U
17	CG4_080066	0.060	0.9990	0	14.58	13.52	14.29	13.24	0.39	U
18	MS-21_REF002	-0.010	1.0003	0	17.75	18.01	18.84	19.11	0.50	U
19	CGR4_110378	0.031	0.9992	0	11.43	10.94	11.27	10.81	0.37	U
20	CG4_010567	0.027	0.9974	0	11.19	10.65	12.50	11.98	0.96	U
21	MS-20 S19068.06	0.033	0.9905	0	25.16	22.61	24.26	22.38	0.56	U
22	CG4_030665	0.043	0.9994	0	11.58	10.95	11.30	10.70	0.41	U
23	IR20-T2_4019	-0.140	0.9995	0	6.932	8.345	7.093	8.568	0.63	U
24	CGR4_160201	0.000	0.9987	0	9.856	9.730	9.661	9.605	0.33	U
25	CGR4_140016	0.000	0.9994	0	11.49	11.42	10.94	10.91	0.41	U
26	CGR4_130648	0.010	0.9993	0	10.91	10.76	10.99	10.82	0.33	U
27	CGR4_070042	0.003	1.0011	0	11.18	10.86	11.01	10.66	0.34	U
28	CGR3_110460	0.104	1.0004	0	14.63	13.01	15.43	13.69	0.35	U
29	CG4_010536	0.026	0.9976	0	9.448	9.021	9.230	8.841	0.44	U
30	EMPIR_01	0.0349	0.9979	0	9.880	9.341	9.973	9.483	0.46	U
31	EMPIR_02	0.053	0.9980	0	10.26	9.504	10.66	9.933	0.54	U
32	CGR4_100210	0.010	0.9989	0	10.37	10.16	10.25	10.07	0.38	U
33	CG4_060869	0.046	0.9996	0	9.122	8.610	9.05	8.57	0.27	U
34	CGR4_170224	-0.011	0.9992	0	12.78	12.89	12.49	12.58	0.43	U
35	CG1_970115	0.030	0.9993	0	11.68	11.25	12.48	12.02	0.31	U
36	PIR_38864F3	0.126	0.9936	8.4	3.091	2.560	3.367	2.839	0.47	U
37	IR20-T2_4041	-0.135	0.9980	0	8.005	9.493	8.437	10.05	0.44	U
38	IR30-A1- T2_101	-0.124	0.9981	0	8.020	9.378	8.370	9.734	0.34	U
39	IR30-A1- T2_102	-0.0164	0.9984	0	7.283	7.361	7.644	7.738	0.32	U
40	IR30-A1-T2- WS_100	-0.106	0.9986	0	7.622	8.708	7.585	8.618	0.29	U

## 5.1 Blackbody versus WISG based calibration

As shown in previous studies, atmospheric downwelling irradiance measurements from pyrgeometers which are only based on blackbody calibrations show large differences. These differences can be quantified from the responsivities  $C_{WISG}$  and  $C_{BB}$ . The relative difference between the two responsivities can be directly expressed in  $W\ m^{-2}$  by multiplying the relative difference by a net irradiance of  $-100\ W\ m^{-2}$ , typical for clear sky conditions. Figure 5 shows the relative difference between  $C_{WISG}$  and  $C_{BB}$  expressed in %.

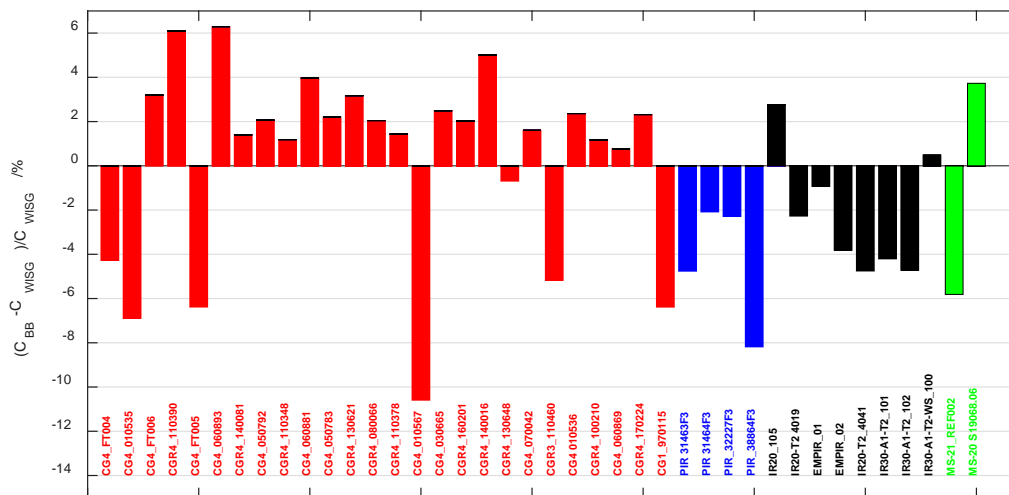


**Figure 5. Relative differences between the blackbody based and WISG based responsivities. The red, blue, black, and green bars represent the Kipp&Zonen CG4/CGR4, Eppley PIR, Hukseflux IR20, and EKO MS- pyrgeometers, respectively.**

As can be seen in Figure 5, discrepancies of up to  $16\ W\ m^{-2}$  can be expected between clear sky atmospheric longwave irradiance measurements from pyrgeometers calibrated in the same blackbody. As discussed in previous studies, these differences are assumed to arise from the spectral mismatch of the spectral dome transmissions and the spectral differences between the blackbody radiation and the atmospheric downwelling radiation.

## 5.2 Solar influence on unshaded pyrgeometers

The solar influence on the unshaded pyrgeometers were calculated by a linear fit to the residuals between each unshaded pyrgeometer and the WISG and extrapolating to  $1 \text{ kW m}^{-2}$  of horizontal direct solar irradiance obtained with a collocated pyrliometer. As can be seen in Figure 6, the impact of the solar irradiance on daytime measurements of unshaded pyrgeometers ranges from  $2.0 \text{ W m}^{-2}$  to  $18.9 \text{ W m}^{-2}$  for a horizontal incident direct solar irradiance of  $1 \text{ kW m}^{-2}$ . This effect can be either due to the differential heating of the dome of the pyrgeometer, or from the shortwave leakage of the interference filter coating applied on the inside of the dome.

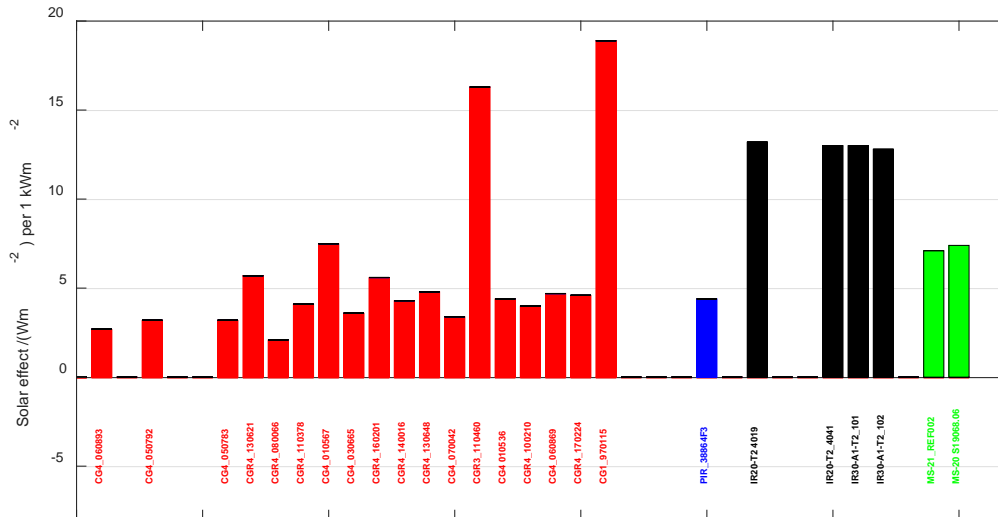


Figure 6. Solar influence on unshaded pyrgeometers relative to the shaded WISG during daytime at  $1 \text{ kW m}^{-2}$  of horizontal direct solar irradiance.

## 6 IRIS, ACP and WISG

Four IRIS and four ACP absolutely calibrated longwave infrared radiometers took part in the IPgC-III. Due to their windowless operation, measurements were only available during clear sky nights. Measurements between 26 September and 18 October were analysed. While measurements of the IRIS radiometers started on 22 September, the ACPs were installed a few days later, on 30 September. The IRIS radiometers measured on 7 clear sky nights, while the ACPs measured on 4 clear sky nights.

## 6.1 The Infrared Integrating sphere radiometers (IRIS)

The downwelling longwave irradiance  $E$  in  $W m^{-2}$  is obtained from the IRIS radiometers [3] using the following measurement equation,

$$E = \frac{U \cos(\theta)}{C(1+dt(7-293.15))} + k\sigma T^4 \quad (3)$$

where  $U$  and  $\theta$  are the signal in Volt and the phase of the IRIS signal obtained from the lock-in amplifier,  $C$  the responsivity in  $V W^{-1} m^2$ ,  $T$  the IRIS temperature in K,  $k$  the emissivity correction factor,  $dt$  the temperature coefficient of the pyroelectric detector in  $K^{-1}$ , and  $\sigma$  the Stefan-Boltzmann constant. The IRIS were calibrated prior to their deployment at the IPgC-III using the PMOD blackbody BB2007. The IRIS calibration coefficients  $C$  and  $k$  are shown in Table 3,

**Table 3. IRIS coefficients in use at the IPgC-III obtained from the calibration with BB2007.**

Instrument	$C$ in $V W^{-1} m^2 \cdot 10^{-3}$	$k$	$dt \cdot 10^{-2}$	Comments
IRIS2	0.1046	0.9949	0.01	Calibrated on 8 September 2021
IRIS3	0.3294	0.9951	-0.10	Calibrated on 19 September 2021 (Calibration certificate Nb. 2021_2379_01)
IRIS4	0.2714	0.9964	0.20	Calibrated on 10 September 2021
IRIS5	0.0892	0.9863	-0.20	Calibrated on 16 September 2021 (Calibration certificate Nb. 2021_2377_02)

## 6.2 The Absolute Cavity Pyrgeometers (ACP)

The downwelling longwave irradiance  $E$  is obtained from the ACP according to [4],

$$E = \frac{K_1 U + (2 - \varepsilon_g) K_2 W_r - (\varepsilon_{cav} + \varepsilon_g) W_c}{\tau} \quad (4)$$

where  $K_1$  is the inverse responsivity in  $W m^{-2} V^{-1}$ ,  $U$  is the thermopile signal in volt,  $\varepsilon_g$  the emissivity of the gold concentrator, equal to 0.0225,  $\varepsilon_{cav}$  the emissivity of the enclosed air volume in the concentrator, equal to 1,  $W_r$  the emitted receiver irradiance in  $W m^{-2}$ ,  $W_c$  the emitted concentrator irradiance in  $W m^{-2}$ , and  $\tau$  the effective throughput of the concentrator. The inverse responsivity  $K_1$  is obtained every 2 hours during an outdoor calibration by cooling the ACP. Then, the concentrator effective throughput  $\tau$  is calculated according to [4],

$$\tau = \frac{0.004903K_1 + 0.004419}{0.007548K_1 + 0.004242} \quad (5)$$

During the IPgC, the calibration constants shown in Table 4 were retrieved for the participating ACPs.

**Table 4. Calibration parameters for the ACPs obtained during the outdoor calibration cooling cycles.**

Date	Time	ACP10F3		ACP57F3		ACP95F3		ACP96F3	
		$K_1 \cdot 10^{-6}$	$\tau^*$	$K_1 \cdot 10^{-6}$	$\tau^*$	$K_1 \cdot 10^{-6}$	$\tau^*$	$K_1 \cdot 10^{-6}$	$\tau^*$
30/9/2021	20:18	0.07348	0.9964	0.06228	1.0026	0.06026	1.0037	0.07511	0.9955
	21:01	0.07152	0.9975	0.06060	1.0036	0.06435	1.0014	0.07511	0.9955
	23:20	0.06913	0.9988	0.06196	1.0028	0.06042	1.0037	0.07555	0.9953
1/10/2021	1:24	0.06492	1.0011	0.06031	1.0037	0.06410	1.0016	0.07264	0.9968
	3:37	0.06511	1.0010	0.05893	1.0045	0.06045	1.0036	0.07196	0.9972
2/10/2021	18:40	0.07186	0.9973	0.06728	0.9998	0.06512	1.0010	0.07691	0.9945
10/10/2021	3:16	0.07159	0.9974	0.06445	1.0013	0.06516	1.0010	0.05993	1.0417
14/10/2021	20:49	0.07930	0.9932	0.06343	1.0020	0.06548	1.0008	0.06677	1.0417
16/10/2021	3:22	0.07371	0.9962	0.06299	1.0022	0.06674	1.0001	0.07918	0.9933
	21:19	0.07435	0.9960	0.06452	1.0013	n/a	n/a	n/a	n/a
17/10/2021	1:00	0.07193	0.9972	0.06218	1.0027	n/a	n/a	n/a	n/a

\* The effective throughput  $\tau$  can have values above 100% since an error in  $\tau$  is a result of a compromised  $K_1$  (see equation 5) (personal communication I. Reda).

### 6.3 Results

The following figures show the downwelling longwave irradiance in  $W m^{-2}$  of the IRIS, ACP, and WISG pygeometers in the upper figures and the corresponding residuals versus the IRIS average in the lower figures.

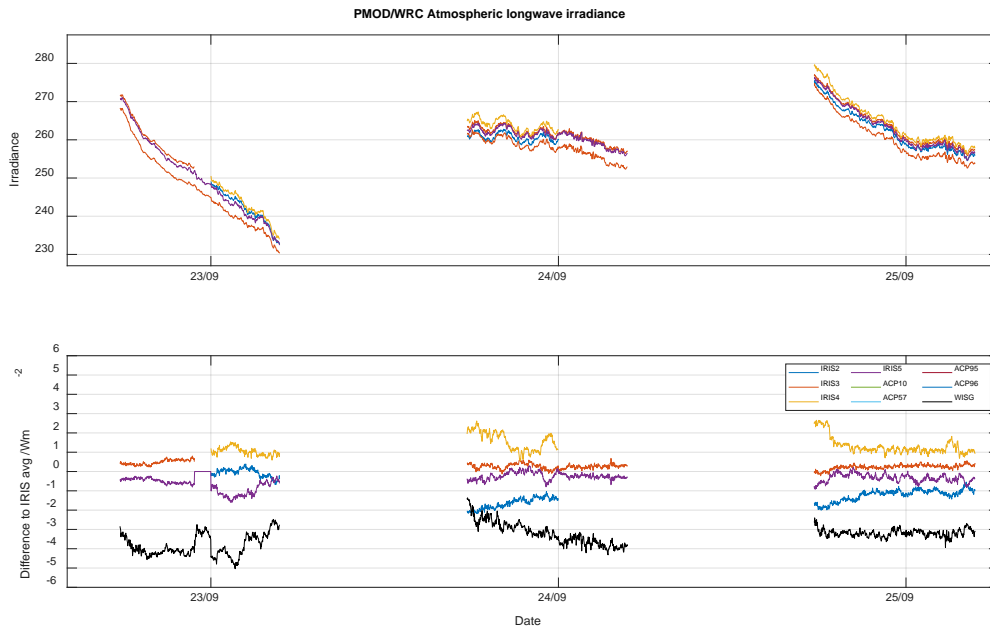


Figure 7. Top: Longwave irradiance measurements for the nights of 22 to 25 September when only the IRIS and the WISG (black) were present. Bottom: Difference to average of IRIS.

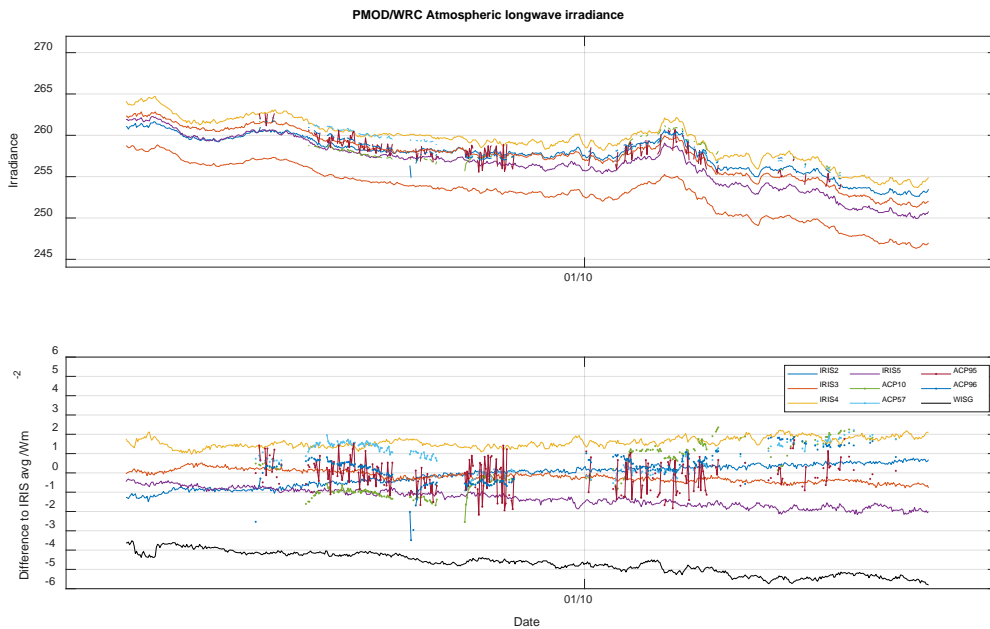
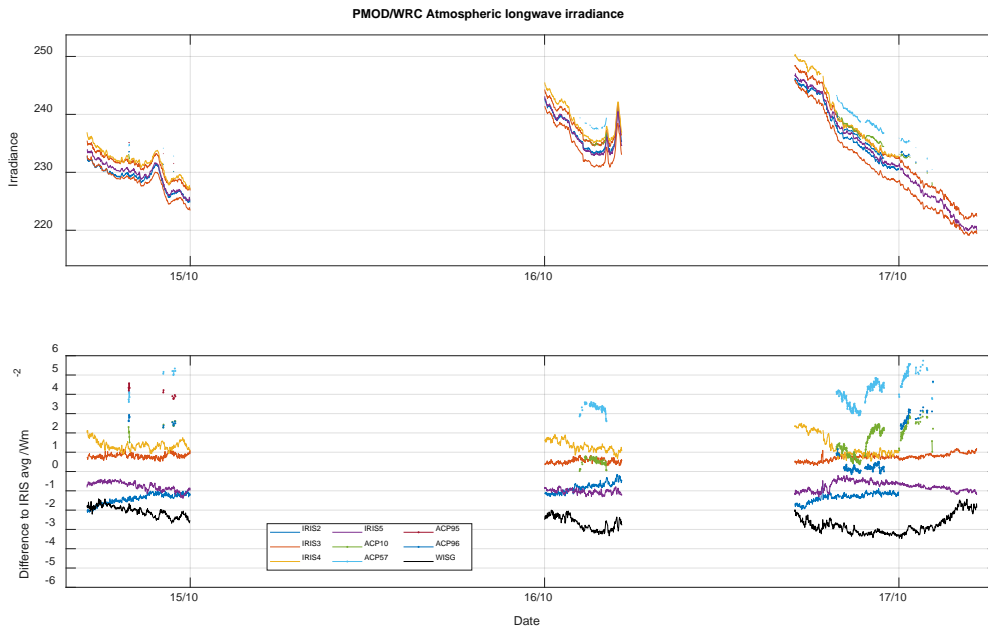


Figure 8. Top: Longwave irradiance measurements for the night of 30 September to 1 October with IRIS, ACP and the WISG. Bottom: Difference to average of IRIS.



**Figure 9. Top: Longwave irradiance measurements for the nights of 14 to 17 October with IRIS, ACP and the WISG. Bottom: Difference to average of IRIS.**

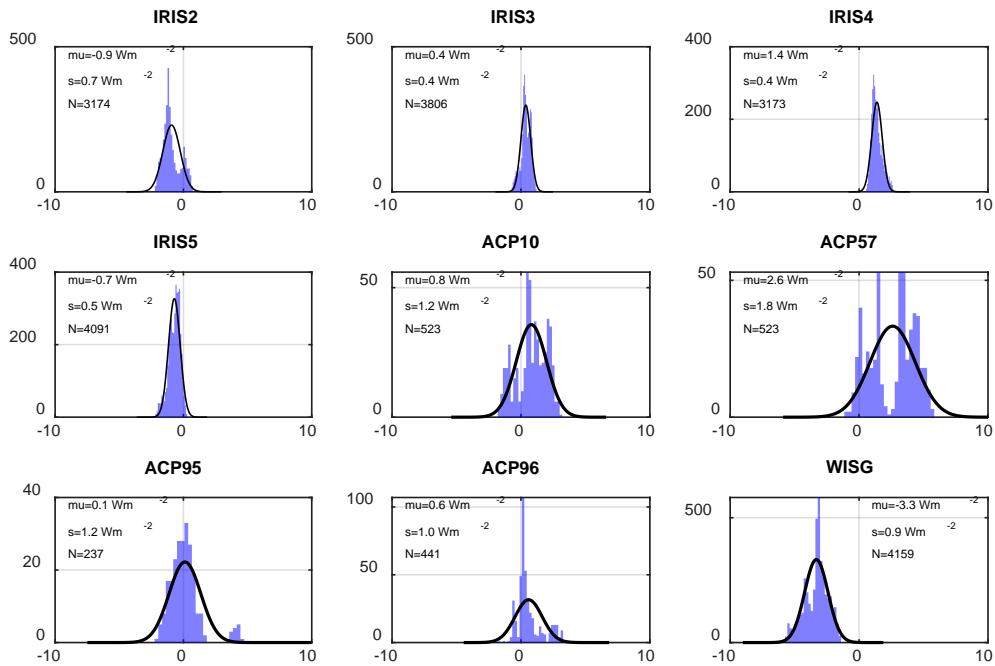


Figure 10. Histogram of the residuals between the radiometers and the average of the IRIS for the selected days shown in the previous figures.

As can be seen in Figure 10 and Table 5 below, the IRIS and ACP radiometers agree well with each other, with average differences between  $-0.9 \text{ W m}^{-2}$  and  $+1.4 \text{ W m}^{-2}$ , with only ACP57 showing a slightly larger average difference of  $2.6 \text{ W m}^{-2}$ . The WISG pyrgeometers measure significantly lower irradiances during the IPgC-III, with an average difference to the IRIS of  $-3.3 \text{ W m}^{-2}$  over the whole period.

Table 5. Statistics of the differences of each radiometer to the IRIS average, as shown in Figure 10.

Instrument	Average / $\text{W m}^{-2}$	Standard dev. / $\text{W m}^{-2}$	Number of points
IRIS2	-0.9	0.7	3174
IRIS3	0.4	0.4	3806
IRIS4	1.4	0.4	3173
IRIS5	-0.7	0.5	4091
ACP10	0.8	1.2	523
ACP57	2.6	1.8	523
ACP95	0.1	1.2	237
ACP96	0.6	1.0	441
WISG	-3.3	0.9	4159



## 7 New WISG coefficients

According to the governance framework for the World Infrared Standard Group (WISG), an advisory group of experts in atmospheric longwave radiation measurements was appointed by the president of INFCOM as per Resolution 1 of CIMO-17 and its annex [5]. The tasks of the advisory group (in the following called Ad-Hoc Committee), are, but not limited to:

- To review the status and stability of the WISG, and evaluate its role as operational reference standard for providing a stable longwave reference, based on the analysis provided by PMOD/WRC;
- To recommend the updating of the calibration factors and changes to the WISG, if necessary;
- To ensure the supervision of the International Pyrgeometer Comparison, scheduled to take place every five years in conjunction with the International Pyrheliometer Comparison;
- To review progress in and provide advice on maintaining and improving traceability to the SI through the International Pyrgeometer Comparison;
- To report their findings and recommendations to the CIMO Management Group.

The WISG pyrgeometers have been characterised annually or in some cases more often in the blackbodies of PMOD/WRC since 2005. Between 2005 and 2007 the characterisations were performed in the blackbody BB1995 [6] and since 2008 in BB2007 [2].

The results of these characterisations are shown in Figures 11 to 14 for WISG1 to WISG4 (note the difference in scales in the figures between pyrgeometers).

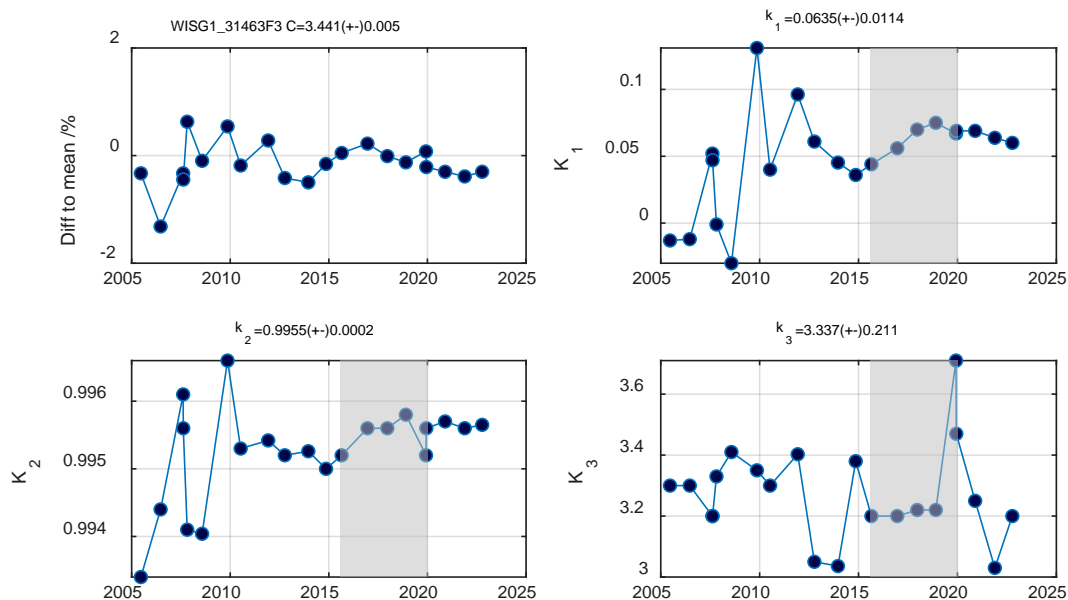


**Figure 11. Characterisation of WISG1, Eppley PIR 31463F3, in the blackbody cavity BB2007, between 2005 and 2021 for responsivity (upper left figure),  $k_1$  (upper right),  $k_2$  (lower left), and  $k_3$  (lower right). The shaded area represents the period between IPgC-II and IPgC-III which was used for the redefinition of the WISG coefficients. The average and standard deviation are shown in the titles of each sub-figure.**

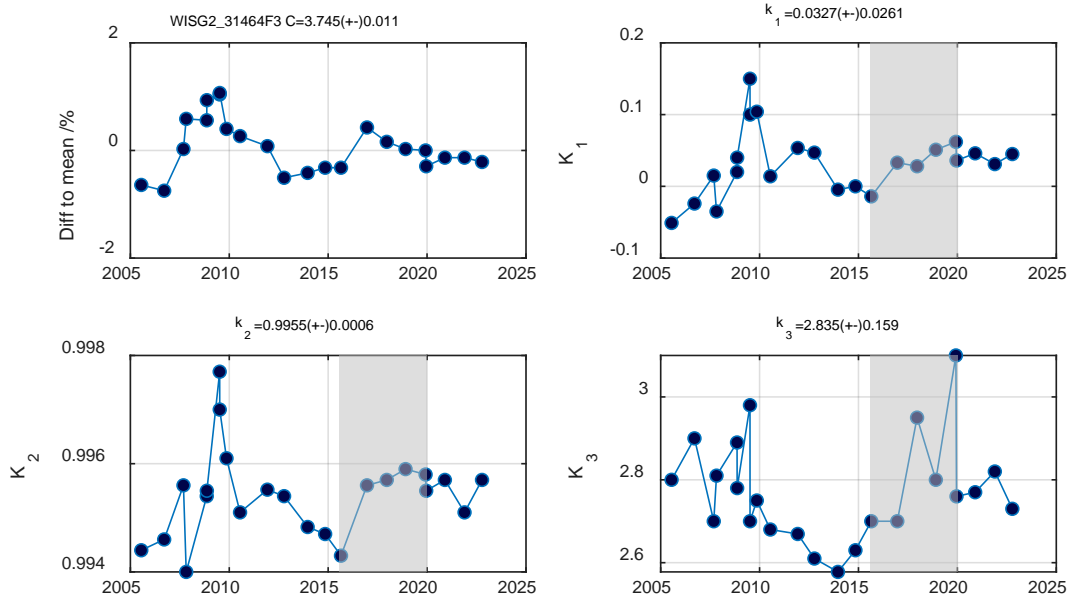


Figure 12. Characterisation of WISG2, Eppley PIR 31464F3, in the blackbody cavity BB2007, between 2005 and 2021 for responsivity (upper left figure),  $k_1$  (upper right),  $k_2$  (lower left), and  $k_3$  (lower right). The shaded area represents the period between IPgC-II and IPgC-III which was used for the redefinition of the WISG coefficients. The average and standard deviation are shown in the titles of each sub-figure.

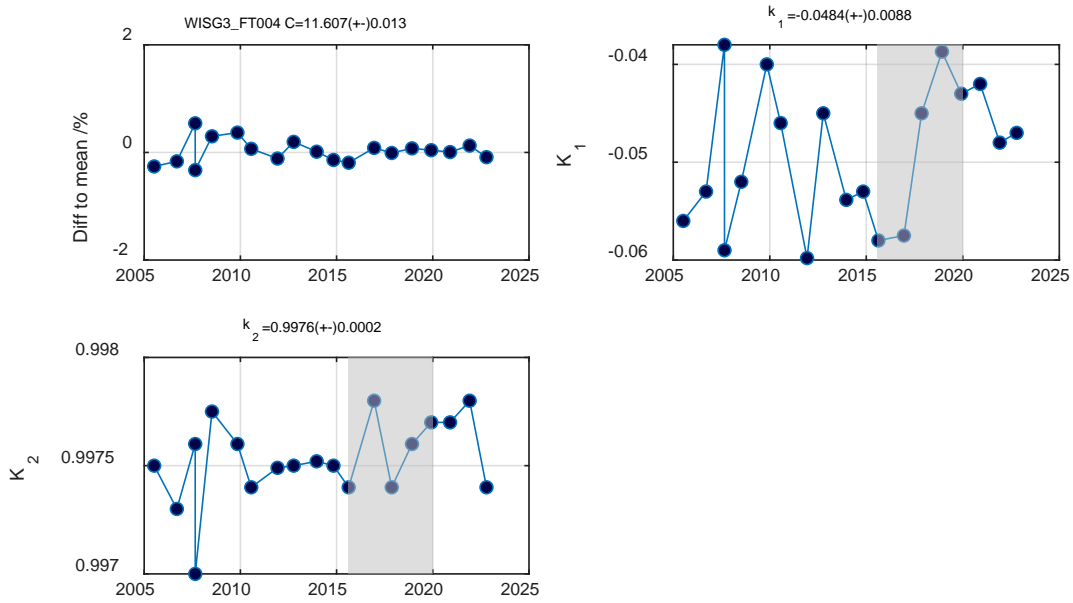
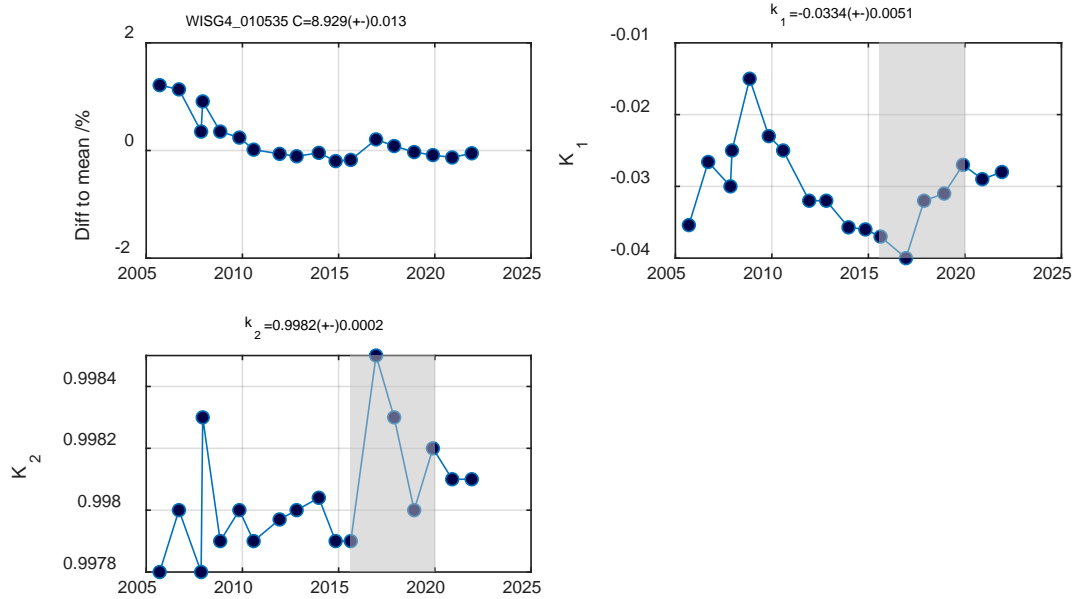


Figure 13. Characterisation of WISG3, Kipp&Zonen FT004, in the blackbody cavity BB2007, between 2005 and 2021 for responsivity (upper left figure),  $k_1$  (upper right), and  $k_2$  (lower left). The shaded area represents the period between IPgC-II and IPgC-III which was used for the redefinition of the WISG coefficients. The average and standard deviation are shown in the titles of each sub-figure.



**Figure 14. Characterisation of WISG4, Kipp&Zonen 010535, in the blackbody cavity BB2007, between 2005 and 2021 for responsivity (upper left figure),  $k_1$  (upper right), and  $k_2$  (lower left). The shaded area represents the period between IPgC-II and IPgC-III which was used for the redefinition of the WISG coefficients. The average and standard deviation are shown in the titles of each sub-figure.**

The coefficients  $k_1$ ,  $k_2$ , and  $k_3$  for each WISG pyrheliometer were determined from the average of the blackbody calibrations performed between the IPgC-II and the IPgC-III, e.g. from September 2015 to December 2019. Note that the IPgC-III was postponed from its nominal date planned for 2020 to 2021 due to the COVID pandemic.

The updated WISG responsivities for each WISG pyrheliometer were then calculated for the period starting in January 2016 to December 2019 by using these updated coefficients  $k_1$ ,  $k_2$ , and  $k_3$  of each WISG pyrheliometer with respect to the three remaining WISG pyrheliometers using their original coefficients. The same calibration procedure as described in [1] was applied. Choosing different periods have no appreciable impact on the results; note that it is important to select a period covering several years in order to sample a representative set of calibration conditions typically between April and October. Table 6 summarises the original and new WISG coefficients retrieved by this procedure.

**Table 6. Original and new WISG coefficients in operational use as per 1 January 2022.**

Instrument	New coefficients				Original coefficients			
	$C/\mu V/(W m^{-2})$	$k_1$	$k_2$	$k_3$	$C/\mu V/(W m^{-2})$	$k_1$	$k_2$	$k_3$
WISG1	3.864	0.064	0.9955	3.3	3.534	0	0.9943	3.27
WISG2	3.969	0.033	0.9955	2.8	3.585	-0.511	0.9945	2.84
WISG3	12.125	-0.048	0.9976	0	12.32	-0.041	0.9970	0
WISG4	9.429	-0.033	0.9982	0	9.590	-0.034	0.9980	0

The internal consistency of the WISG has improved with the new coefficients, in particular during the calibration season between approximately April and October, while the overall irradiance level of the WISG is maintained throughout the year. Table 7 shows the offset of each WISG pyrheliometer to their mean using the original and updated WISG coefficients (see Table 6).

**Table 7. Differences of the WISG pyrgeometers to their average using the original and updated coefficients. The last row shows the standard deviation of the WISG average.**

Instrument	Difference to [...] in $W m^{-2}$	
	WISG (original)	WISG <sub>2022</sub>
WISG1	-0.46	0.41
WISG2	-0.07	-0.13
WISG3	0.05	-0.30
WISG4	0.44	0.03
Std (WISG)	0.37	0.30

As per the self-consistency of the applied procedure, the irradiance of the average of the WISG instruments during the period from January 2016 to December 2020 does not change when using the original or the new WISG coefficients, as shown in Figure 15, with an average difference of  $0.0 W m^{-2}$  and a standard deviation of  $0.15 W m^{-2}$ .

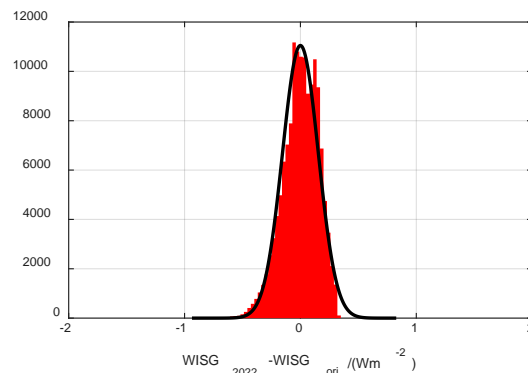


**Figure 15. Irradiance difference between the average of the WISG pyrgeometers using the original and updated coefficients from Table 6 for the period January 2016 to December 2020.**

Furthermore, the updated WISG coefficients also improve the consistency of the WISG during daytime as shown in Figure 16.

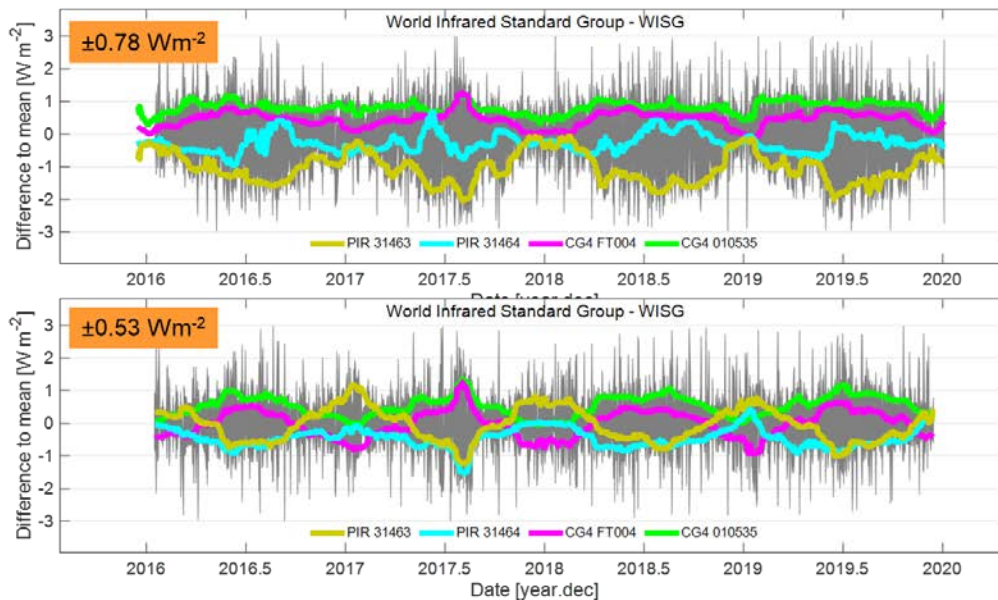


**Figure 16. Differences of the WISG pyrgeometers to their mean using the original (upper figure) and the updated 2022 coefficients (lower figure). The values shown in the respective upper left corner represent the standard deviation of the mean.**

As a final verification, the IPgC-III participating pyrgeometers were also calibrated with respect to the new WISG coefficients, yielding relative differences in the retrieved responsivities of typically less than 0.4% as shown in Table 8. Note that the corresponding change in downwelling longwave irradiance will

be significantly less than these changes since the responsivity only affects the net radiation component (see equation 1).

**Table 8. Pyrgometer responsivities retrieved with the original and updated (new) WISG coefficients. The last column shows the relative difference between the responsivities.**

Nb	Pyrgometer	$k_1$	$k_2$	$k_3$	C_WISG in $\mu\text{V}/(\text{W m}^{-2})$		$(C_{\text{new}} - C_{\text{ori}}) / C_{\text{ori}}$ in %
					Original ( $C_{\text{ori}}$ )	New ( $C_{\text{new}}$ )	
1	PIR 31463F3	0.069	0.9957	3.2	3.885	3.867	-0.46
2	PIR 31464F3	0.046	0.9957	2.8	4.026	4.031	0.12
3	CG4_FT004	-0.042	0.9977	0	12.23	12.27	0.33
4	CG4_010535	-0.029	0.9981	0	9.460	9.479	0.20
5	CG4_FT006	0.072	1.0003	0	11.62	11.62	0.00
6	IR20_105	-0.029	1.0009	0	15.08	15.08	0.00
7	CGR4_110390	0.000	0.9993	0	8.398	8.405	0.08
8	CG4_FT005	0.049	0.9983	0	9.673	9.674	0.01
9	CG4_060893	-0.010	0.9979	0	7.435	7.439	0.05
10	CGR4_140081	-0.010	0.9980	0	9.405	9.418	0.14
11	CG4_050792	0.053	0.9991	0	8.783	8.791	0.09
12	CGR4_110348	0.040	0.9978	0	11.55	11.56	0.09
13	CG4_060881	0.016	0.9979	0	8.215	8.218	0.04
14	CG4_050783	0.020	0.9974	0	9.619	9.627	0.08
15	PIR_32227F3	-0.046	0.9956	2.5	3.833	3.833	0.00
16	CGR4_130621	-0.0231	0.9986	0	11.39	11.39	0.00
17	CG4_080066	0.060	0.9990	0	14.29	14.30	0.07
18	MS-21_REF002	-0.010	1.0003	0	18.84	18.88	0.21
19	CGR4_110378	0.031	0.9992	0	11.27	11.28	0.09
20	CG4_010567	0.027	0.9974	0	12.50	12.54	0.32
21	MS-20 S19068.06	0.033	0.9905	0	24.26	24.28	0.08
22	CG4_030665	0.043	0.9994	0	11.30	11.31	0.09
23	IR20-T2_4019	-0.140	0.9995	0	7.093	7.106	0.18
24	CGR4_160201	0.000	0.9987	0	9.661	9.673	0.12
25	CGR4_140016	0.000	0.9994	0	10.94	10.96	0.18
26	CGR4_130648	0.010	0.9993	0	10.99	11.00	0.09
27	CGR4_070042	0.003	1.0011	0	11.01	11.02	0.09
28	CGR3_110460	0.104	1.0004	0	15.43	15.45	0.13
29	CG4_010536	0.026	0.9976	0	9.230	9.231	0.01
30	EMPIR_01	0.0349	0.9979	0	9.973	9.993	0.20
31	EMPIR_02	0.053	0.9980	0	10.66	10.69	0.28
32	CGR4_100210	0.010	0.9989	0	10.25	10.26	0.10
33	CG4_060869	0.046	0.9996	0	9.053	9.086	0.36
34	CGR4_170224	-0.011	0.9992	0	12.49	12.49	0.00
35	CG1_970115	0.030	0.9993	0	12.48	12.48	0.00
36	PIR_38864F3	0.126	0.9936	8.4	3.367	3.371	0.12
37	IR20-T2_4041	-0.135	0.9980	0	8.437	8.424	-0.15
38	IR30-A1-T2_101	-0.124	0.9981	0	8.370	8.404	0.41
39	IR30-A1-T2_102	-0.0164	0.9984	0	7.644	7.673	0.38
40	IR30-A1-T2-WS_100	-0.106	0.9986	0	7.585	7.614	0.38

The Ad-Hoc Committee established for the IPgC-III recommended to INFCOM (formerly CIMO) to approve the update of the WISG coefficients, based on the evidence presented during the IPgC-III that the WISG coefficients  $k_1$ ,  $k_2$ , and  $k_3$  in operational use since its inception have changed, based on the characterisation performed annually in the PMOD BB2007 blackbody.

The new WISG coefficients have been used operationally by PMOD/WRC since 1 January 2022.

## 8 Conclusion

- 1) The WISG has been measuring continuously since 2004. Between 2004 and 2021, the four pyrgeometers comprising the WISG show an internal consistency of  $1 \text{ W m}^{-2}$ , demonstrating that the WISG can be used as a stable reference for long-term atmospheric longwave irradiance measurements.
- 2) As shown in this IPgC-III, pyrgeometers can be calibrated relative to an outdoor reference like the WISG with an expanded uncertainty ( $k=2$ ) of less than  $1 \text{ W m}^{-2}$ . The reported expanded uncertainty of measurement is stated as the standard uncertainty of measurement multiplied by the coverage factor  $k = 2$ , which for a normal distribution corresponds to a coverage probability of approximately 95%.
- 3) The solar influence on unshaded pyrgeometers is correlated to the incoming direct solar irradiance and can be as high as  $19 \text{ W m}^{-2}$  for  $1000 \text{ W}$  horizontal direct solar irradiance (see Figure 6 and the corresponding figures for each unshaded pyrgeometer in the Annex).
- 4) Atmospheric longwave irradiance measurements from different pyrgeometers based on a blackbody calibration (even if it is the same cavity) can give discrepancies of up to  $16 \text{ W m}^{-2}$ .
- 5) Atmospheric longwave irradiance measurements of the IRIS and ACP absolute radiometers give consistent results to within  $1.4 \text{ W m}^{-2}$  (discarding ACP57 which behaved erratically for yet unknown reasons, personal communication I. Reda), which is well within their stated uncertainties. The average difference between WISG and the IRIS mean is  $3.3 \text{ W m}^{-2}$  during cloud free nights at the IPgC-III, with WISG measuring lower irradiances. These results are consistent with previous findings as published in [7].

## Acknowledgments

We would like to thank the Ad-Hoc Committee of the IPgC-III, Stefan Wacker, Nozomu Ohkawara, Shun Sasaki, Bruce Forgan, Wael Khaled, Michael Milner, Edgardo Sepúlveda, Adriana Elizabeth Gonzalez, Ibrahim Reda, Tom Kirk, and Thomas Carlund for their helpful comments to a previous version of this report.

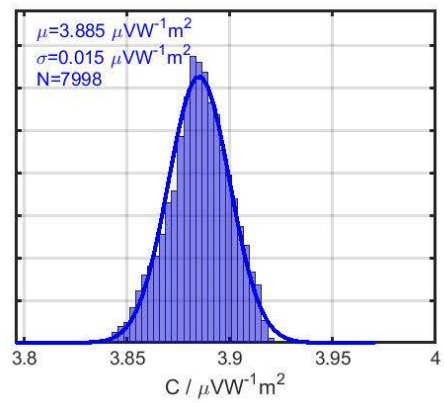
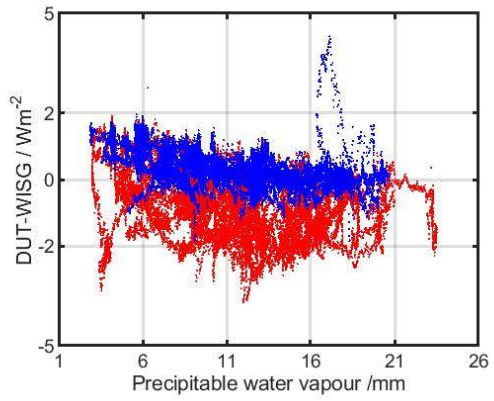
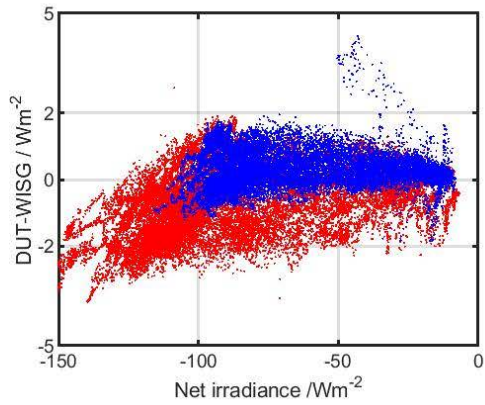
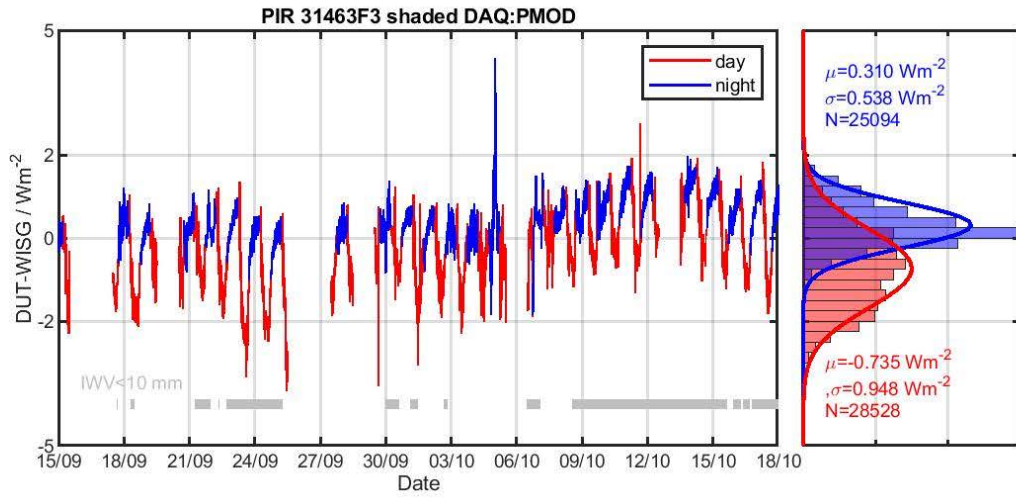
## References

- [1] Gröbner, J., and S. Wacker, 2015: Pyrgeometer calibration procedure at the PMOD/WRC-IRS, IOM Report No. 120, WMO. [https://library.wmo.int/doc\\_num.php?explnum\\_id=7365](https://library.wmo.int/doc_num.php?explnum_id=7365)
- [2] Gröbner, J., 2008: Operation and Investigation of a tilted bottom cavity for pyrgeometer characterizations, Applied Optics, 47, 4441-4447.
- [3] Gröbner, J., 2012: A Transfer Standard Radiometer for atmospheric longwave irradiance measurements, Metrologia, 49, S105-S111.
- [4] Reda, I., J. Zeng, J. Scheuch, L. Hanssen, B. Wilthan, D. Myers, and T. Stoffel, 2012: An absolute cavity pyrgeometer to measure the absolute outdoor longwave irradiance with traceability to International System of Units, SI, J. Atmos. Sol. Terr. Phys., 77, 132–143, doi:10.1016/j.jastp.2011.12.011.
- [5], WMO, Commission for Instruments and methods of Observation, Abridged Final Report of the Seventeenth Session, Amsterdam, 12-16 October 2018, [https://library.wmo.int/doc\\_num.php?explnum\\_id=5683](https://library.wmo.int/doc_num.php?explnum_id=5683)
- [6] Philipona, R., C. Fröhlich, and Ch. Betz, 1995: "Characterization of pyrgeometers and the accuracy of atmospheric long-wave radiation measurements," Appl. Opt. 34, 1598–1605.
- [7] Gröbner, J., I. Reda, S. Wacker, S. Nyeki, K. Behrens, and J. Gorman, 2014: A new absolute reference for atmospheric longwave irradiance measurements with traceability to SI units, J. Geophys. Res. Atmos., 119, doi:10.1002/2014JD021630.

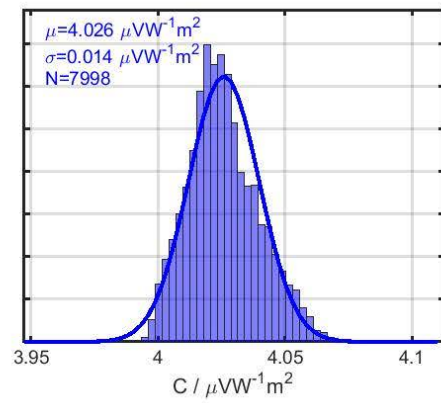
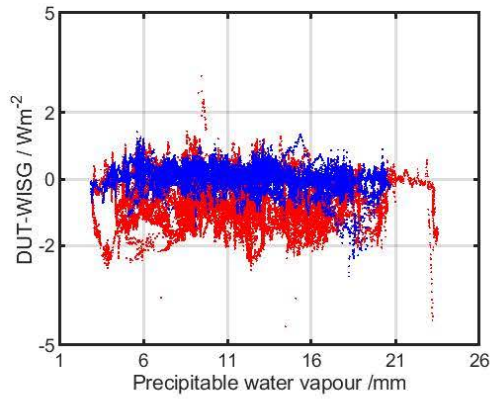
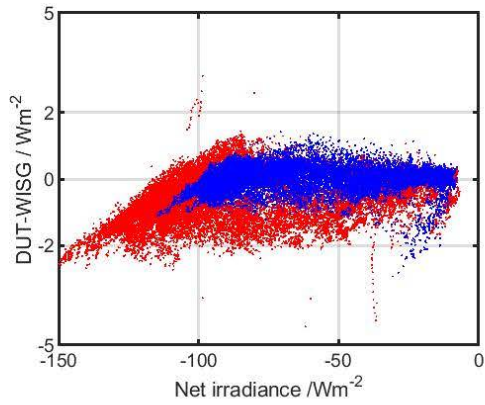
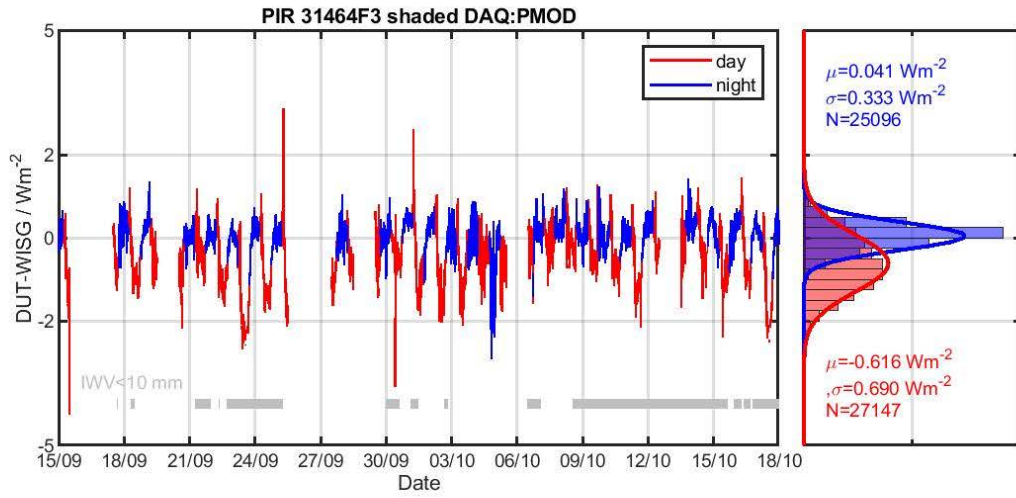
## **9 Annex**

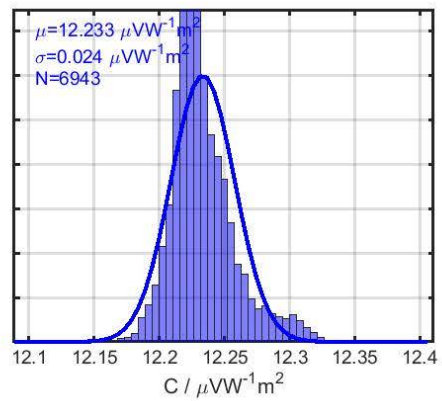
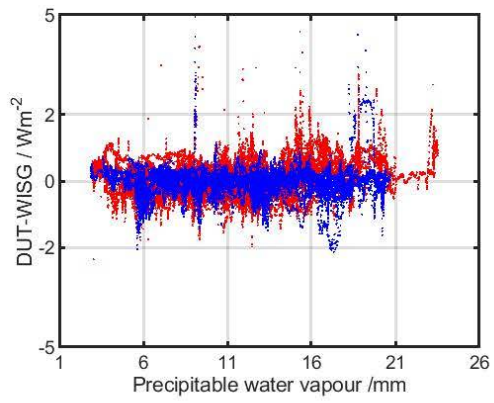
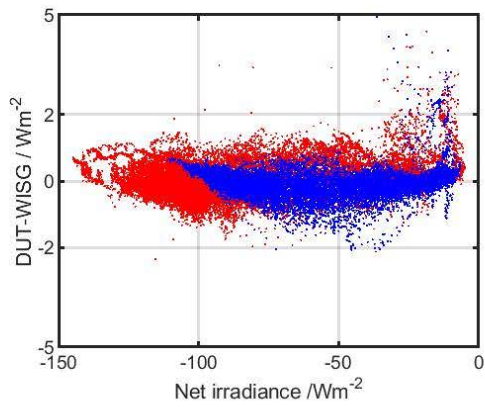
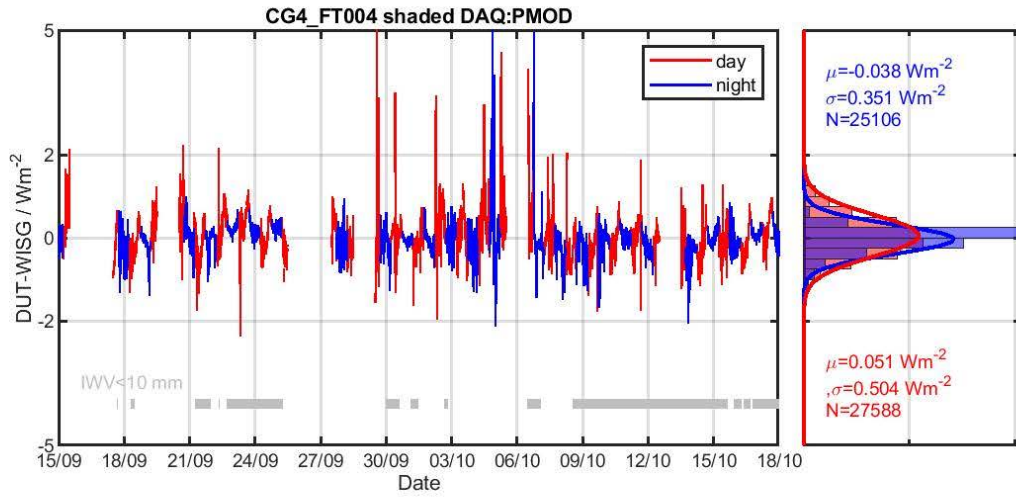
Measurement results for individual pyrgeometers, following the Table 2 listing order.

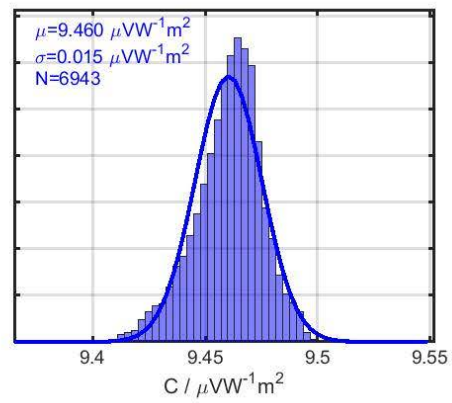
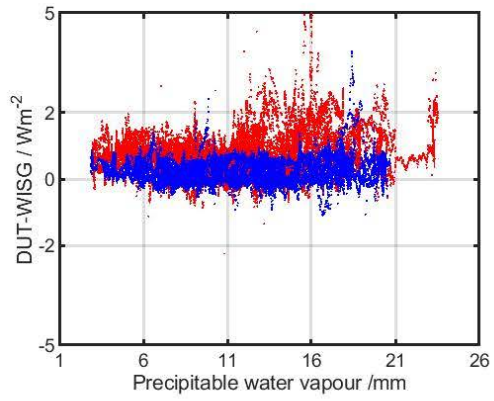
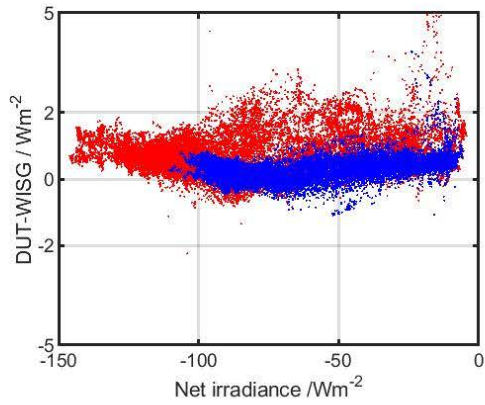
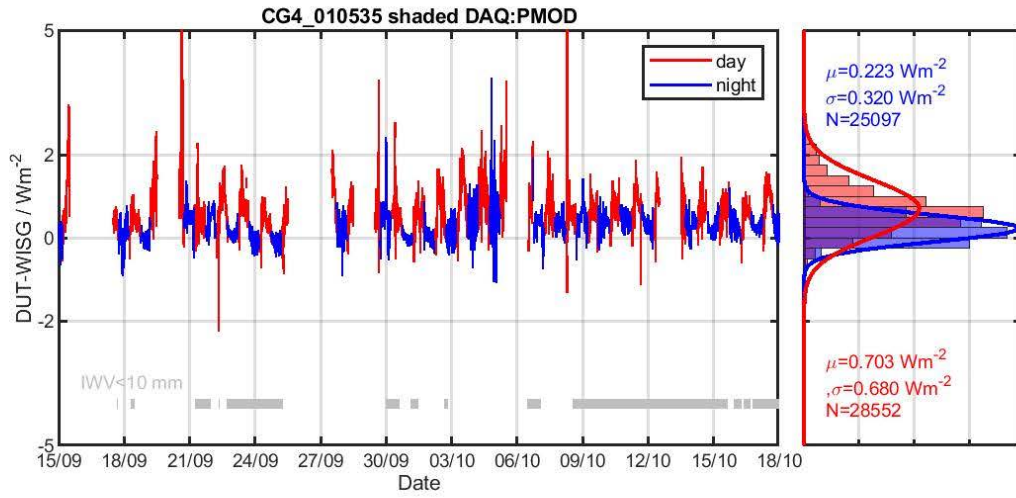
DUT – Device under Test

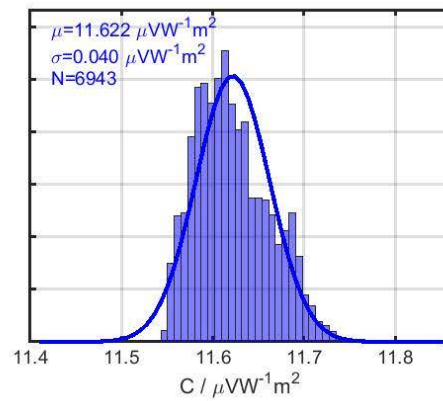
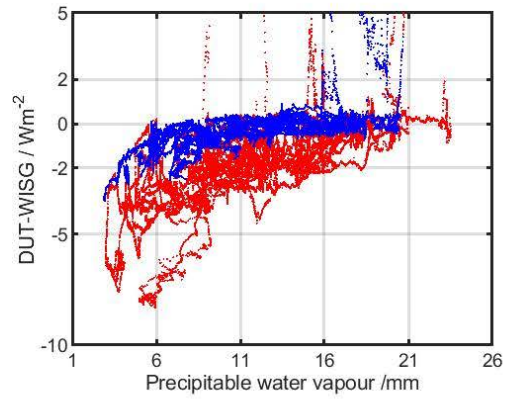
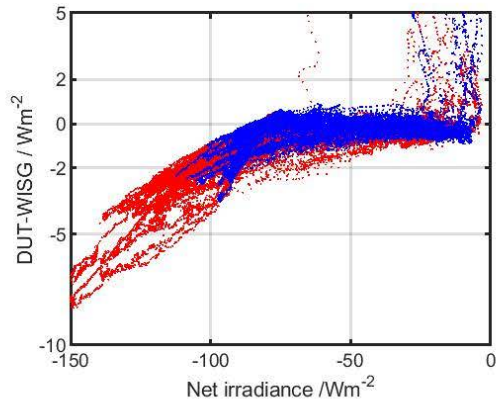
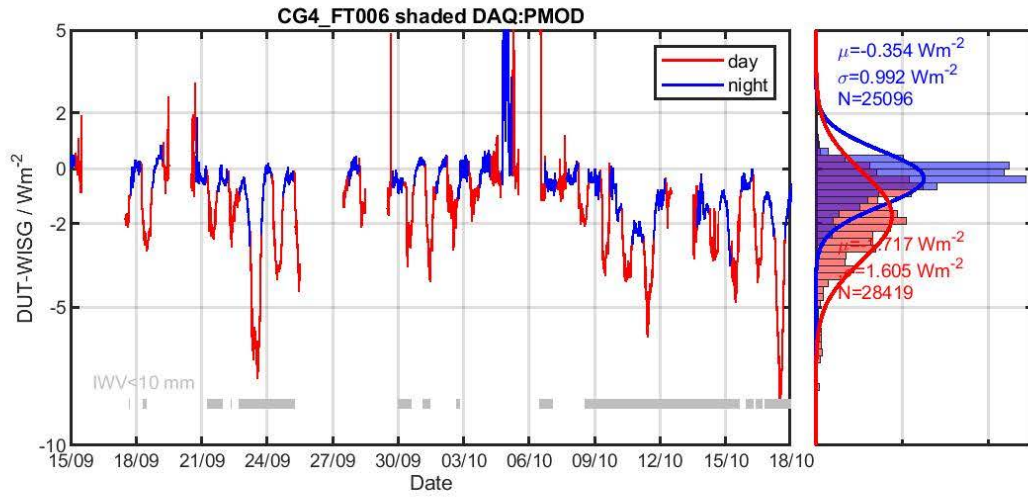


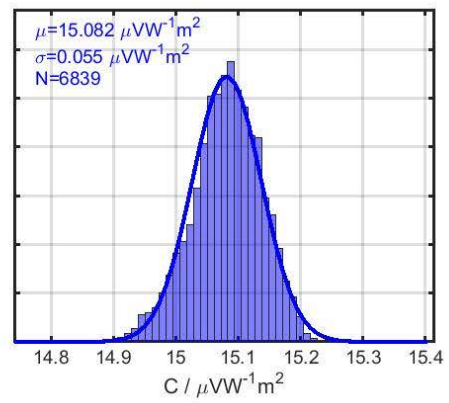
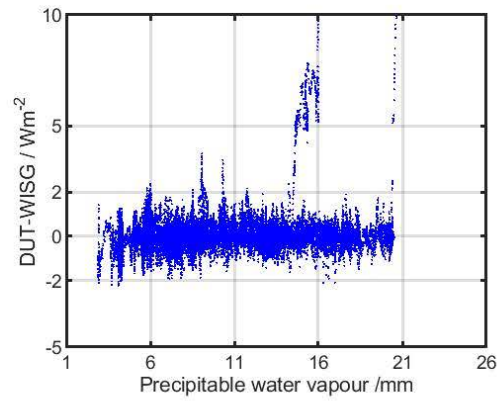
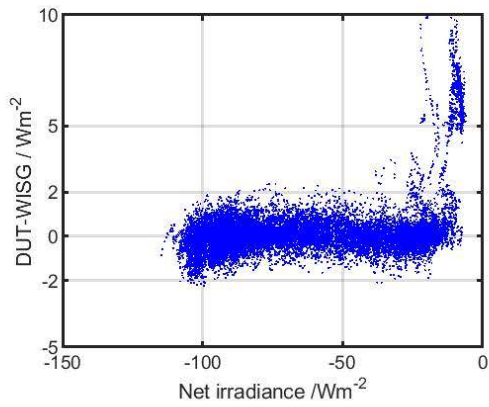
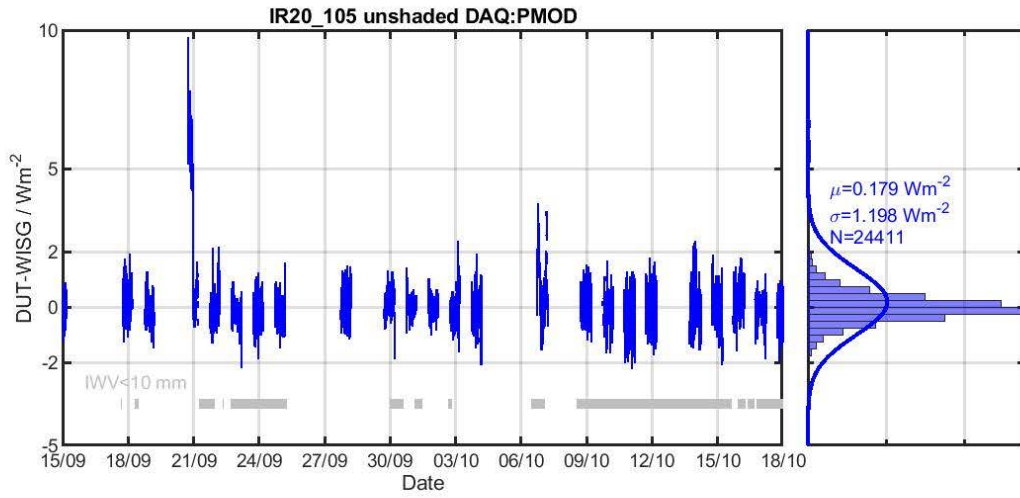


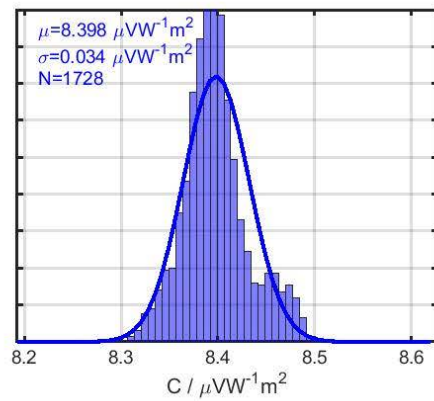
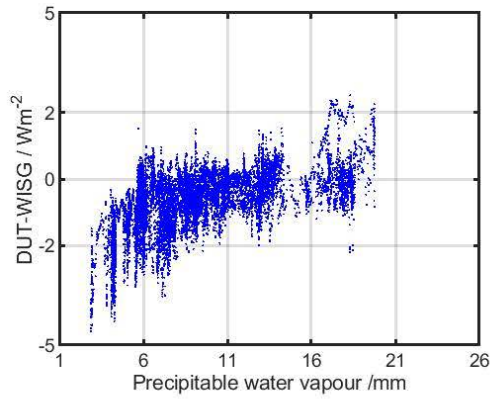
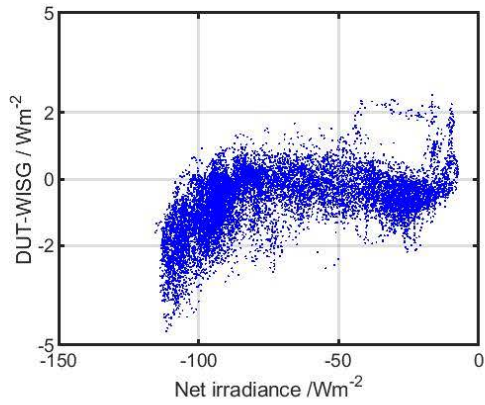
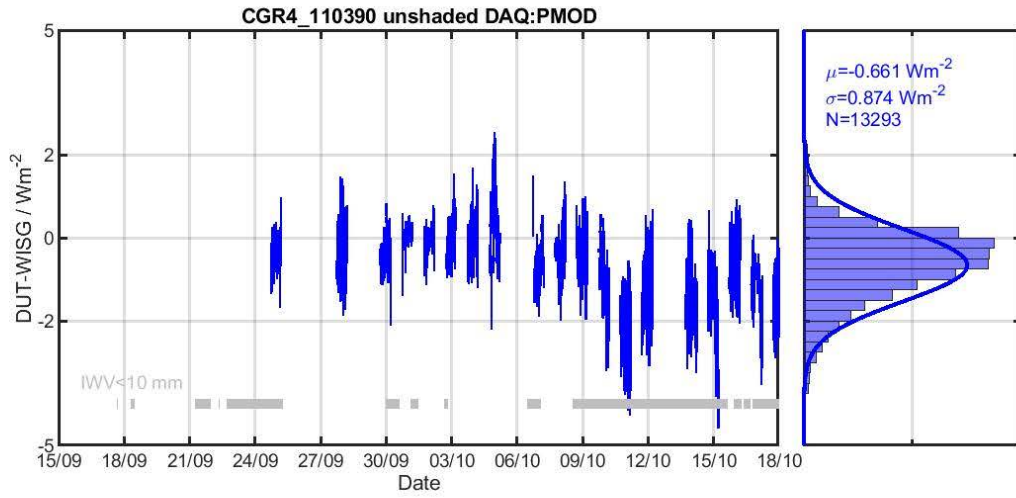


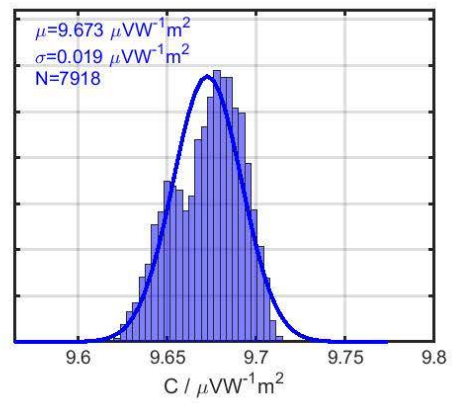
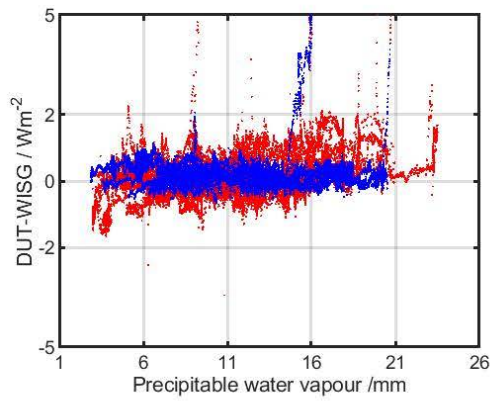
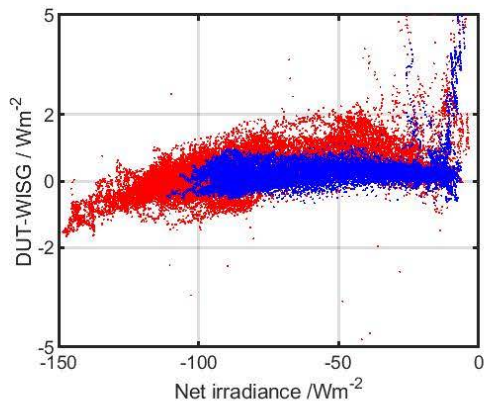
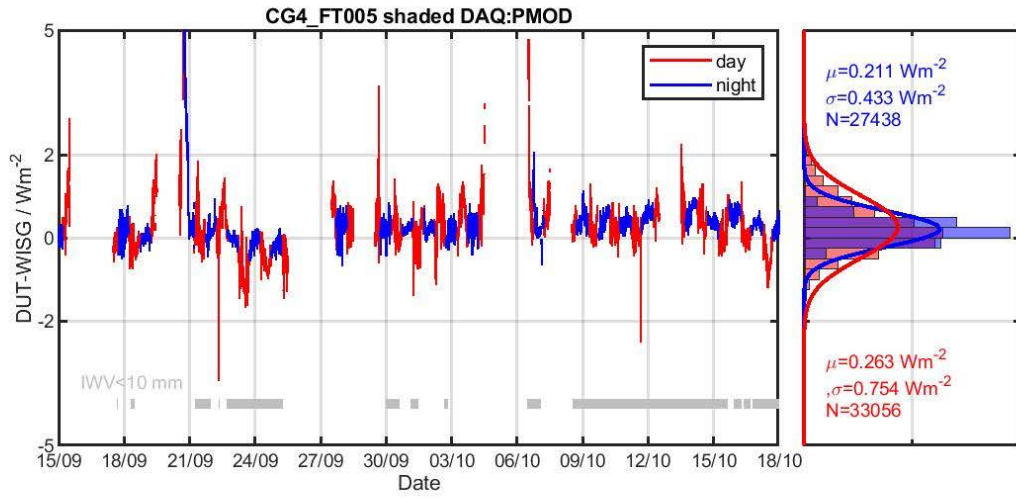


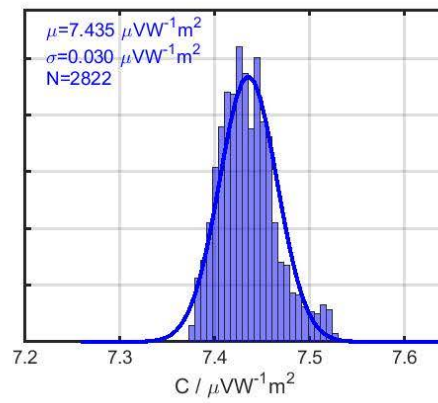
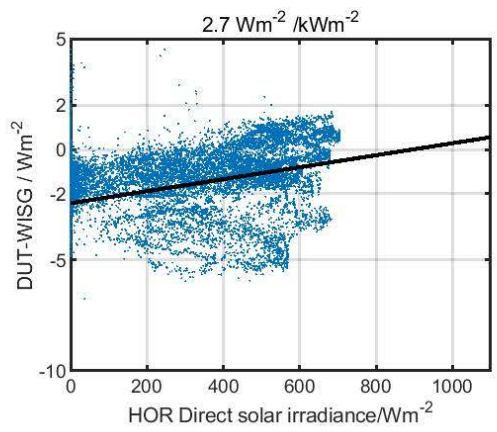
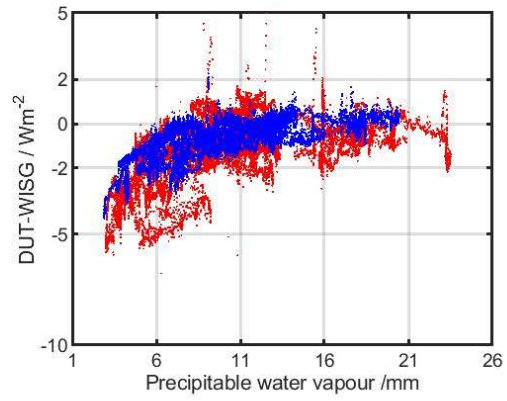
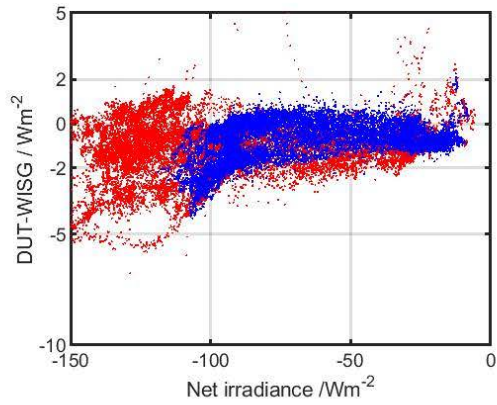
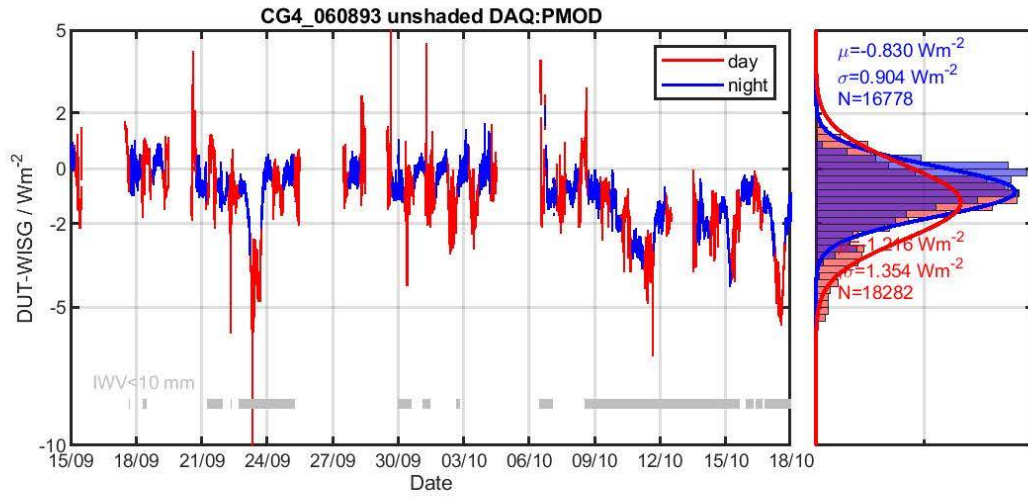




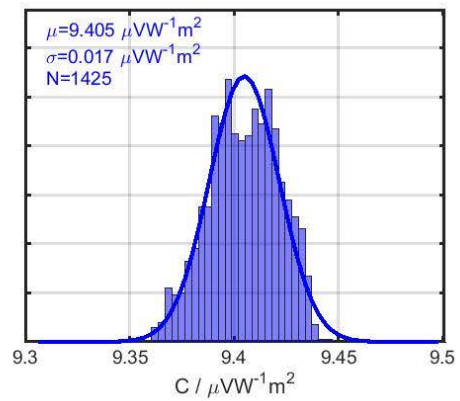
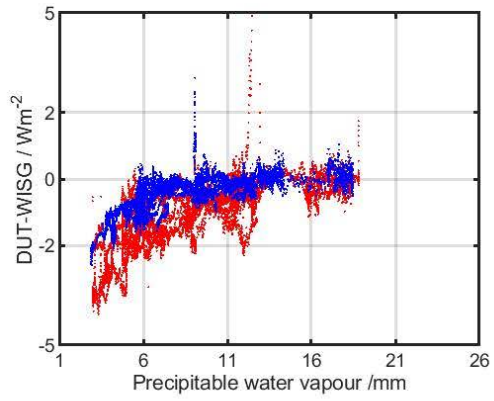
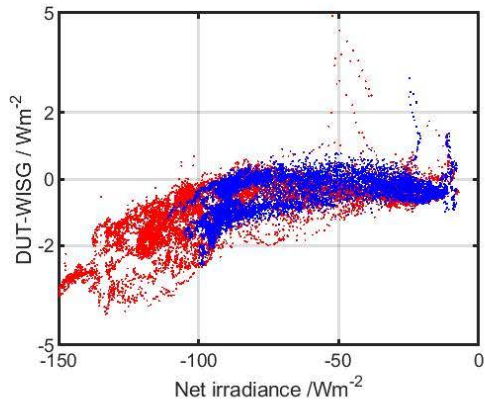
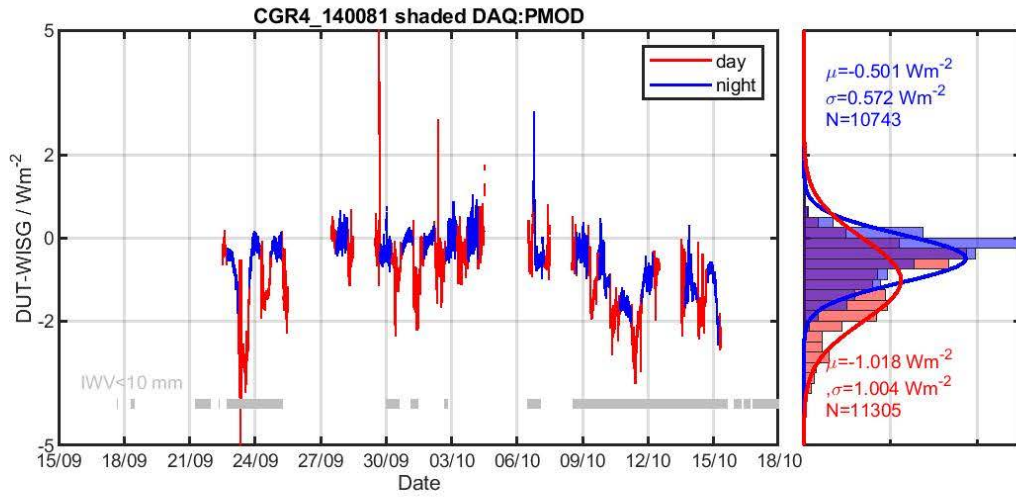


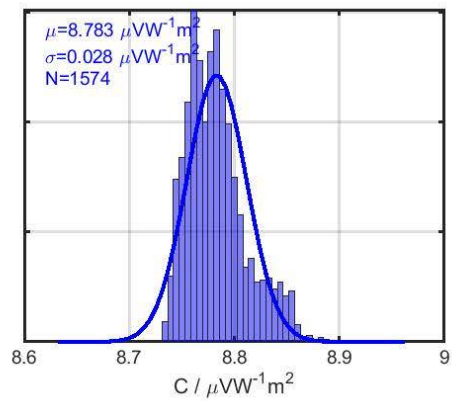
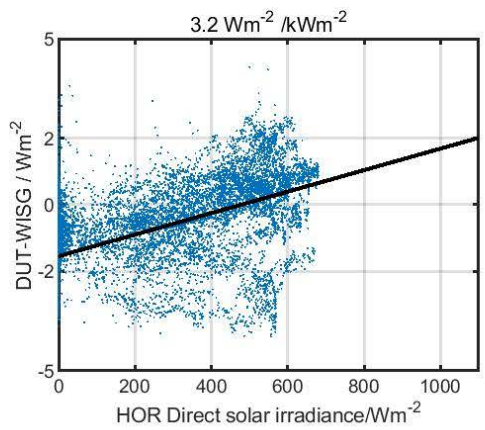
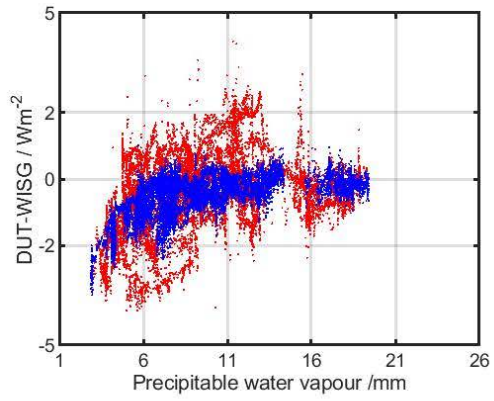
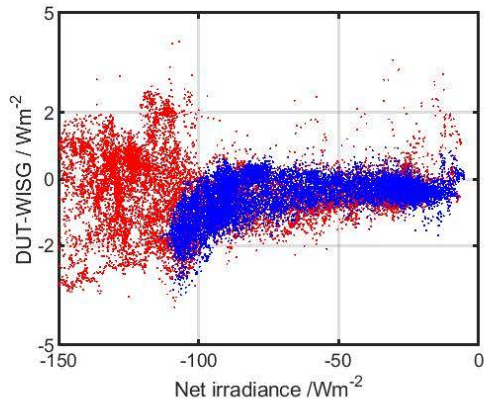
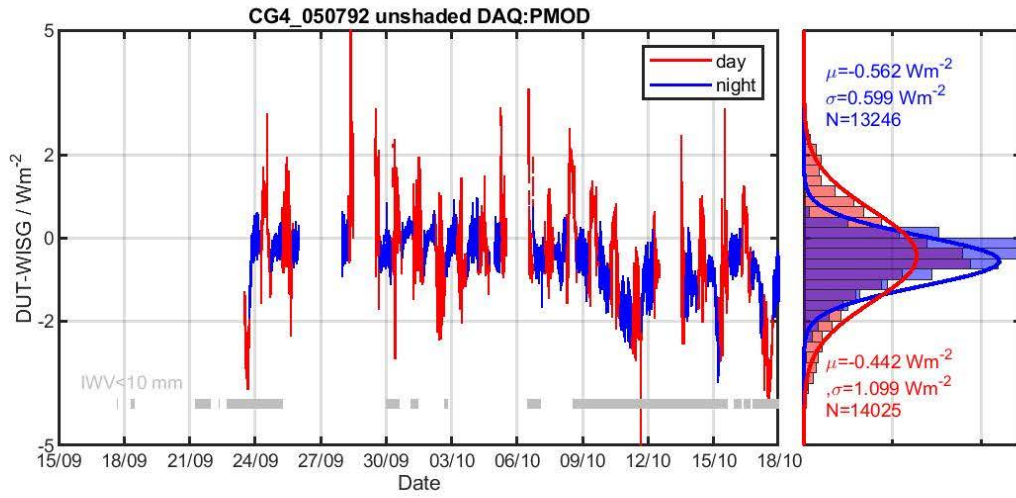


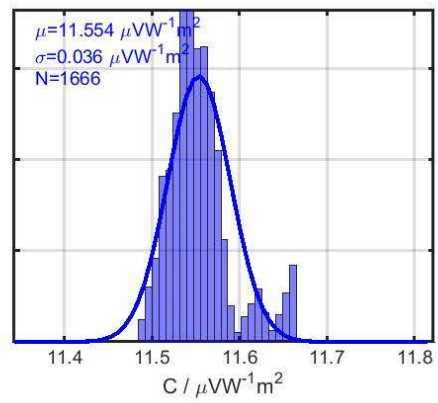
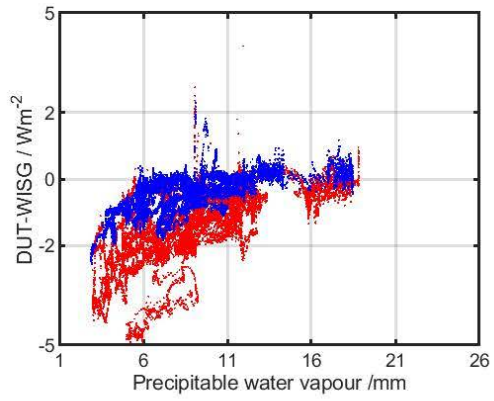
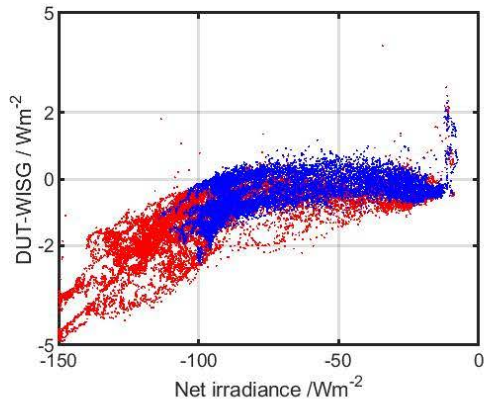
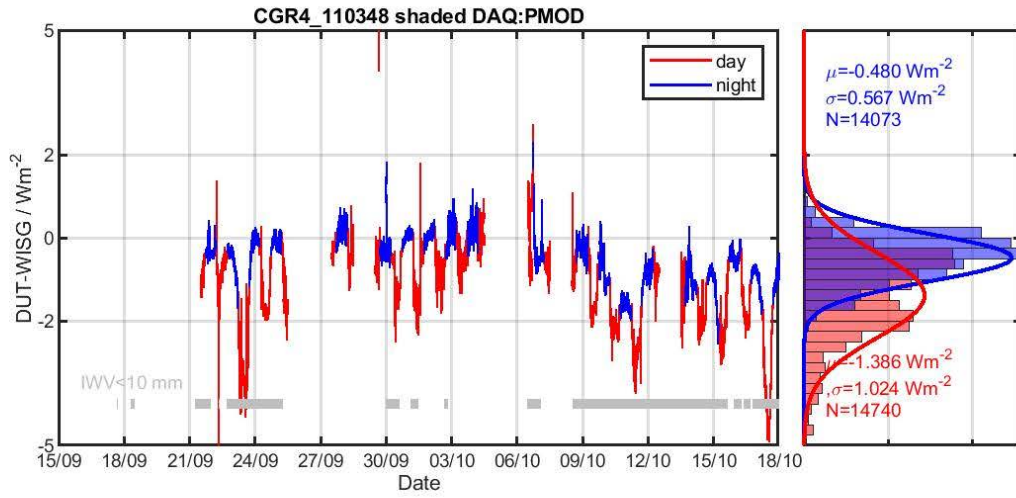


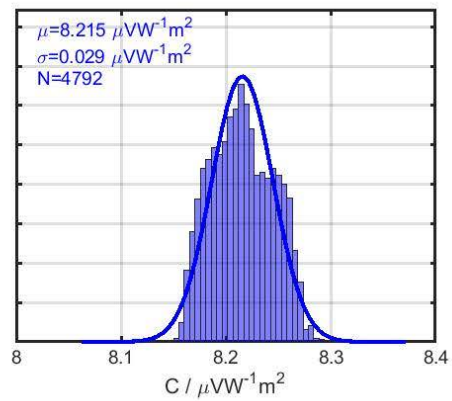
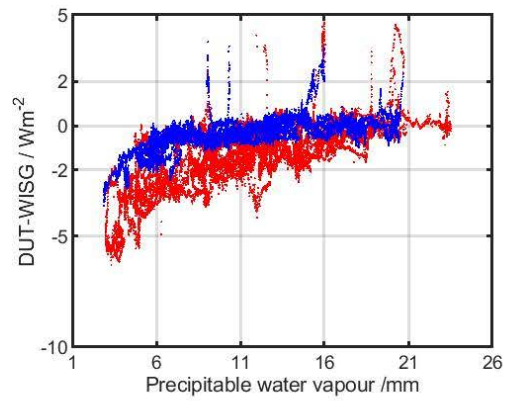
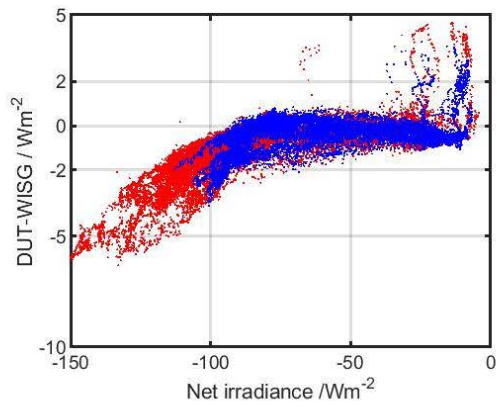
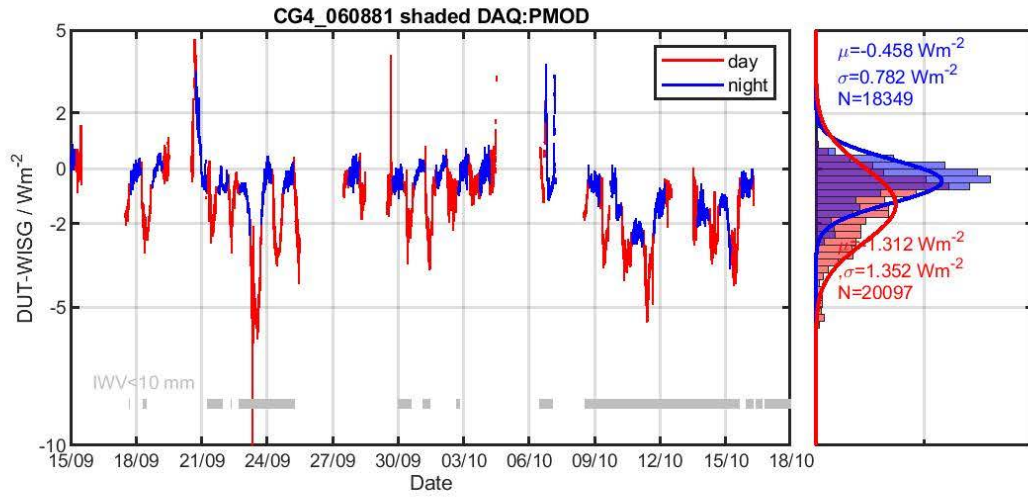


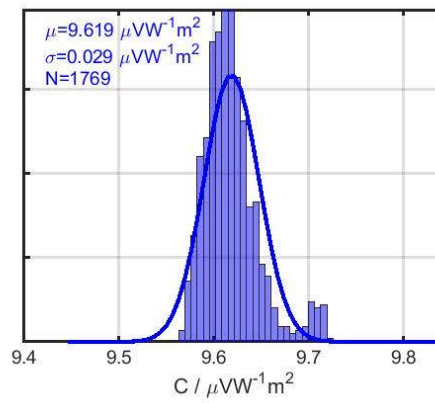
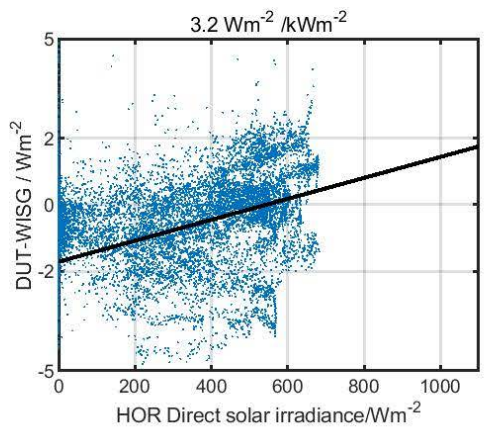
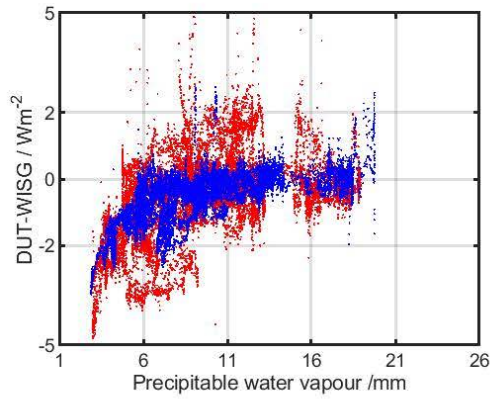
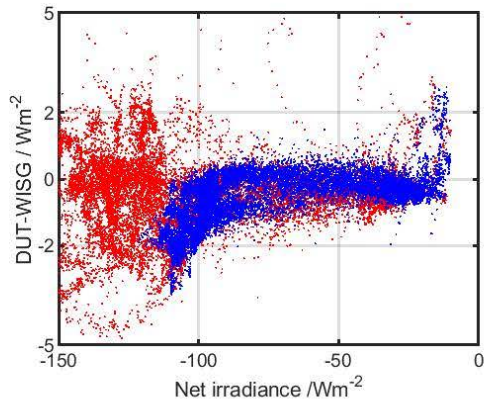
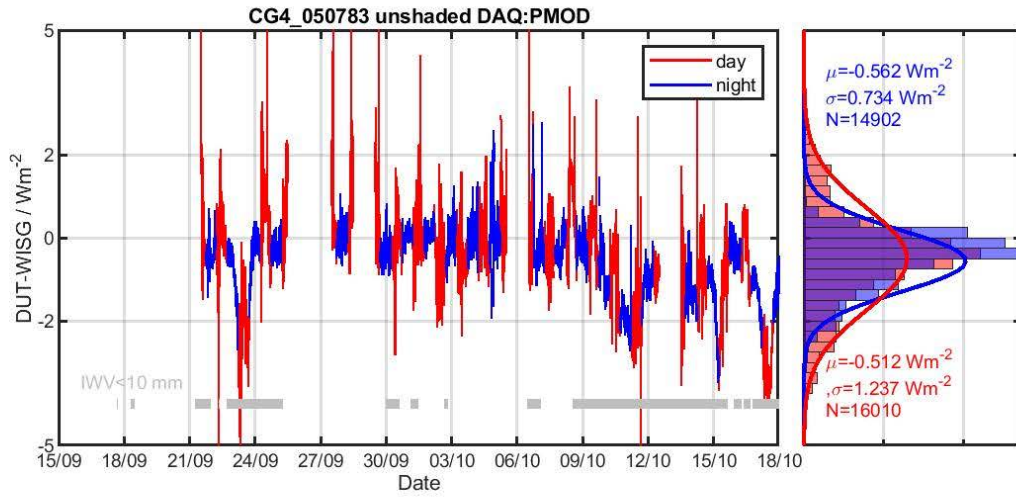


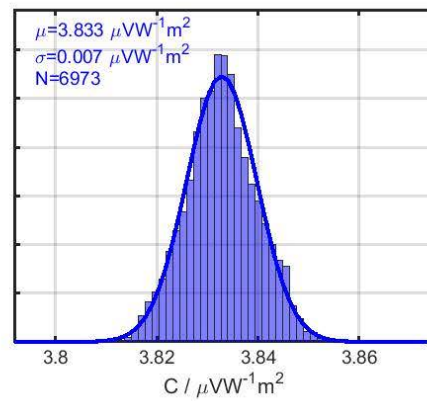
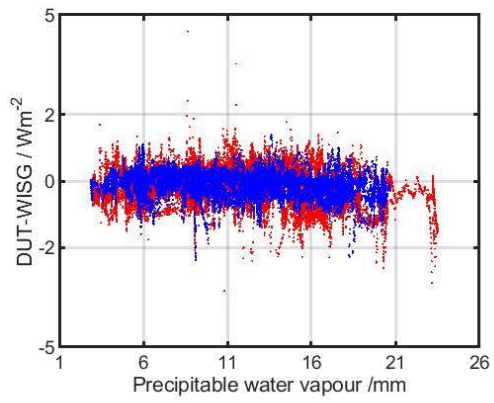
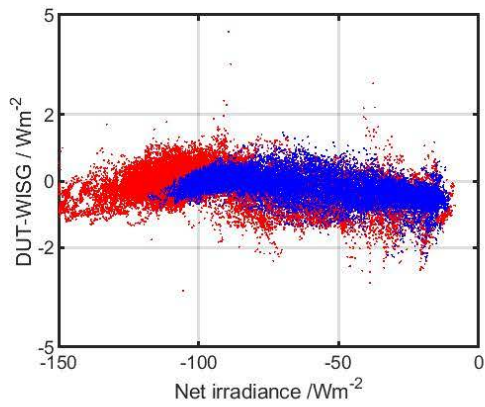
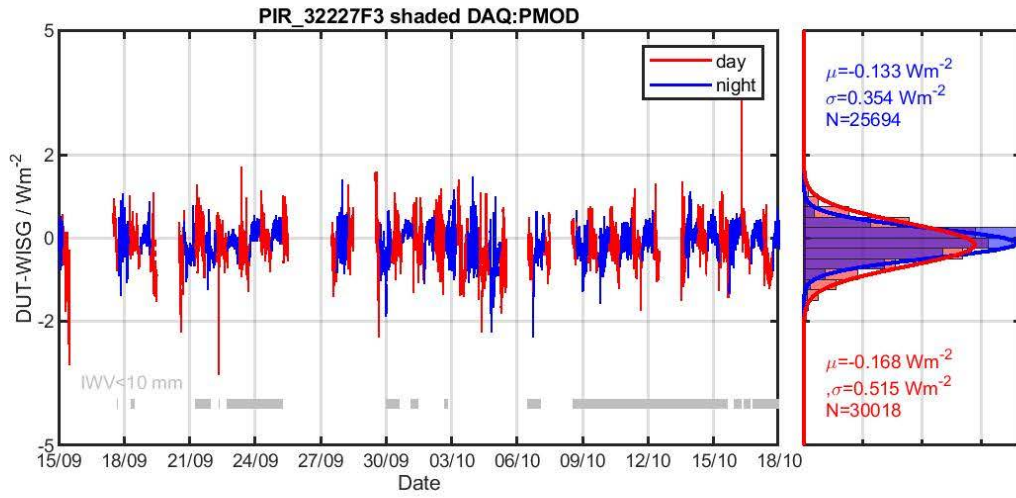


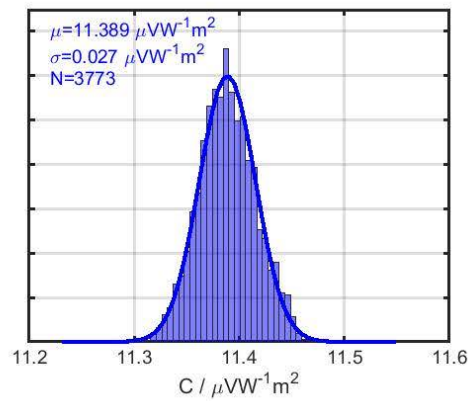
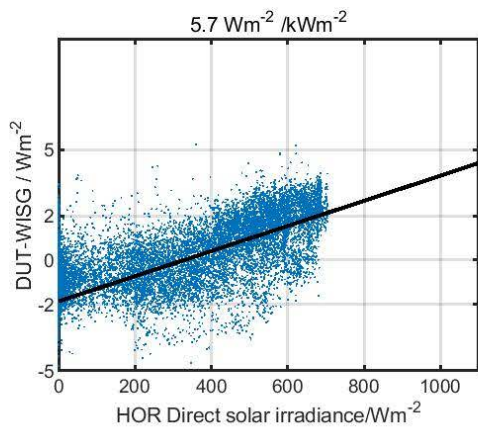
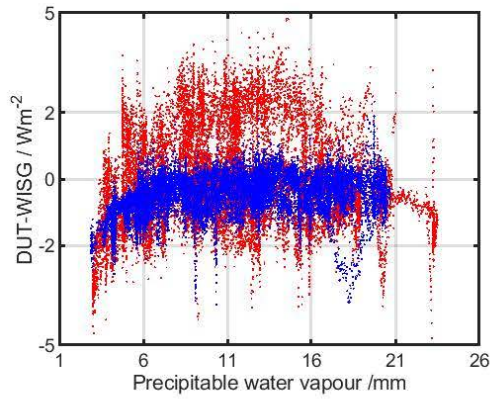
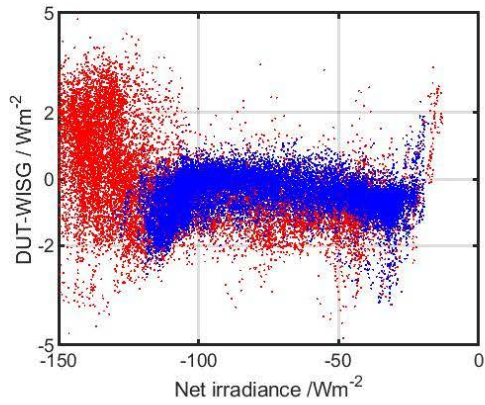
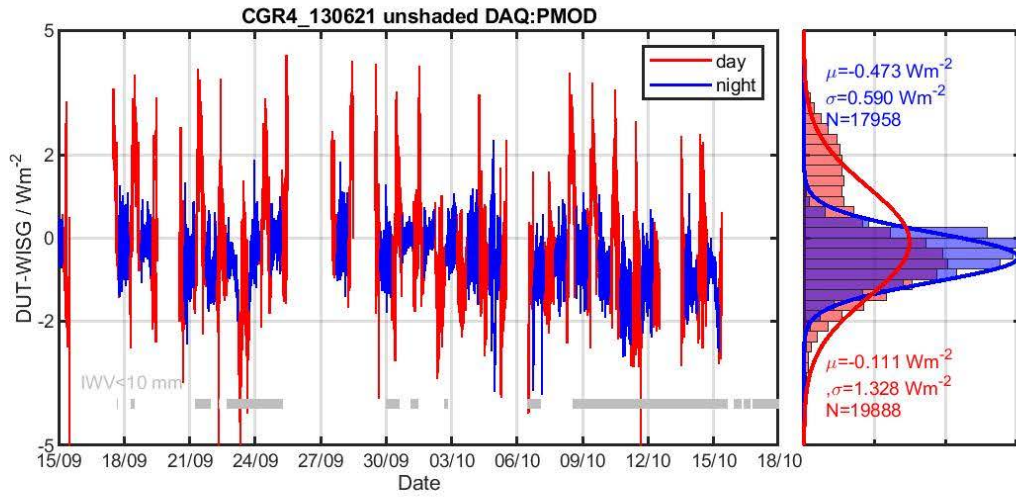


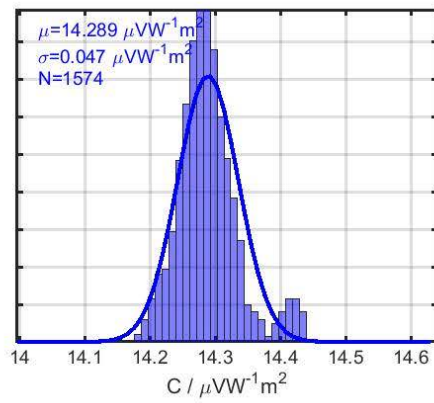
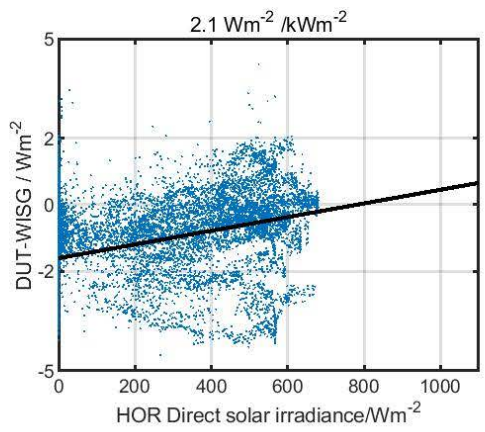
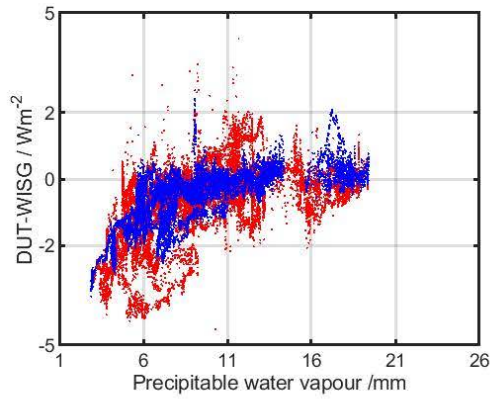
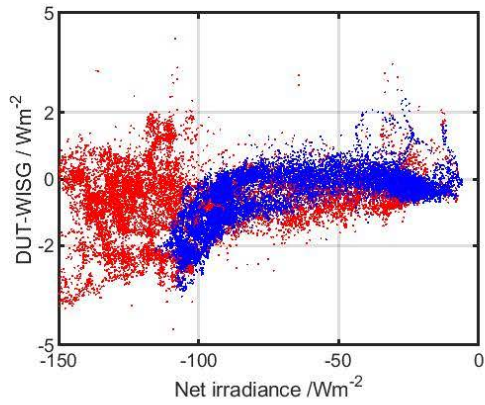
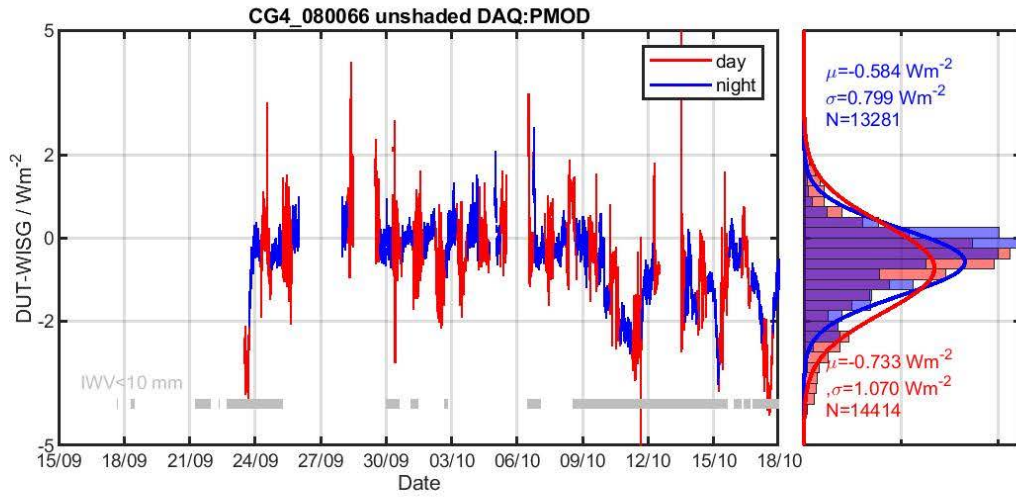




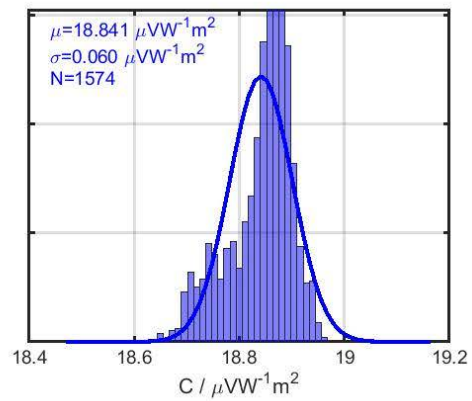
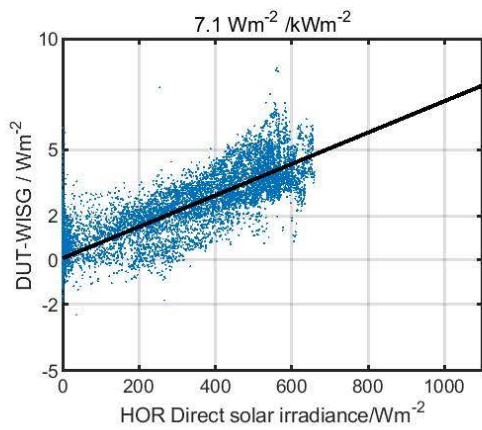
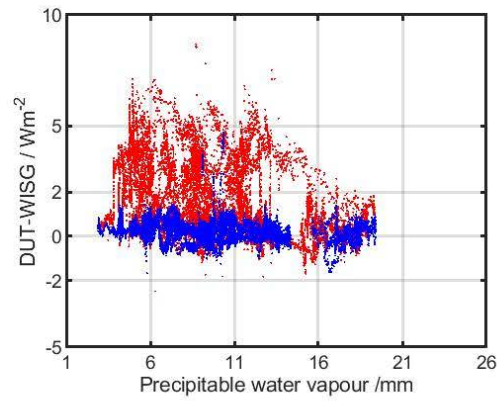
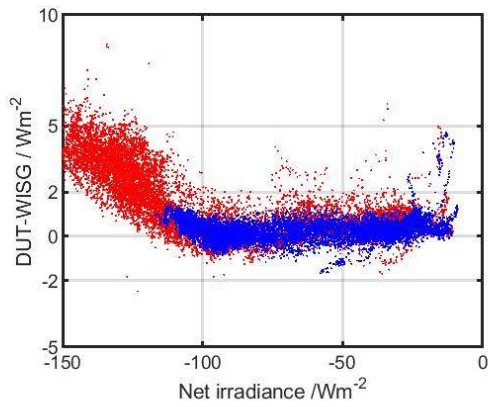
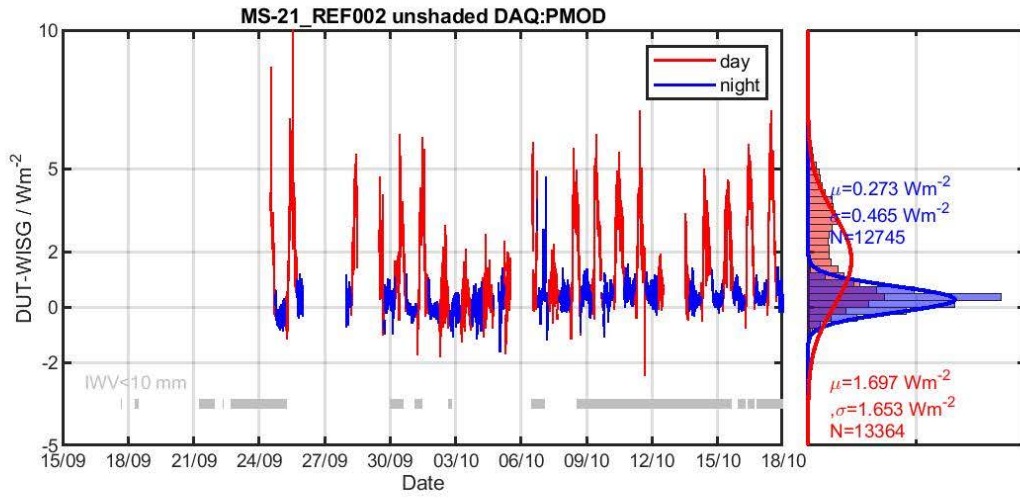


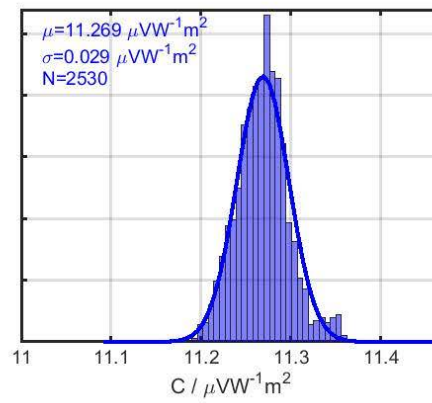
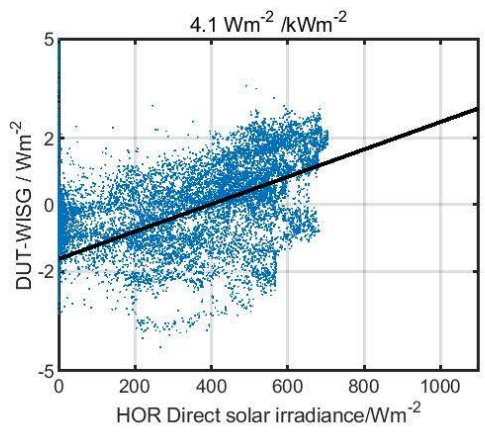
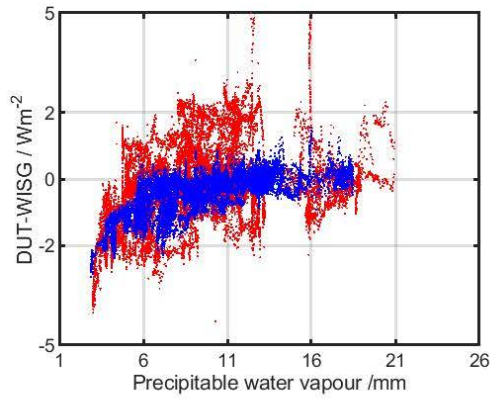
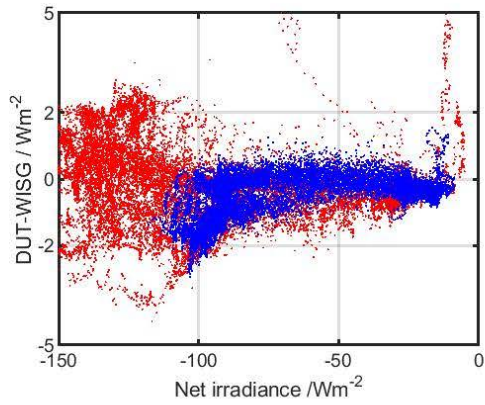
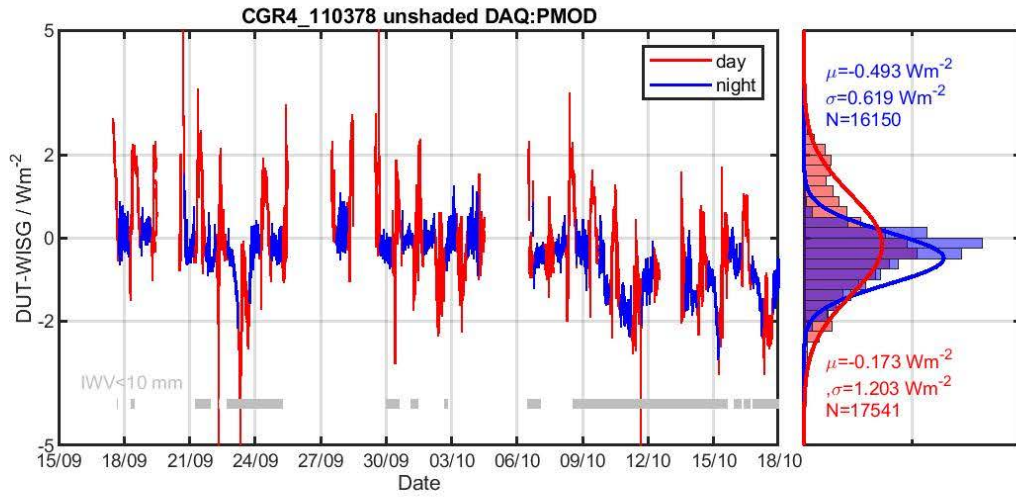


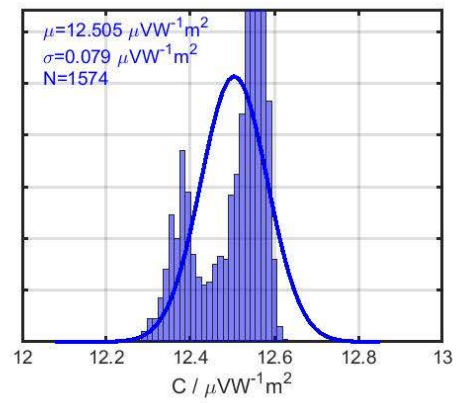
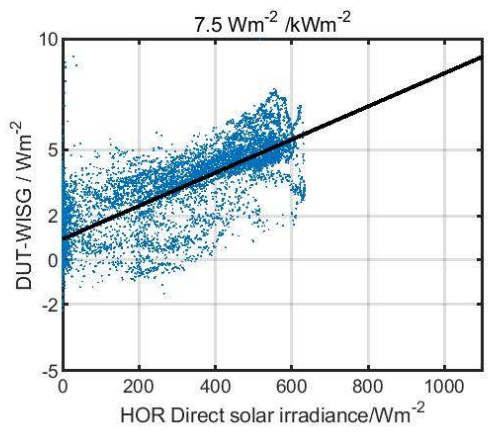
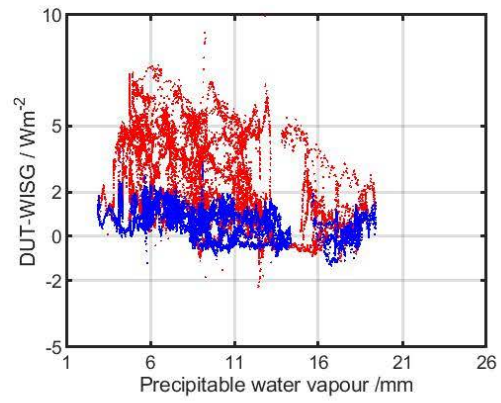
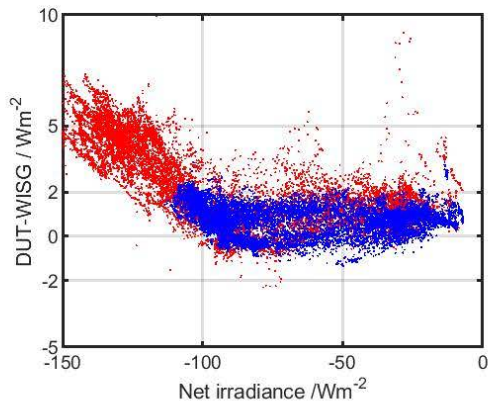
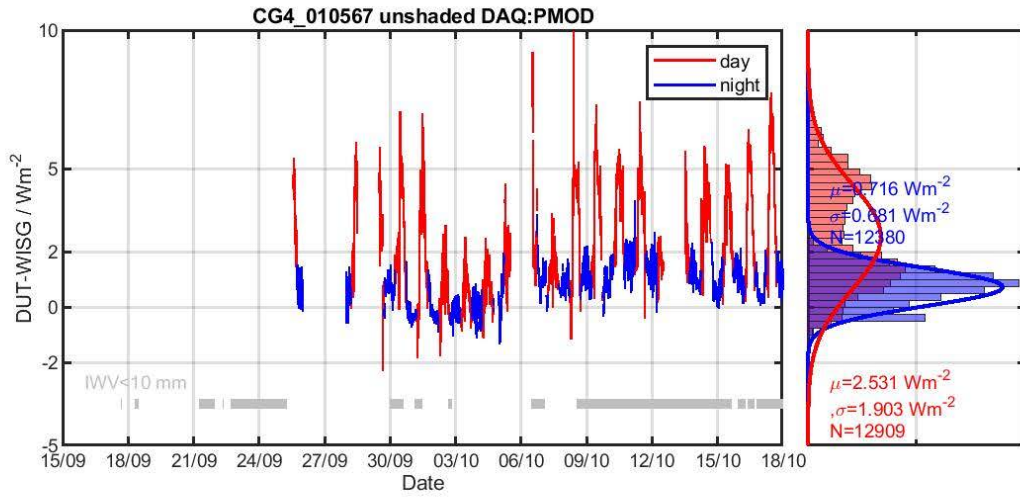


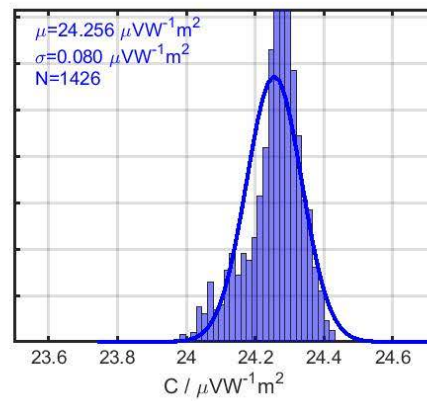
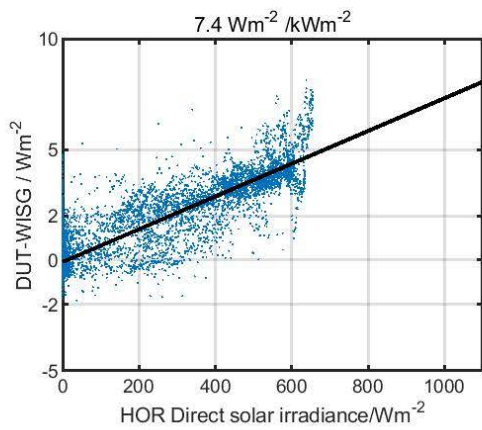
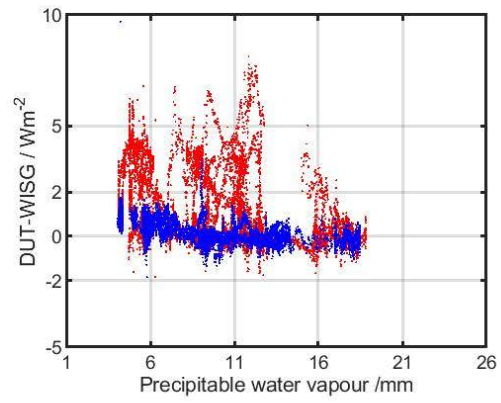
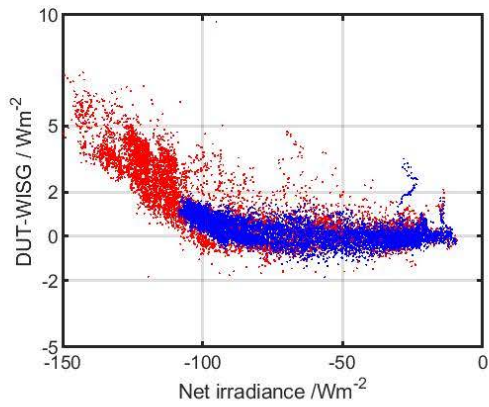
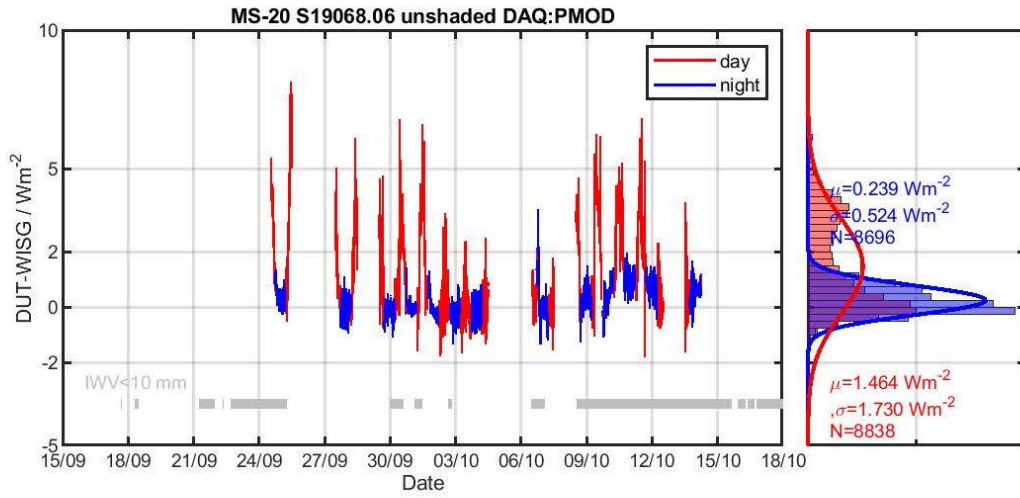


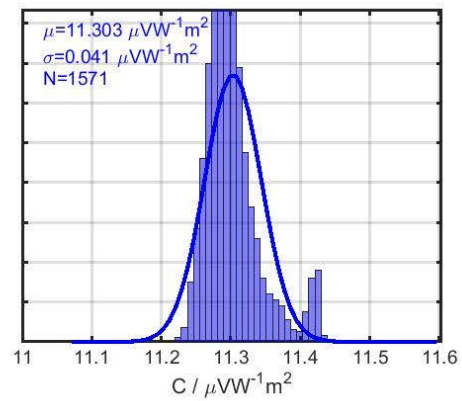
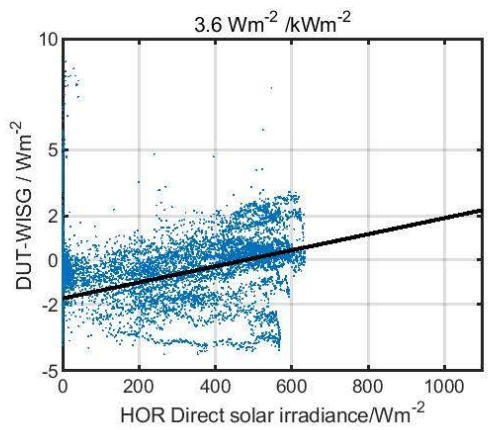
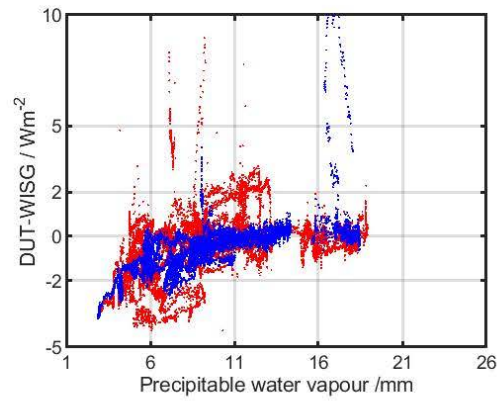
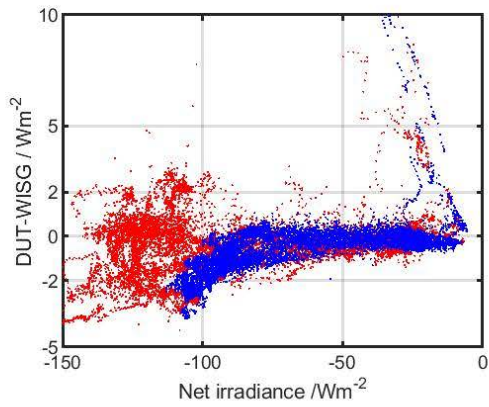
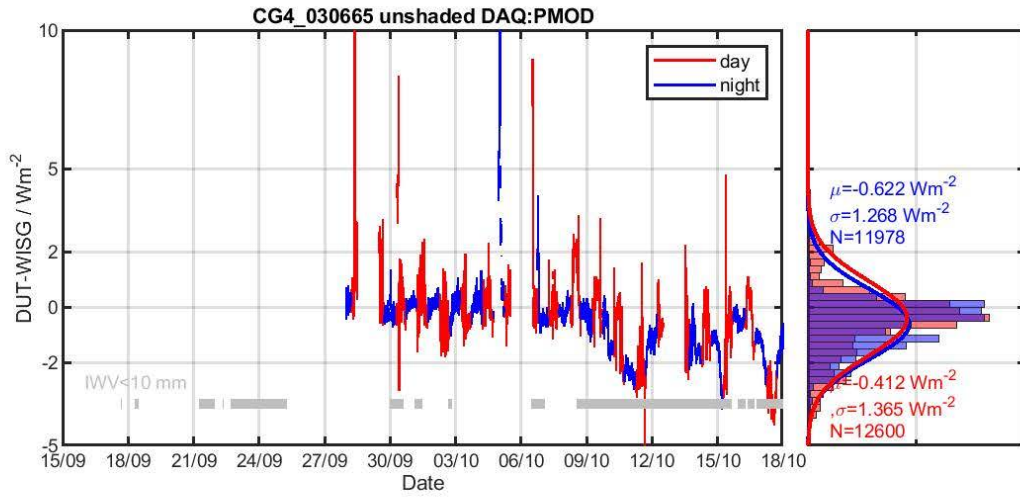


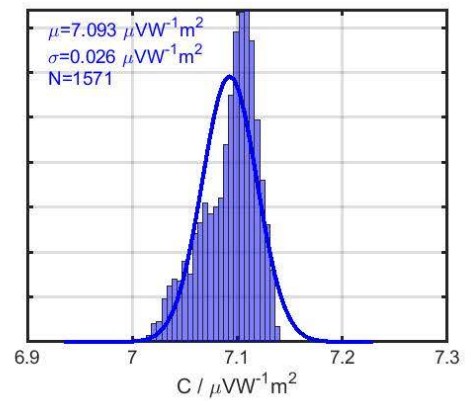
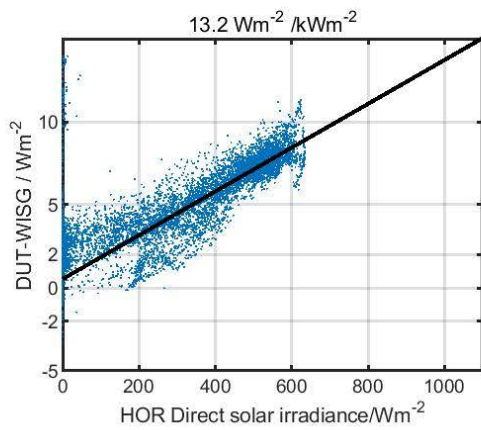
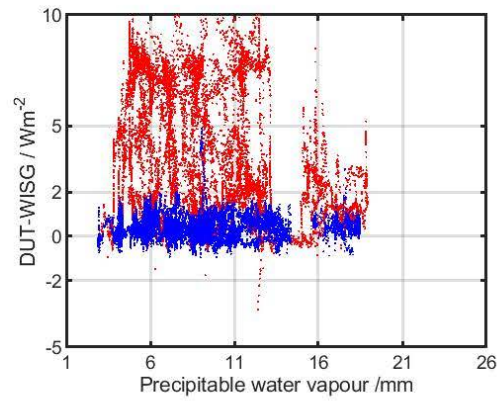
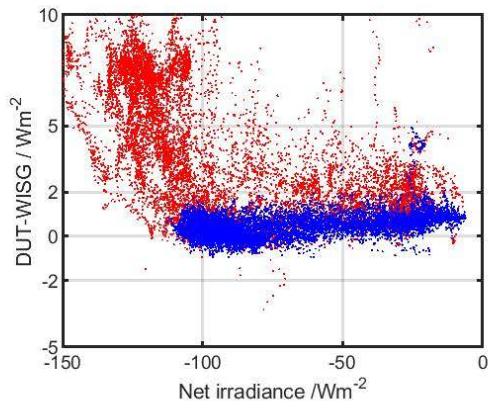
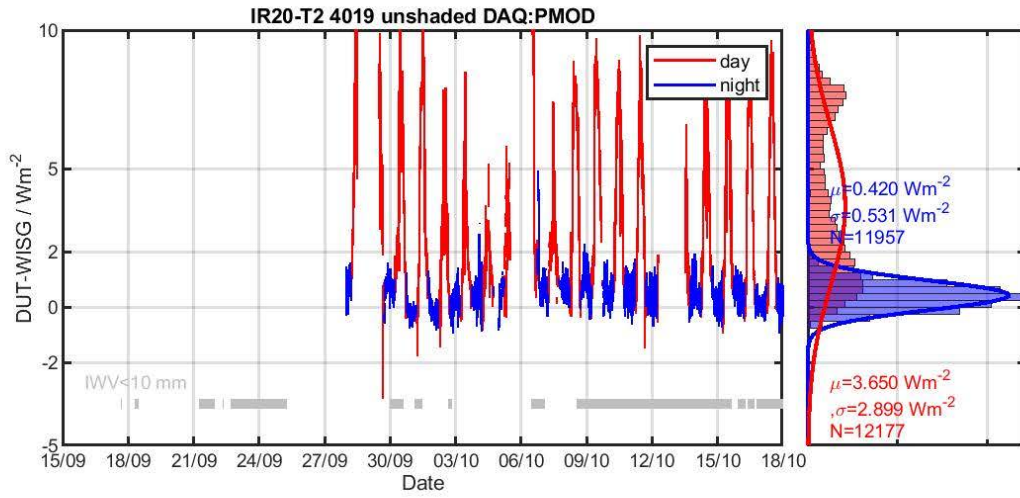


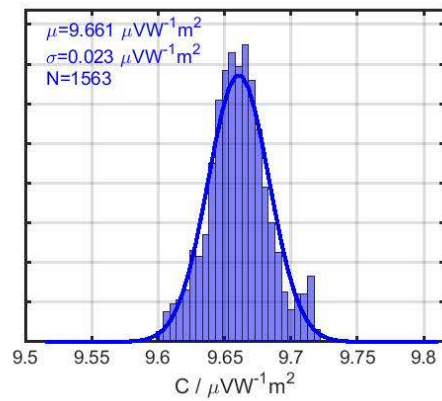
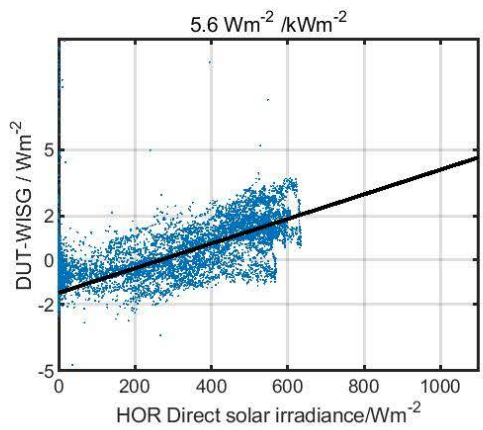
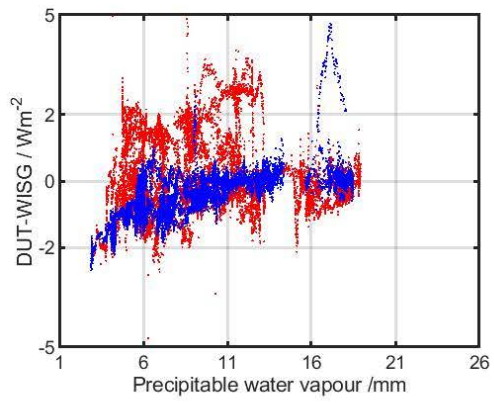
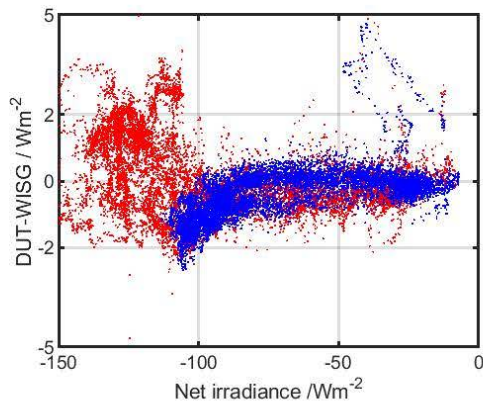
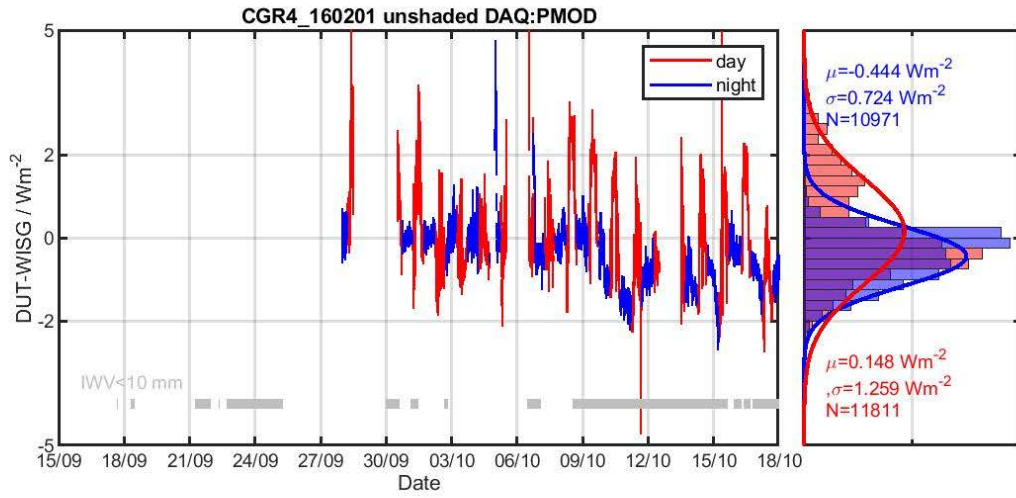


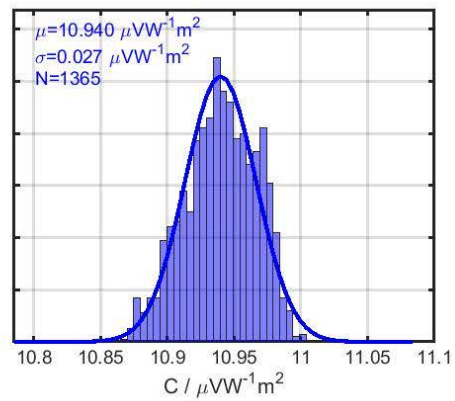
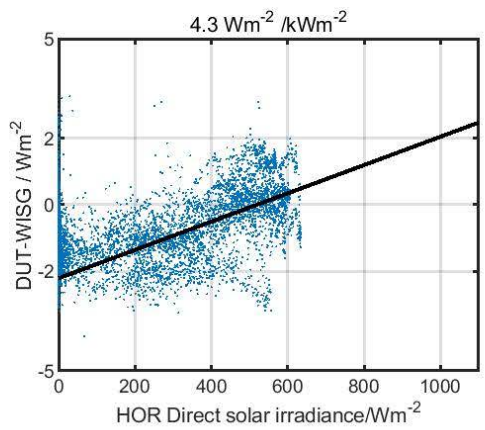
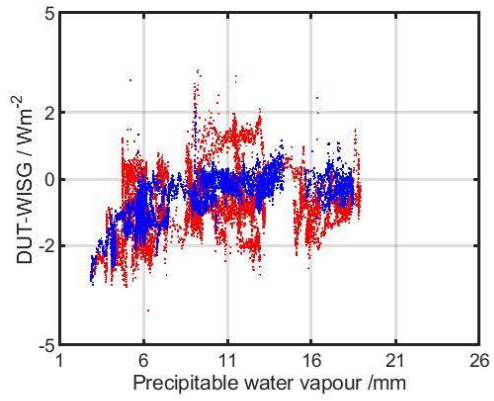
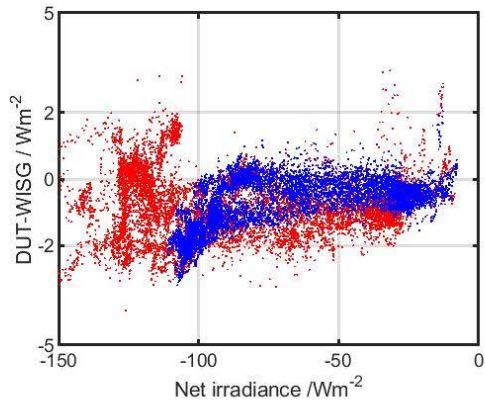
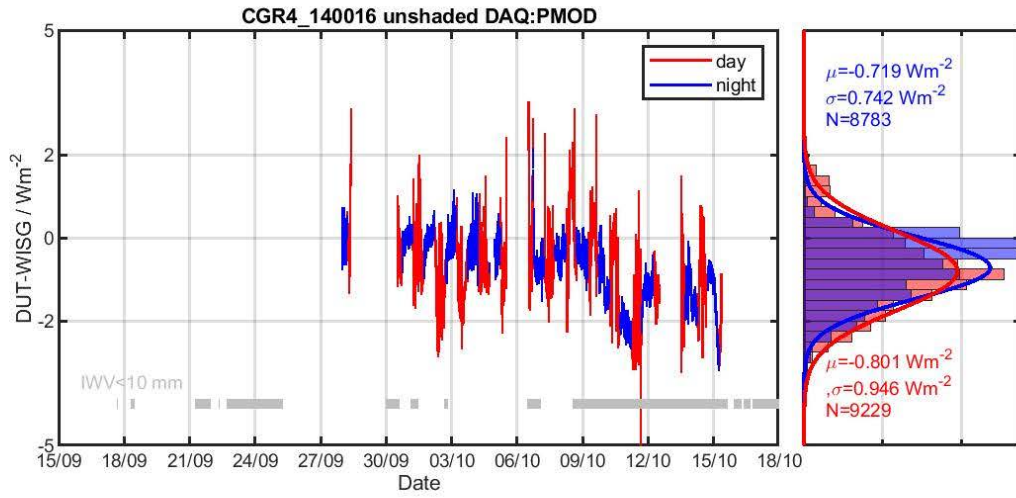




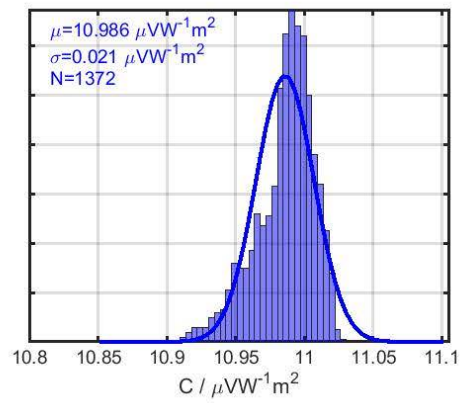
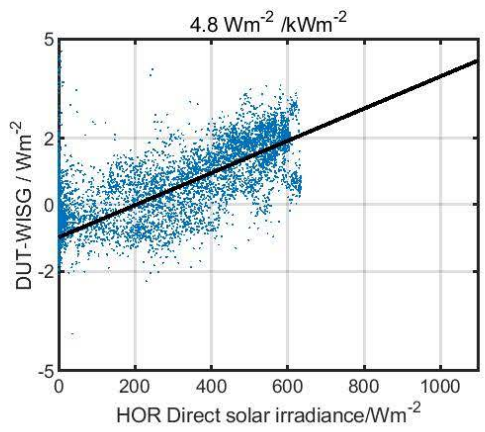
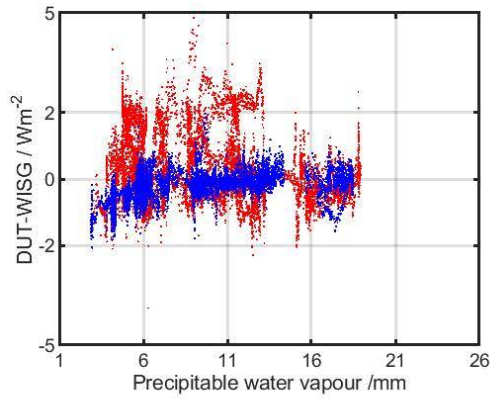
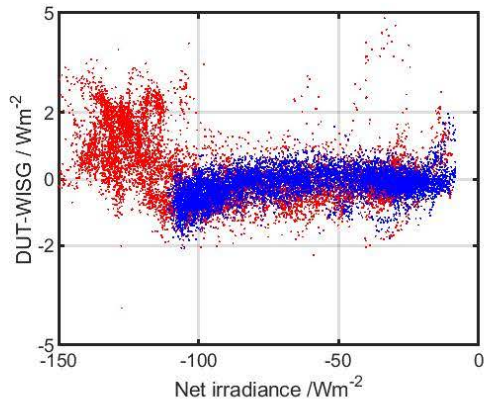
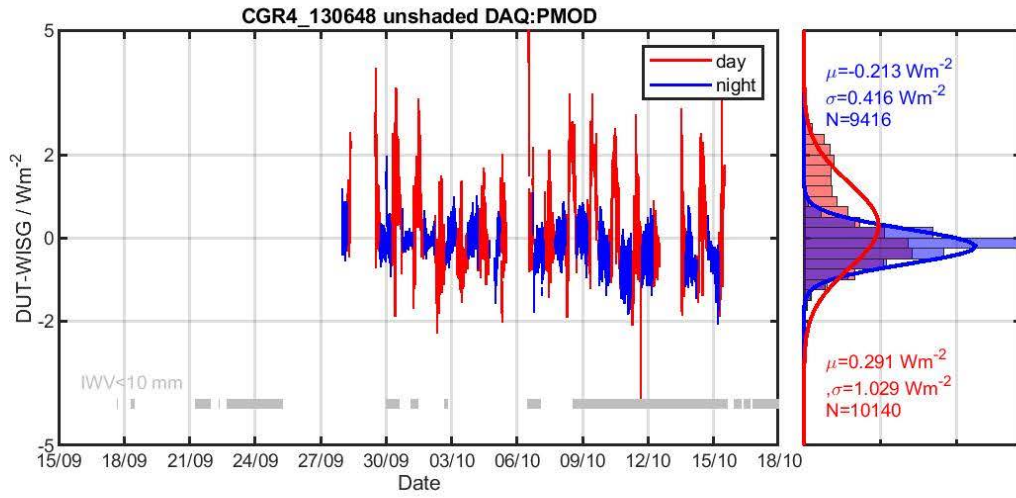


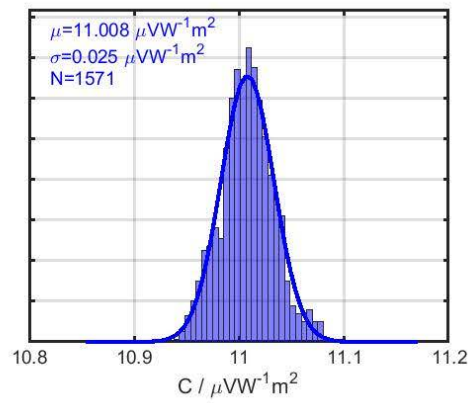
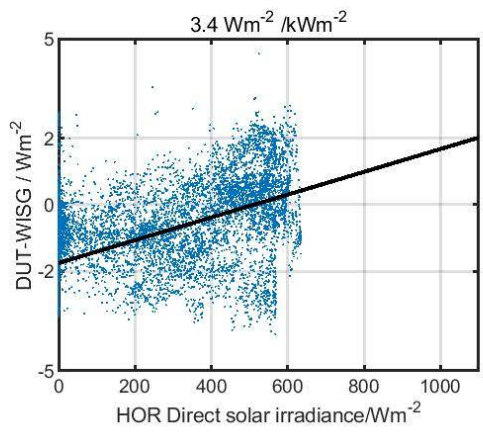
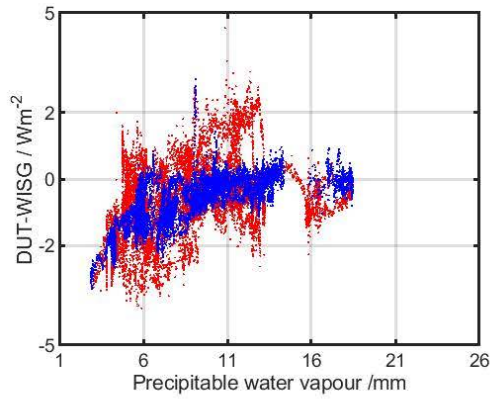
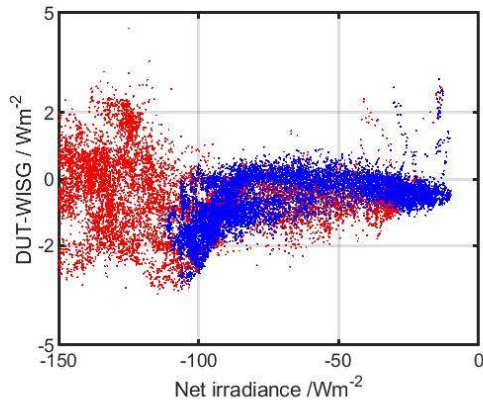
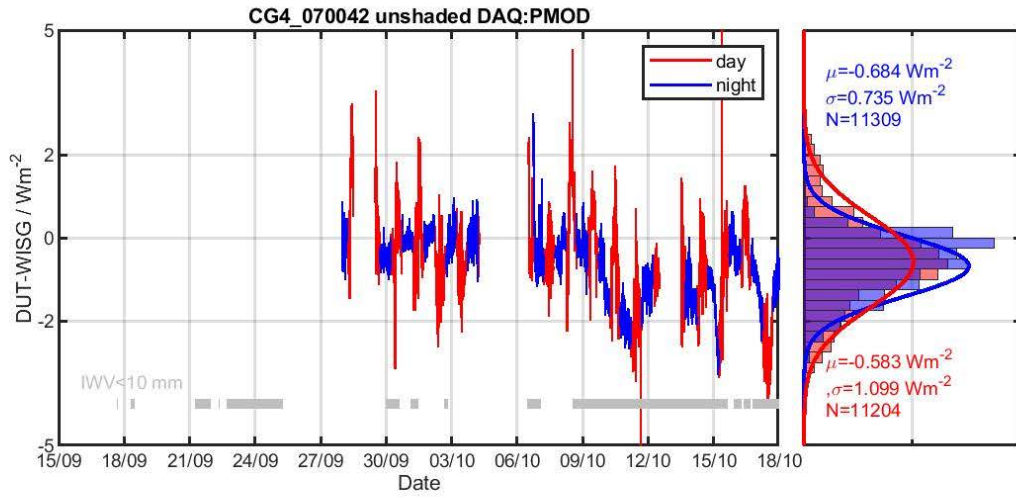


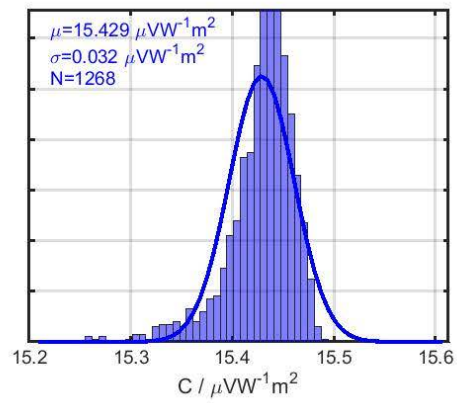
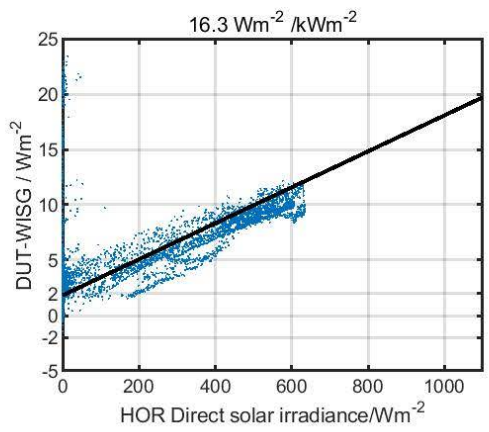
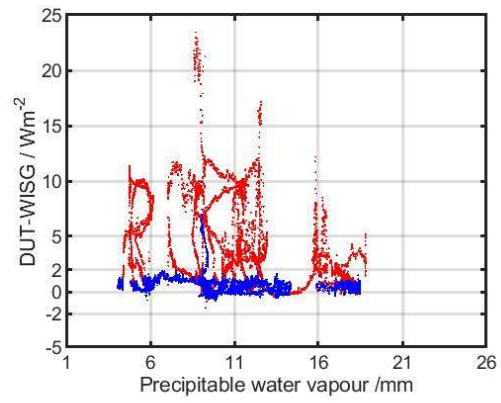
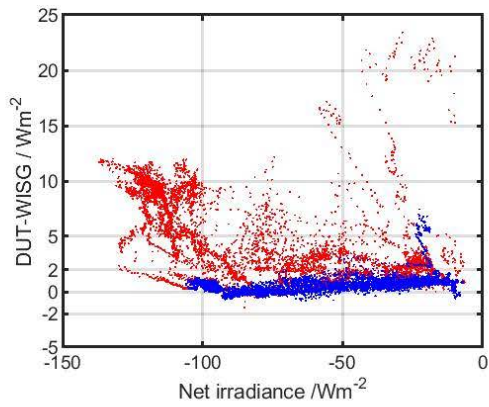
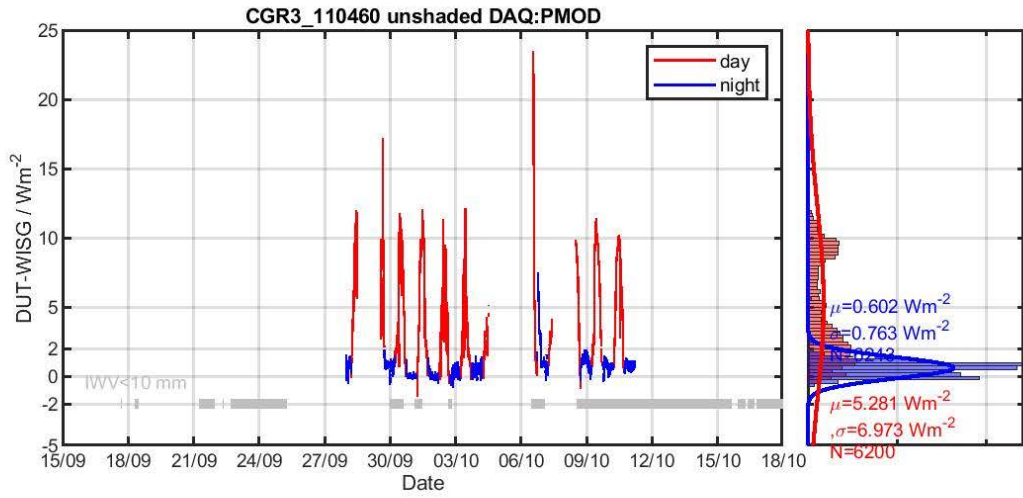


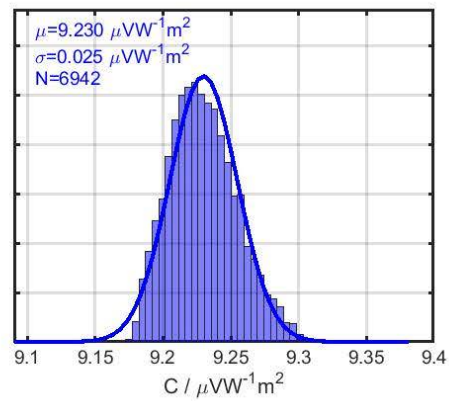
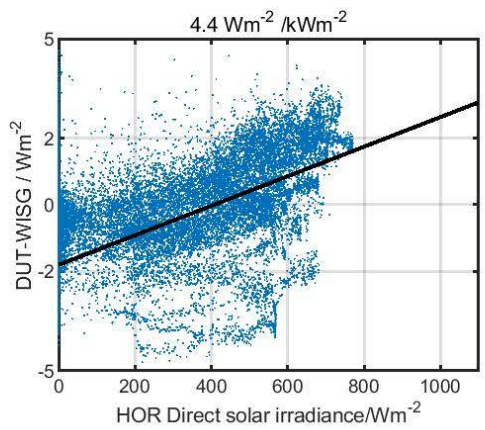
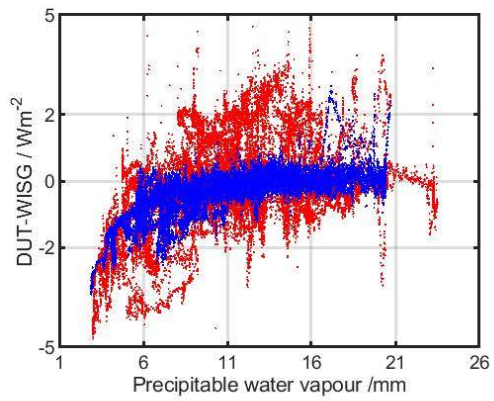
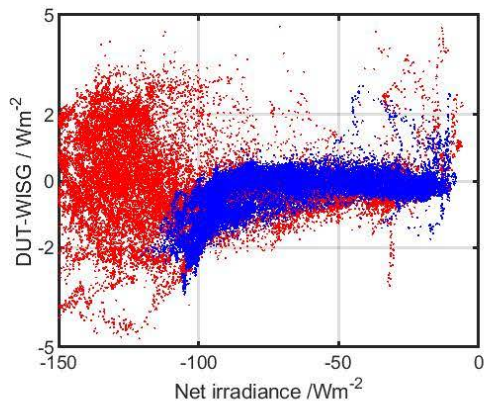
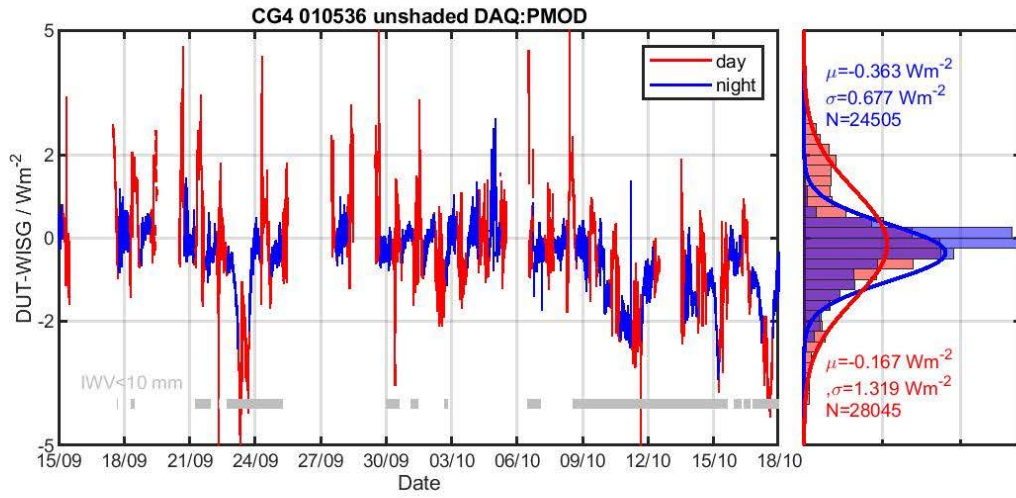


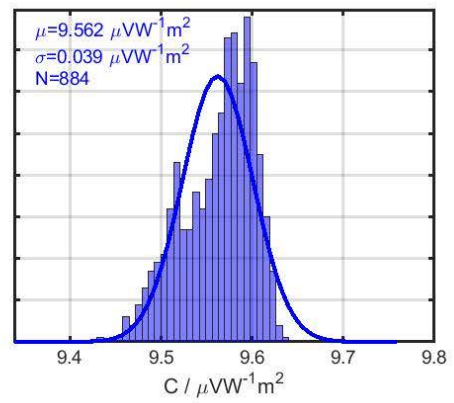
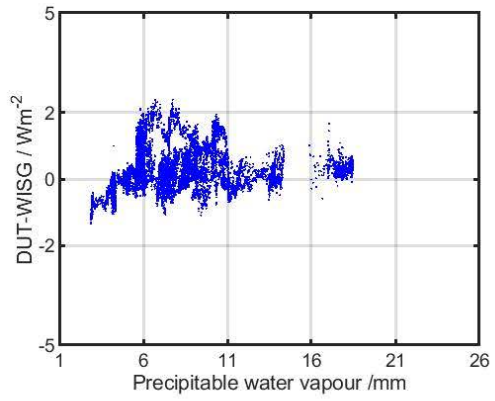
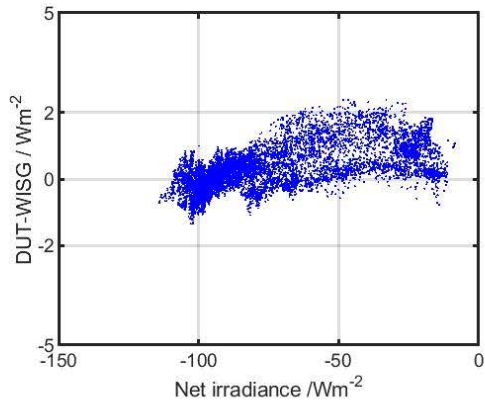
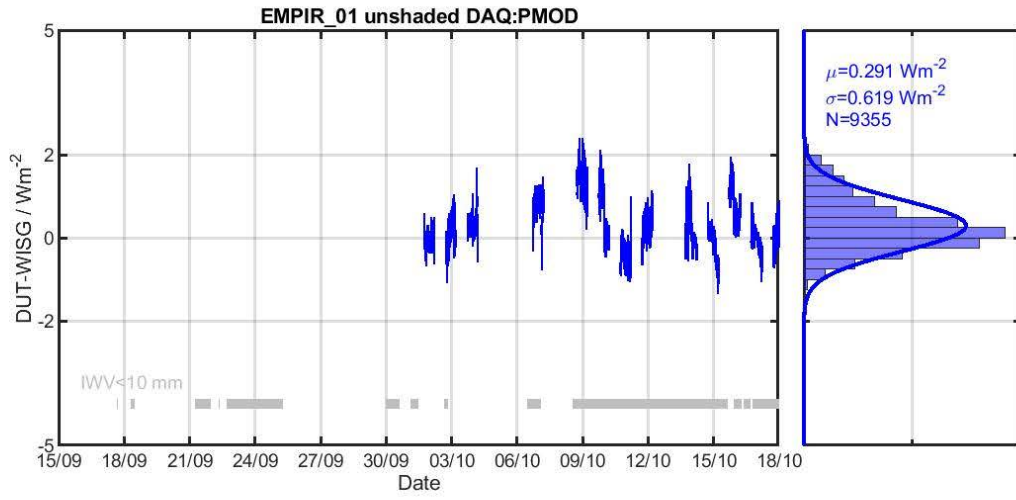


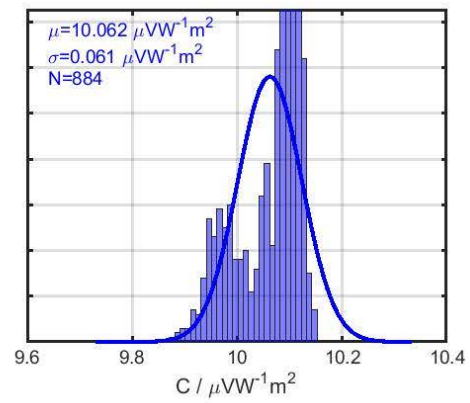
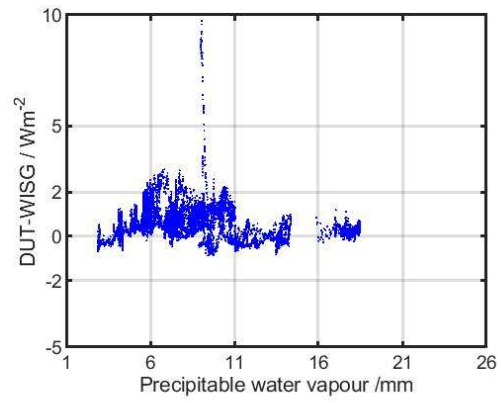
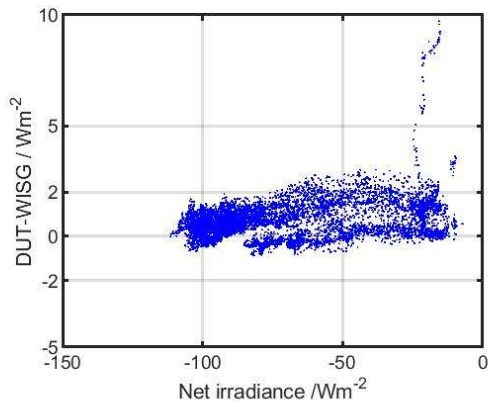
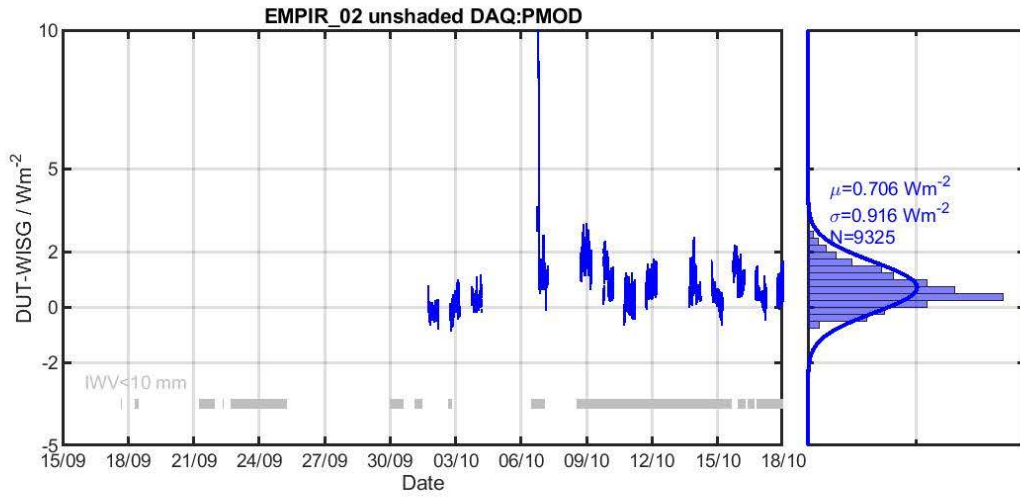


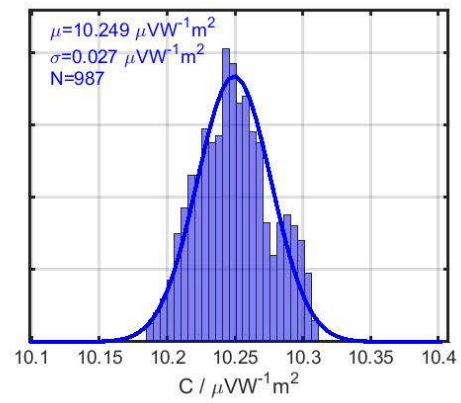
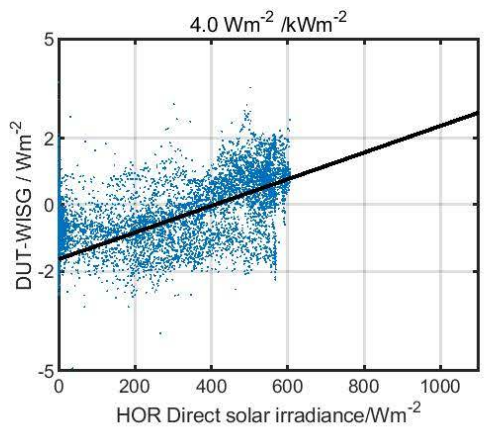
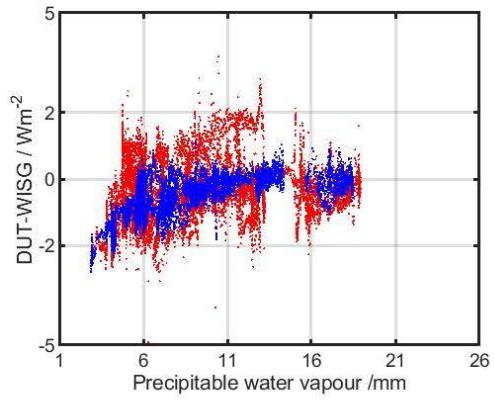
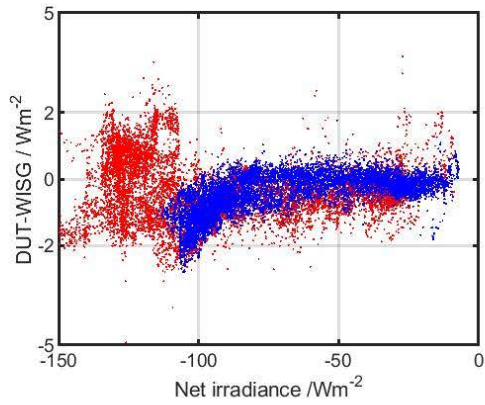
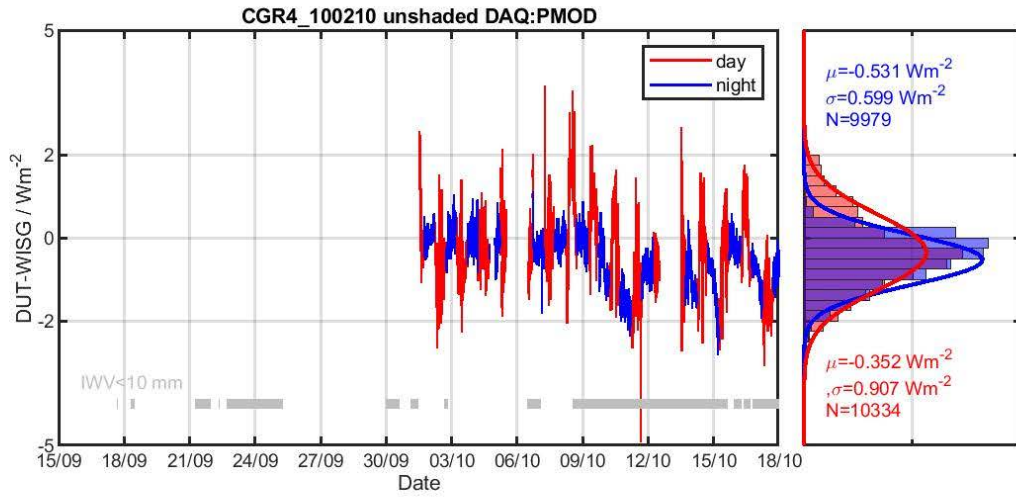


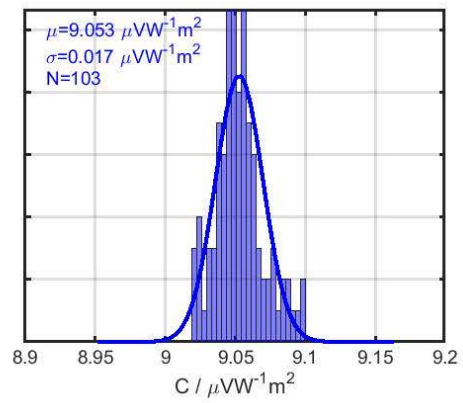
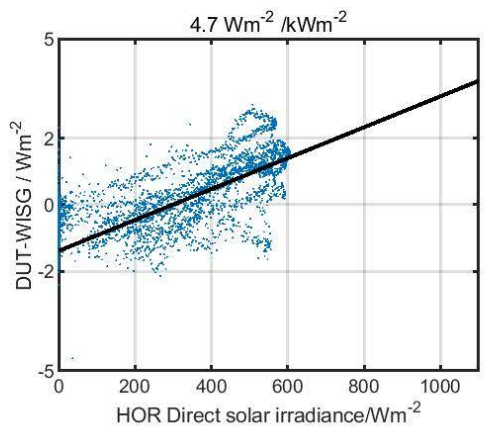
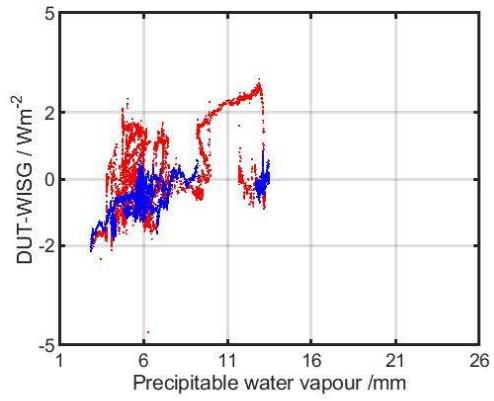
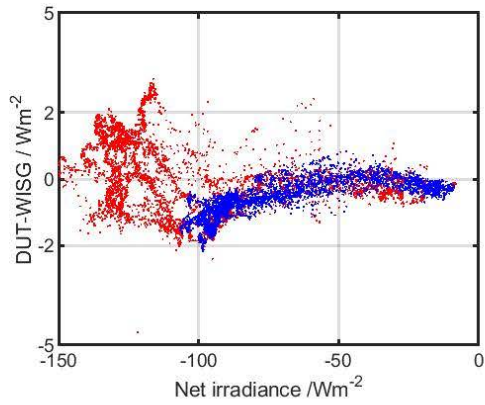
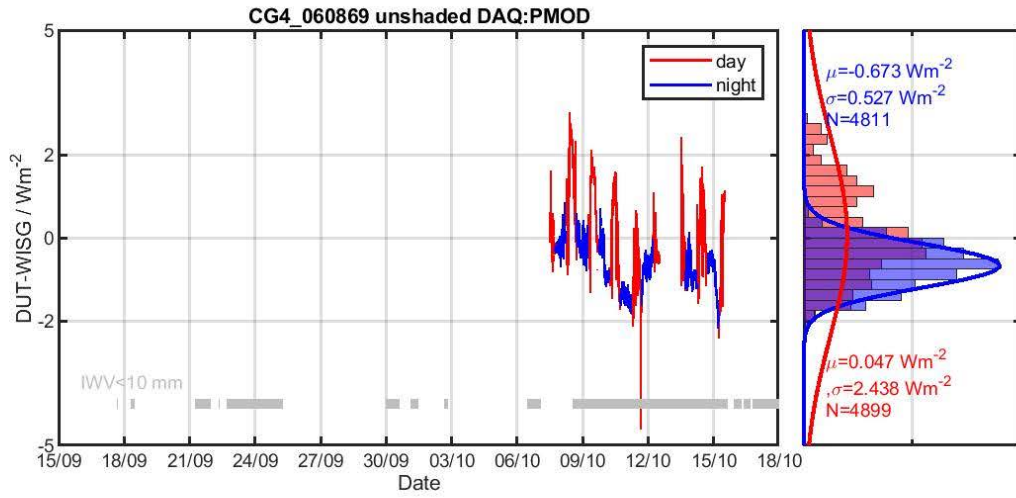




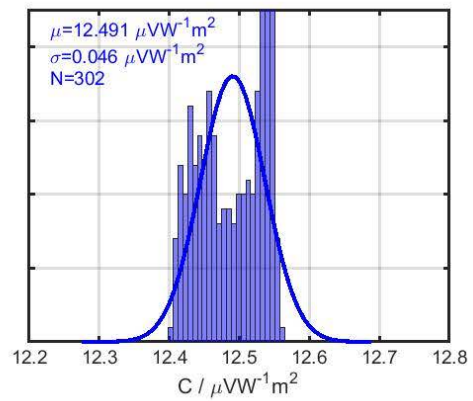
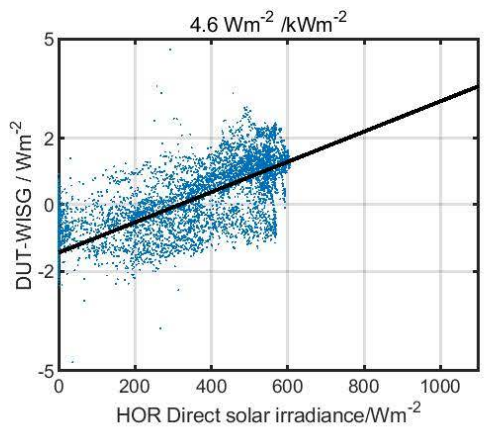
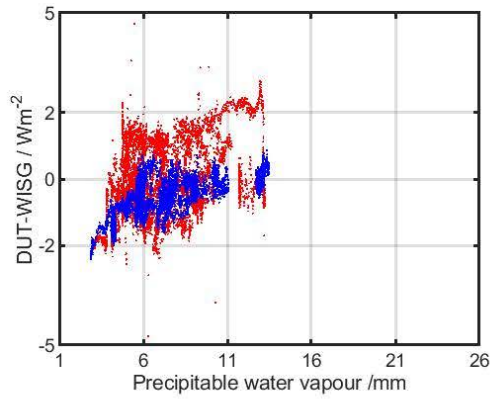
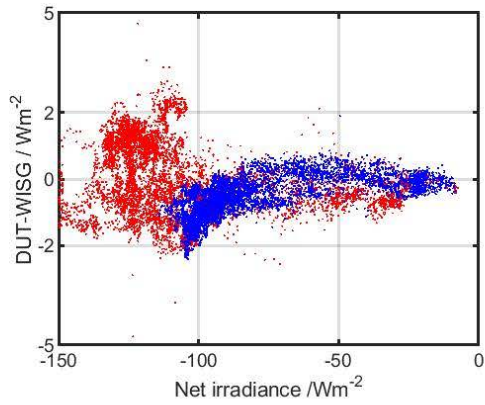
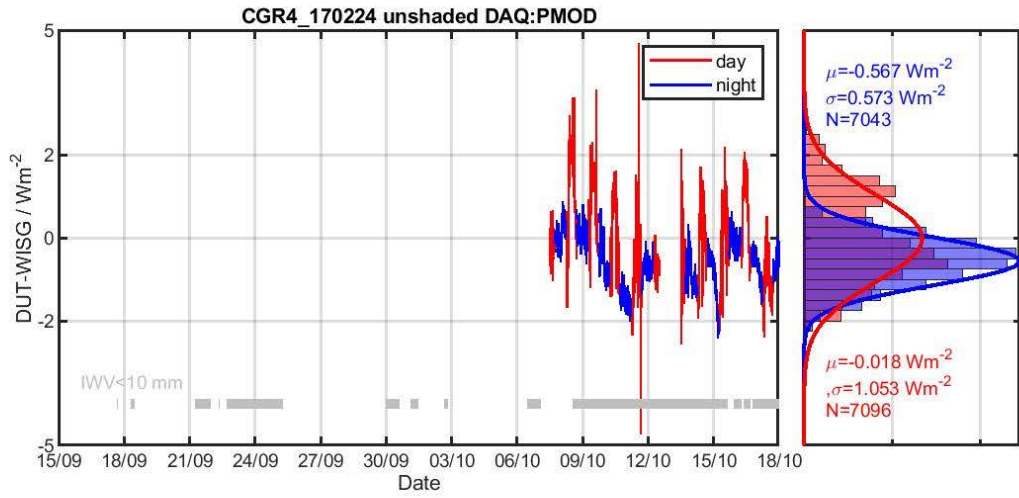


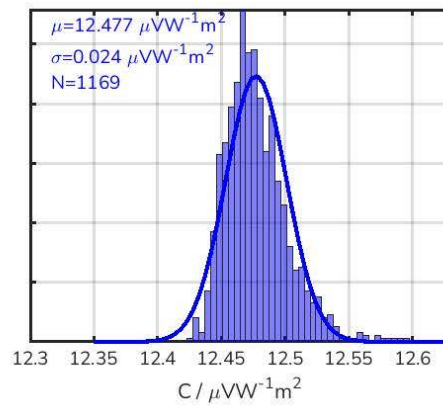
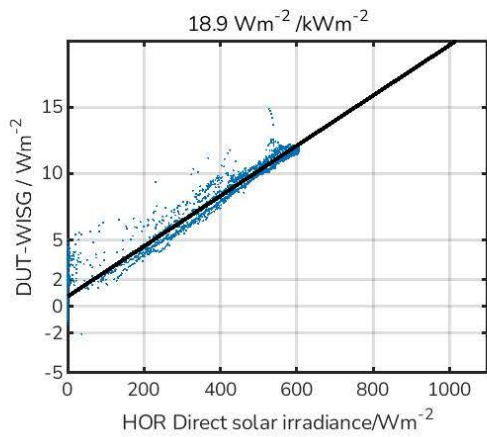
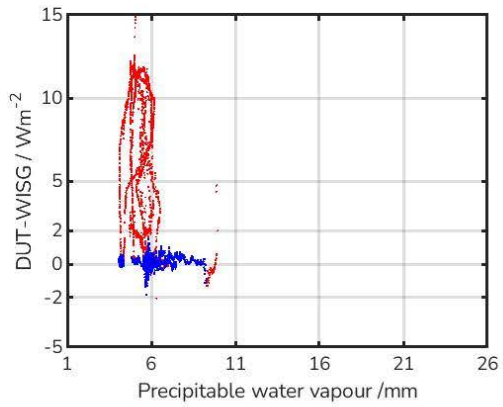
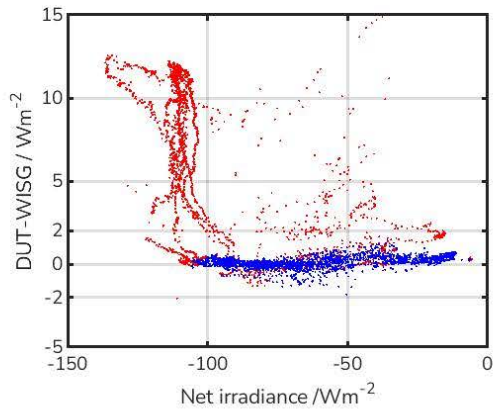
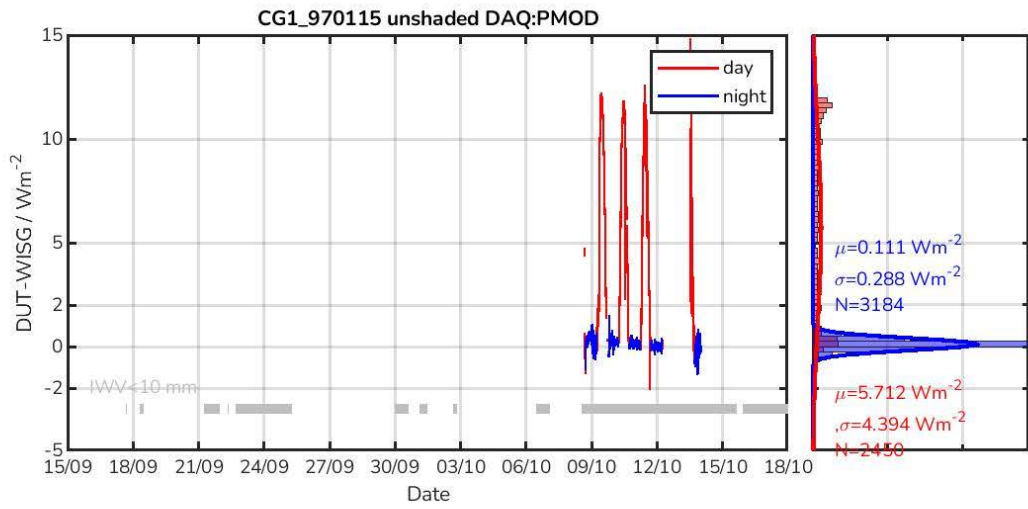


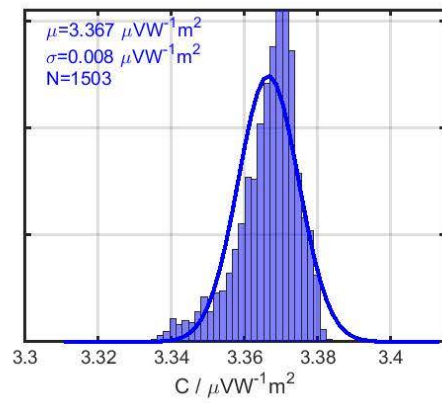
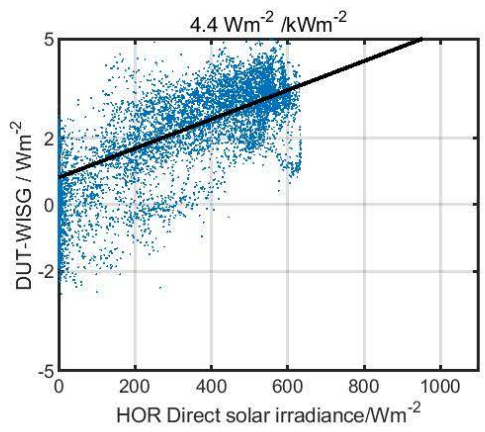
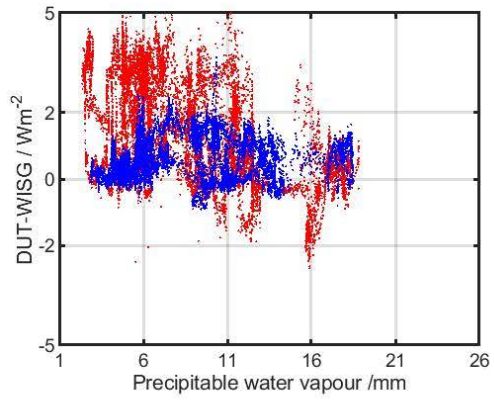
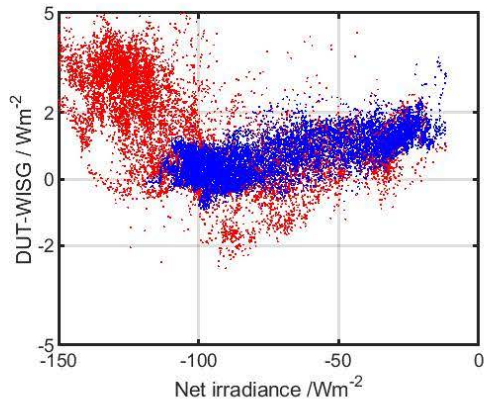
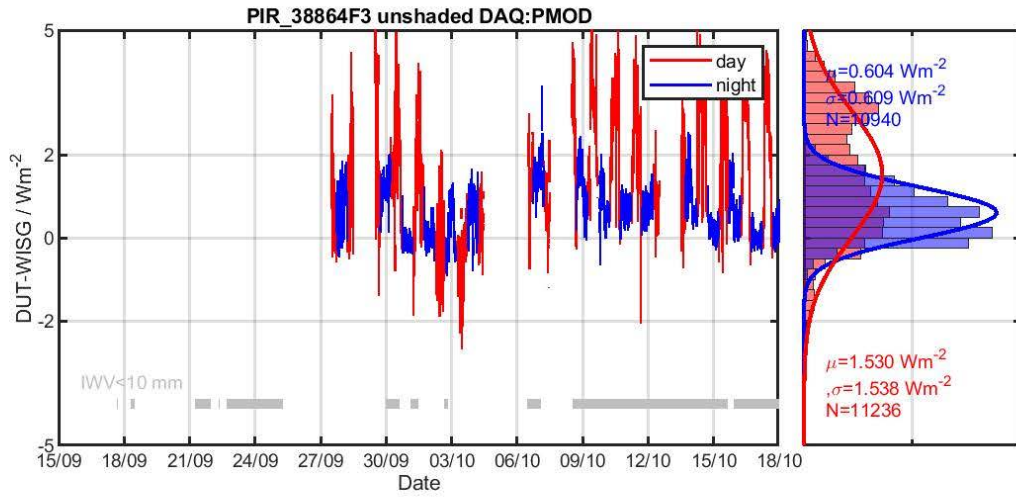


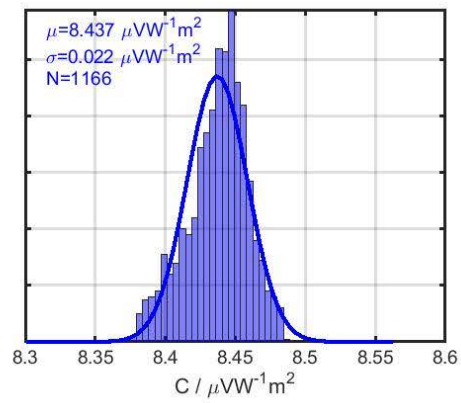
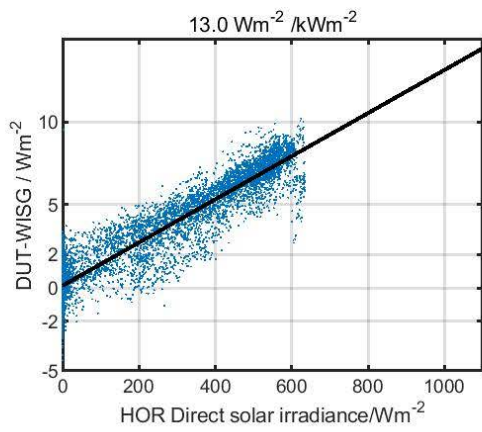
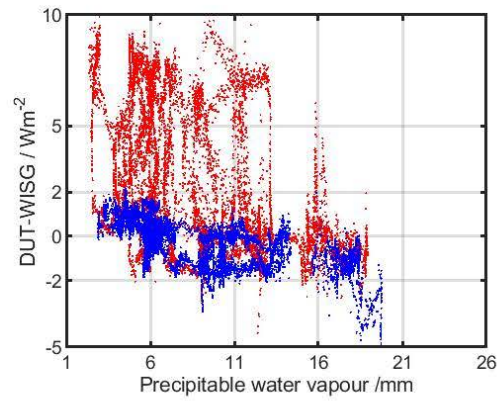
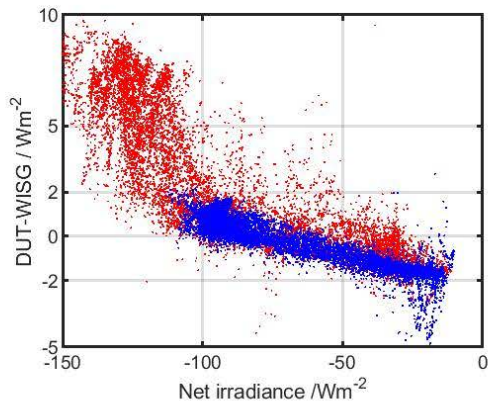
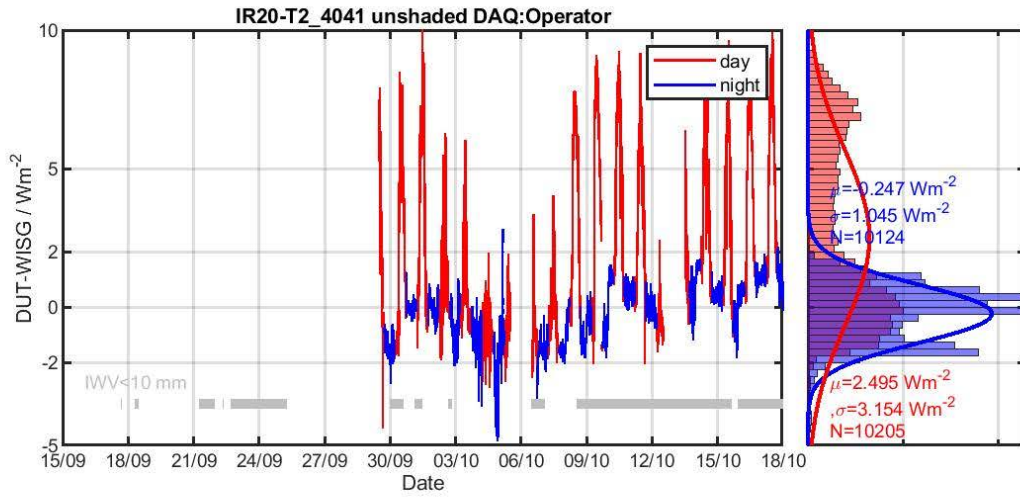


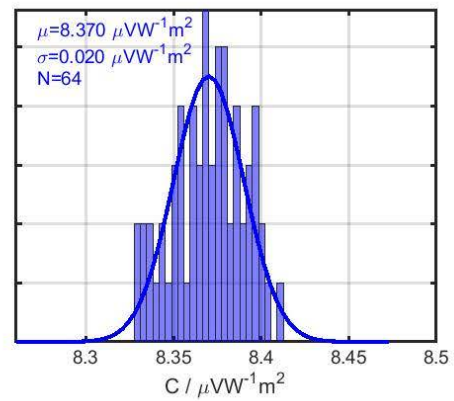
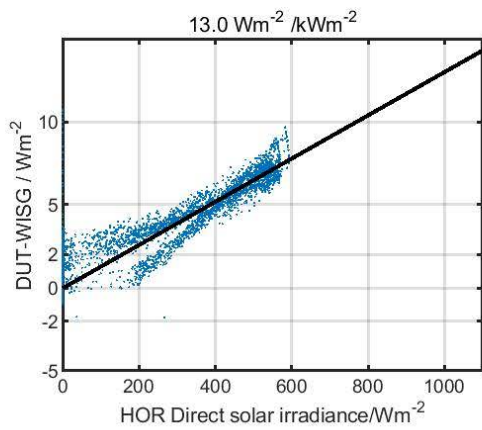
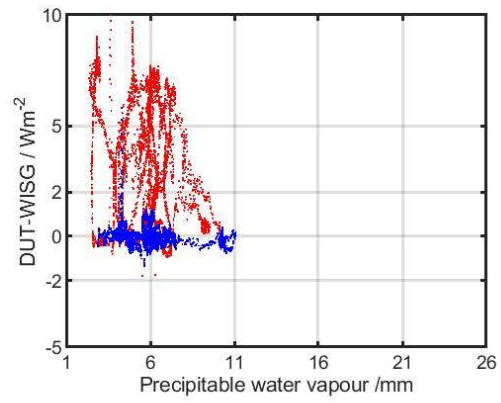
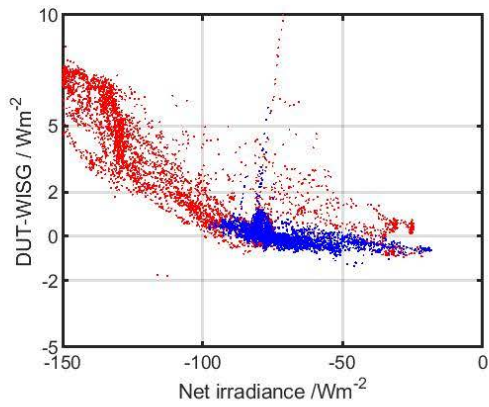
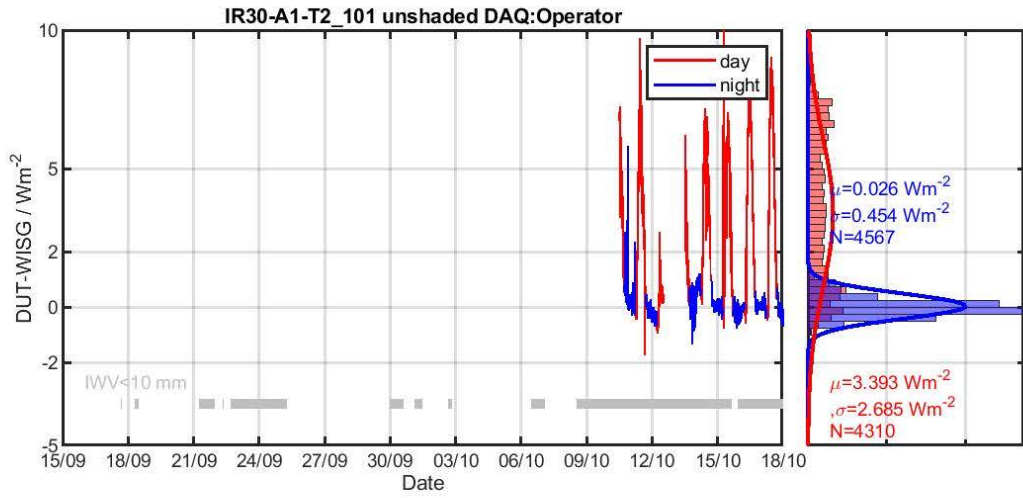


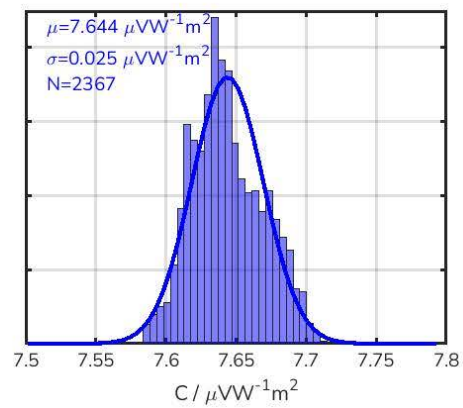
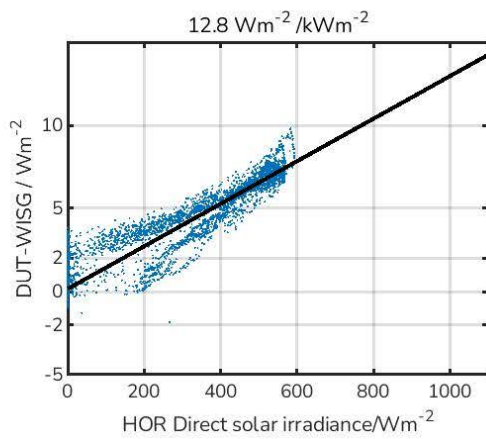
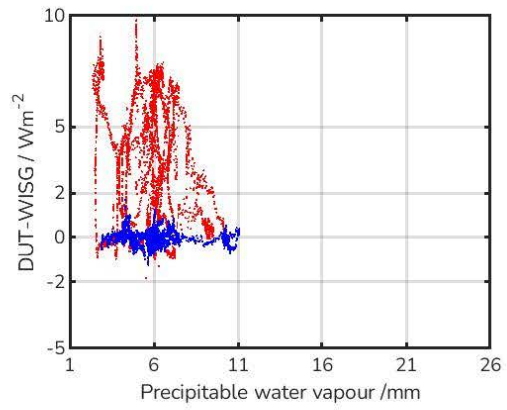
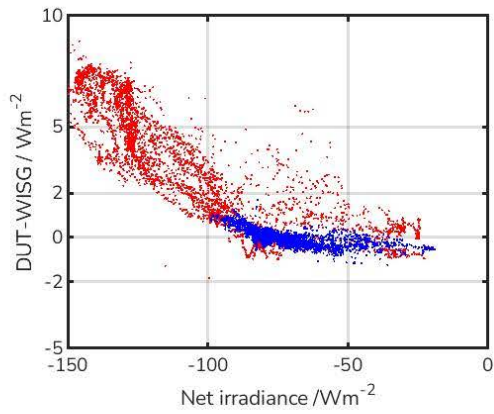
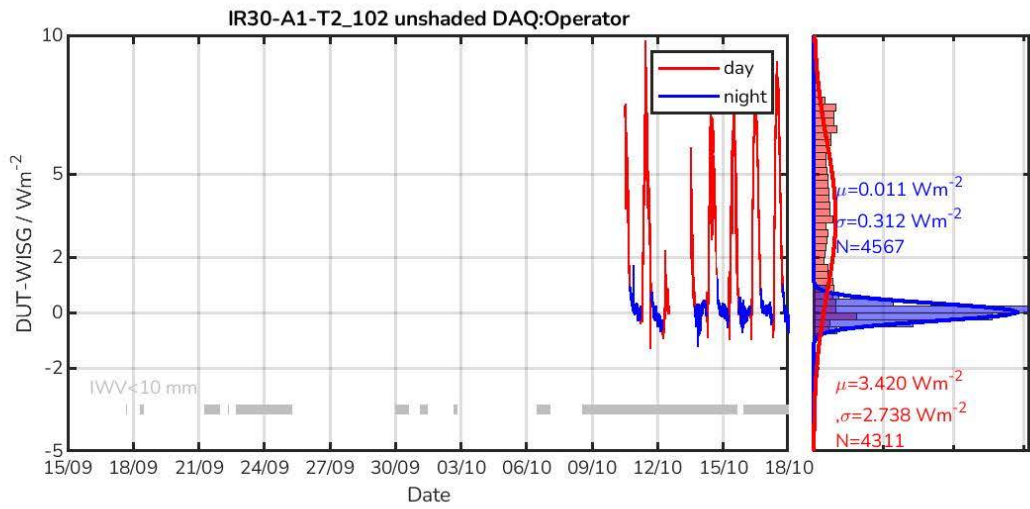


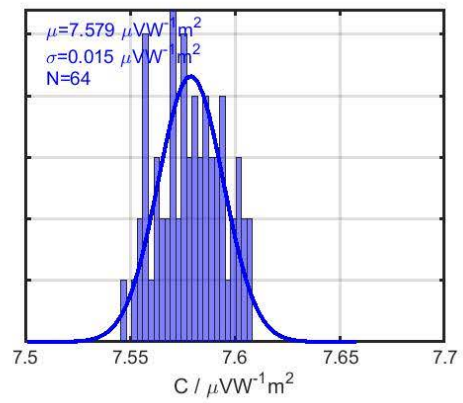
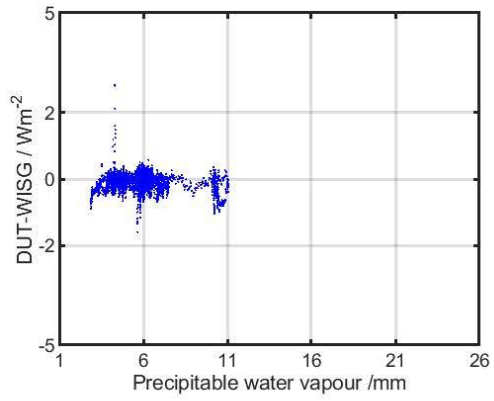
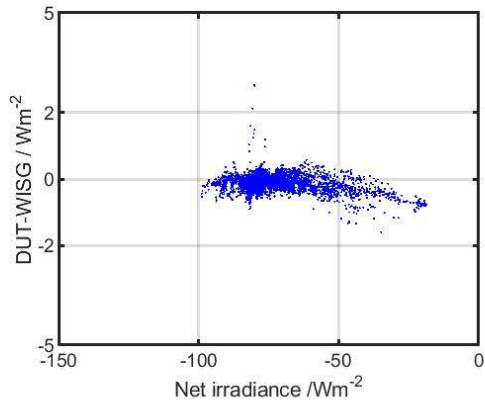
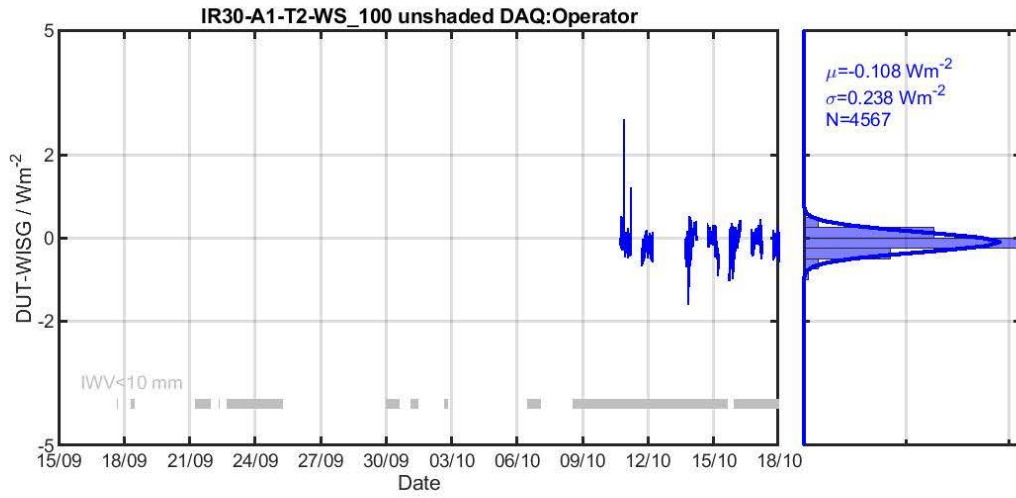












For more information, please contact:

**World Meteorological Organization**

7 bis, avenue de la Paix – P.O. Box 2300 – CH 1211 Geneva 2 – Switzerland

**Communication and Public Affairs Office**

Tel.: +41 (0) 22 730 83 14 – Fax: +41 (0) 22 730 81 71

E-mail: [cpa@wmo.int](mailto:cpa@wmo.int)

[public.wmo.int](http://public.wmo.int)